LAWRENCE
LIVERMORE
NATIONAL
LABORATORY

LLNL-TH-700178

Determining the Role of Sost and Sostdc1 During Fracture Healing

C. S. Yee

August 10, 2016

Disclaimer

This work performed under the auspices of the U.S. Department of Energy by Lawrence Livermore National Laboratory under Contract DE-AC52-07NA27344.

University of California, Merced

Determining the Role of Sost and Sostdc1 During Fracture Healing

A dissertation submitted in partial satisfaction of the requirements for the degree Doctor of Philosophy

in

Quantitative Systems Biology

by

Cristal Sook Ngei Yee

Committee in charge:
Dr. Jennifer O. Manilay, Chair
Dr. Katrina K. Hoyer
Dr. Masashi Kitazawa
Dr. Gabriela G. Loots

2016

The Dissertation of Cristal Sook Ngei Yee is approved, and it is acceptable in quality and form for publication on microfilm and electronically:

Katrina K. Hoyer

Masashi Kitazawa

Gabriela G. Loots

Jennifer O. Manilay, Chair

Date

University of California, Merced
2016

Table of Contents

Signature Page iii
Table of Contents iv
List of Figures v
List of Tables vi
Acknowledgements vii
Curriculum Vita ix
Abstract xi
Chapter 1: Introduction 13
1.1 Overview of Fracture Repair 13
1.2 Overview of Diabetes & Bone 13
1.3 Insulin Treatment in TYpe 1 Diabetes Mellitus and Bone Fracture 14
1.4 High Glucose Environment & Bone 16
1.5 Current Osteoporosis Therapy 17
1.6 Type 1 Diabetic Mellitus Animal Models 19
1.7 Wnt Signaling Role in Bone & Fracture 21
1.8 Sost as a Wnt Antagonist & Sost Antibody 22
1.9 Sostdc1, a Paralog of Sost 23
1.10 Objective of Study and Hypothesis Tested 24
Chapter 2: Sclerostin Antibody Treatment Improves Fracture Outcomes in a Type I Diabetic Mouse Model 30
2.1 Introduction 30
2.2 Methods 32
2.3 Results 35
2.4 Discussion 39
Chapter 3: Akita Fracture Healing Characterization 58
3.1 Introduction 58
3.2 Materials and Methods 59
3.3 Results 60
3.4 Discussion 61
Chapter 4: *Sostdc1* Deficiency Accelerates Fracture Healing by Promoting the Expansion of Periosteal Mesenchymal Stem Cells 68
4.1 Introduction 68
4.2 Material and Methods 69
4.3 Results 72
4.4 Discussion 77
Chapter 5: Conclusion and Future Directions 94
References 97

List of Figures

Chapter 1: Introduction 13
Figure 1. Insulin Signaling. 25
Figure 2. Wnt Signaling. 27
Figure 3. Phenotype of Sclerosteosis and Van Buchem Patients. 29
Chapter 2: Sclerostin Antibody Treatment Improves Fracture Outcomes in a Type I Diabetic Mouse Model 30
Figure 1. SostAb treatment Improves Low Bone Mass in STZ mice. 44
Figure 2. Histology and MicroCT reveals SostAb Enhances Endochondral Healing. 46
Figure 3. SostAb Rescues Abnormal Osteoblast Maturation in STZ Observed by Immunofluorescence. 47
Figure 4. SostAb Anabolic Effect During Repair Continued After Treatment Termination. 49
Figure 5. Immunohistochemistry Reveals Altered Wnt Signaling in Treated Groups. 50
Figure 6. Histology Reveals Increased Adipogenesis in STZ mice that is Reversed with SostAb Treatment 52
Figure 7. Osteoclast Activity was Unchanged in Treated Groups. 53
Figure 8. Negative Antibody Control Stains Show No Evidence of Cross-reactivity or Non-specific Signal 54
Chapter 3: Akita Fracture Healing Characterization 58
Figure 1. Blood Glucose Levels of Akita Mice. 63
Figure 2 Akita Mice has Insignificant Changes Compared to Controls 64
Figure 3. Akita Mice Have Delayed Fracture Healing. 65
Chapter 4: *Sostdc1* Deficiency Accelerates Fracture Healing by Promoting the Expansion of Periosteal Mesenchymal Stem Cells 68
Figure 1. Histological Characterization of Early Time Points in Fracture Repair of Sostdc1-/- Mice. 80
Figure 2. Fracutre Healing Observed in Calluses of Sostdc1-/- Mice. 82
Figure 3. Stem Cells Co-localize with Sosdc1 During Fracture Healing. 83
Figure 4. Elevated Osteoblast Precursors During Fracture Repair in Sostdc1-/- Mice. 85
Figure 5. Quantification of Mesenchymal Stem Cells and Osteoblasts Population During Fracture Repair. 86
Figure 6. Elevated Beta-Catenin During Fracutre Repair in Sostdc1-/- Mice. 87
Figure 7. Micro-CT parameters for intact cortical bone in WT and Sostdc1-/- mice at 12 weeks of age. 88
Figure 8. Quantification of osteoclast development in WT and Sostdc1-/- mice 89
Figure 9. Histological characterization of LacZ expression [as a surrogate for Sostdc1 expression] in Sostdc1+/LacZ mice. 90
Figure 10. Histological characterization of LacZ expression [as a surrogate for Sostdc1 expression] in cartilage of Sostdc1+/LacZ mice. 91

List of Tables

Chapter 2: Sclerostin Antibody Treatment Improves Fracture Outcomes in a Type I Diabetic Mouse Model 30
Table 1. Bone Phenotyping Based on uCT Parameters in the Cancellous Bone Compartment of the L4 Vertebrae and Cortical Bone of uninjured 11-week old Male Mice Compared to Controls. 56
Table 2. Bone Phenotyping Based on uCT Parameters in the Cancellous Bone Compartment of the L4 Vertebrae and Cortcal Bone of uninjured 14-week old Male Mice Compared to Controls 56
Table 3. Bone Phenotyping Based on uCT Parameters in the Cancellous Bone Comparment of 21-day and 42-day fracture calluses of Male Mice Compared to Controls 57
Chapter 3: Akita Fracture Healing Characterization 58
Table 1. Blood Glucose Levels in Control and Akita Male Mice at 6 Weeks of Age 66
Table 2. Bone Phenotyping Based on Micro-CT Parameters data on Trabecular Bone Compartment of the Distal Femur Region and Cortical Bone of Uninjured 11 and 14 Week Old Akita Male Mice Compared to Controls 66
Table 3. Bone Phenotyping Based on Micro-CT Parameters in the Trabecular Bone Compartment of the L4 Vertebrae of Uninjured 11 and 14 Week old Akita Male Mice Compared to Controls 66
Table 4. Bone Phenotyping Based on Micro-CT Parameters in 21 and 42 days post fracture calluses of Akita Male Mice Compared to Controls 67
Chapter 4: *Sostdc1* Deficiency Accelerates Fracture Healing by Promoting the Expansion of Periosteal Mesenchymal Stem Cells 68
Table 1. Bone Phenotyping Based on uCT Parameters in the Cancellous Bone Compartment of the Distal Femur, L4 Vertebrae and Cortical Bone of 5.5-Month-Old Sostdc1$^{-/-}$ Mice Compared to WT Controls. 92
Table 2. Histomorphometric analysis of Periosteal and Endocortical region of 5.5 Month-Old Sostdc1$^{-/-}$ Femurs Compared to WT Controls. 92
Table 3. Biomechanical properties determined by uCT and Torsional Testing of the Mature Callus Compartment of Sostdc1$^{-/-}$ Mice Compared to WT Controls, at 28 Days Post-Fracture. 92
Table 4. Cell populations in the Femur during Fracture Repair in Sostdc1-/- Mice Compared to WT Controls. 93

Acknowledgements

I would like to thank my family, especially my parents and grandparents for their continuous support and patience. Without them, I would have never pushed myself in my capabilities within the science research field and in pursuing a higher education. My mother Elaine Lim-Yee has always been a positive role model in teaching me to always pursue my goals without hesitation. My father, Cy Ward Yee, who first introduced me to the world of science and biology. With our similar curiosity in science, you have lit the spark of fire that would become my goal in pursuing biology research. To my loving grandfather, Ernest Lim, and grandmother, Barbara Lim, who have always taught me respect and with that, I have found respect towards my friends, colleagues, and research. I would also like to thank my significant other, Matthew Richard Moy, for all the patience, love, and support, which is more than I could have ever ask for. Thank you for being encouraging, positive, and being with me during my graduate studies.

I like to give special thanks to Dr. Gabriela G. Loots for her investment in my growth as a graduate student and scientist in the field of bone biology. Her patience and encouragement has continuously pushed my limits as a student and scientist. Dr. Loots has been an important support system that has displayed professional grace and guidance and for that, I am glad I had the opportunity to have her as my mentor.

I have been very fortunate to have worked with the technicians, post-doctoral, and fellow graduate students in Dr. Loots lab. I would like to especially thank Dr. Nicole Collette, who have provided me technical support and scientific contributions in learning how to design an experiment and analyzed data. Your guidance and support have encouraged me to persist in my projects and always to stay positive. A special thanks to the Loots Lab technician, Deepa, who have provided assistance with the animal husbandry, genotyping, and technical assistance. My fellow colleagues, Jiun Chang and Aimy Sebastian, have also provided much support in believing me and encouraging me to persist in my graduate program. Other contributions I would like to thank is members of my committee: Dr. Jennifer O. Manilay, Dr. Masashi Kitazawa, and Dr. Katrina K. Hoyer for their support and advise.

The text of Chapter 2, *Sost Antibody Treatment Improves Fracture Outcomes in a Type I Diabetic Mouse Model* is a reprint of the material as it appears in *Bone* (Elsevier, 2016), published under the Creative Commons Attribution-NonCommercial-No Derivatives License (CC BY NC ND). The dissertation author was the first author of this material. The text of Chapter 4, *Sostdc1 Deficiency Accelerates Fracture Healing by Promoting the Expansion of Periosteal Mesenchymal Stem Cells* is a reprint of the material as it appears in *Bone* (Elsevier, 2016), published under the Creative Commons Attribution-NonCommercial-No Derivatives License (CC BY NC ND). The dissertation author was the second author of this material. Dr. Gabriela Loots, listed in these two publications as co-author, directed and supervised research which forms the basis for this dissertation.

The study in Chapter 2, *Sost Antibody Treatment Improves Fracture Outcomes in a Type I Diabetic Mouse Model* received funding from National Institutes of

HealthDK075730 and Laboratory-directed Research and Development Grant11-ERD-060. This work was conducted under the auspices of the United States Department of Energy by Lawrence Livermore National Laboratory (Contract #DE-AC52-07NA27344) (Manuscript release number LLNL-JRNL-666626)

In Chapter 4, *Sostdc1 Deficiency Accelerates Fracture Healing by Promoting the Expansion of Periosteal Mesenchymal Stem Cells*, I would like to thank the National Institutes of Health (NIH) Knock-Out Mouse Program (KOMP) and Regeneron for providing the *Sostdc1* knockout mice. The researchers on this study were supported in part by NIH grant DK075730 and LLNL LDRD ER (11-ERD-060). This work was performed under the auspices of the U.S. Department of Energy by Lawrence Livermore National Laboratory under Contract DE-AC52-07NA27344.

Curriculum Vita

2011-2016	Ph.D. Graduate Student, Quantitative Systems Biology, University of California, Merced
2007- 2011	Bachelor of Science, University of California, Merced
2012-2016	Teaching Assistant, School of Natural Science, University of California, Merced

Awards

Quantitative and Systems Biology Graduate Program 2016 Summer Research Fellowship
University of California, Merced

Quantitative and Systems Biology Graduate Program 2015 Summer Research Fellowship
University of California, Merced

ASBMR 2015 Young Investigator Travel Grant

Quantitative and Systems Biology Graduate Program 2013 Summer Research Fellowship
University of California, Merced

Publication

- **Cristal S. Yee**, LiQin Xie, Sarah Hatsell, Nicholas Hum, Deepa Murugesh, Aris N. Economides, Gabriela G. Loots, Nicole M. Collette, Sclerostin Antibody Improves Fracture Outcomes in a Type I Diabetic Mouse Model, *Bone* (2015)
- Nicole M. Collette, **Cristal S. Yee**, Deepa Murugesh, Aimy Sebastian, Leila Tahner, Nicholas W. Gale, Aris N. Economides, Richard M. Harland, and Gabriela G. Loots, Sost and its Paralog Sostdc1 coordinate digit number in a Gli3-dependent manner. *Developmental Biology* (2013)
- Nicole M. Collette, **Cristal S. Yee**, Nicholas R. Hum, Deepa K. Murugesh, Blaine A. Christiansen, LiQin Xie, Aris N. Economides, Jennifer O. Manilay, Alexander G. Robling, Gabriela G. Loots, Sostdc1 Deficiency Accelerates Fracture Healing by Promoting the Expansion of Periosteal Mesenchymal Stem Cells. *Bone* (2016)

Presentations

May 16, 2016	QSB Spring 2016 Retreat Poster Presentation University of California, Merced
March 5-8, 2016	Poster Presentation Orthopaedic Research Society (ORS) 2016 Annual Meeting

October 9-12, 2015	Oral Poster Presentation The American Society for Bone and Mineral Research (ASBMR) 2015 Annual Meeting
May 20, 2015	QSB Spring 2015 Retreat Poster Presentation University of California, Merced
March 28-32, 2015	Poster Presentation Orthopaedic Research Society (ORS) 2015 Annual Meeting
November 6, 2014	QSB Fall 2014 Retreat Oral Presentation University of California, Merced
September 12-15, 2014	Poster Presentation The American Society for Bone and Mineral Research (ASBMR) 2014 Annual Meeting

Abstract

Determining the Role of Sost and Sostdc1 During Fracture Healing

by

Cristal Sook Ngei Yee

Doctor of Philosophy

University of California, Merced, 2016

Dr. Gabriela G. Loots, Advisor
Dr. Jennifer O. Manilay, Chair
Dr. Masashi Kitazawa
Dr. Katrina K. Hoyer

The bone is a dynamic organ, often changing throughout the course of the human lifespan with its continuous remodeling, laying down new bone and resorbing old bone. With age, the bone becomes increasingly porous and mechanically unstable, leading to the development of osteoporosis in some individuals. Elderly patients with osteoporosis are at an increased risk of fracturing their bones which contributes to a higher mortality rate. Recent studies have revealed that type 1 diabetic mellitus (T1DM) patients also have an osteoporotic bone phenotype and impaired fracture healing, independent of age. Currently, there is a lack of available treatments that can improve impaired healing and directly enhance bone formation. Therefore, there is a great need for developing new therapies that can not only aid type 1 diabetic patients with osteoporosis to improve bone phenotype, but that could also aid patients with difficult or impaired fracture healing. In this thesis, I will be discussing the role of Wnt signaling and Sclerostin, a Wnt antagonist that negatively regulates bone formation, in the content of fracture repair.

Wnt signaling is involved during development and homeostasis in both mammals and non-mammals, revealing its conservative role throughout evolution [1]. In *Drosophila melanogaster* development, Wingless (wg), an orthologue of Wnt-1, is involved in segment polarity by restricting engrailed expression and forming parasegments. In *Caenorhabditis elegans*, Wnt signaling is involved in gut development by inducing endoderm-mesoderm precursor cells (EMS) division to endodermal (E) cells (gut lineage founder cells) and in body axis formation in *Xenopus laevis* development. Wnt signaling is also involved in bone formation as observed in both loss-of-function and gain-of-function of Sost, a Wnt antagonist, which results in either increased bone formation or decreased bone formation respectfully [2]. Sostdc1, a paralog of Sost, is also a Wnt antagonist that has been shown to regulate tooth development [3] and most recently to be expressed in the periosteum, a source of stem cells that is active upon fracture injury, suggesting that Sostdc1 may have a potential role during fracture repair. In this dissertation, we will also be discussing how Sostdc1 is involved during bone fracture repair and potential therapy applications.

Using a drug induced type 1 diabetic mouse, a model of impaired fracture healing, we will examine how Sost antibody treatment can improve both the osteoporosis phenotype as well as the impaired fracture healing in diabetic mice by enhancing bone formation. We will also briefly characterize another type 1 diabetic mouse model, the Akita mice, which carries a mutation in the insulin gene [4], to provide another potential diabetic mouse model to be used in fracture healing studies. Lastly, we will examine Sostdc1 role during fracture healing and reveal enhanced periosteum activity observed in Sostdc1 knockout mice.

Chapter 1: Introduction

1.1 Overview of Fracture Repair

Fracture repair recapitulates or mimics what occurs during embryonic bone development. There are two types of fracture repair, intramembranous, where mesenchymal stem cells differentiate into osteoblasts to form bone, and endochondral, where a cartilage template is formed prior to bone formation [5-7]. Once a bone fracture occurs, there are specific stages that occur during the healing and repair process. First, a hematoma forms where the body's immune responses localize to the site of injury and form a blot clot. Granulocytes and monocytes, followed later by lymphocytes localize to the site of injury to target foreign pathogens to clean-up the damage, begin repair, and release cytokines to recruit stem cells from the periosteum, bone marrow, and surrounding tissue to the site of injury [5-7].

In the next phase of fracture repair, stems cells recruited from surrounding sites of injury invade the fracture site where during endochondral bone formation, chondrogensis occurs to form a soft callus of cartilage template to provide stability and structural support. Osteoclasts then remove mineralized cartilage and angiogenesis occurs simultaneously, bringing osteochondral progenitor cells at the site of injury. As cartilage is removed, osteoblasts replaces cartilage with woven bone, which are highly unstable and unorganized trabecular bone being rapidly formed, to form a hard callus. During intramembranous bone formation, similar events occur. However recruited osteochondral progenitor cells differentiate directly into osteoblasts and woven bone is formed immediately instead of forming a cartilage template [5-7]. The final stage of healing, remodeling, occurs when woven bone is replaced with organized and structurally stable bone, thus replacing the initial broken cortical bone.

1.2 Overview of Diabetes & Bone

Insulin, a hormone secreted by beta cells in the islets of the pancreas, is required for trafficking glucose from the blood stream into the adjacent tissues and cells and functions to regulate blood glucose levels. In the absence of insulin, glucose cannot enter most cells leading to cellular starvation and apoptosis [8]. When individuals do not produce enough insulin they become hyperglycemic and develop diabetes mellitus (DM). There are two main types of diabetes mellitus (DM): 1. Type 1 diabetes mellitus (autoimmune-mediated loss of insulin) 2. Type 2 diabetes mellitus (insulin-resistance caused by a metabolic disorder).

Type 1 diabetes mellitus (T1DM) is an autoimmune disease where T cells attack the beta cells within the pancreas, leading to insulin deficiency and hyperglycemia [9]. T cells mature in the thymus, where autoreactive T cells are removed, to allow self-tolerance. Though some autoreactive T cells are not removed, autoreactive T cells are suppressed by regulatory T cells. Impaired removal of autoreactive T cells and defective regulatory T cells can contribute to diabetes mellitus. Those with T1DM are diagnosed at a young age, having to monitor their blood glucose levels frequently and are provided with insulin treatment [9].

Type 2 diabetes mellitus (T2DM) (insulin independent mellitus) occurs when cells no longer respond to insulin normally (insulin resistance) and/or when beta cells are not able to compensate or produce enough insulin (insulin deficient) and therefore leads to a hyperglycemic environment. This type of diabetes is often diagnosed in middle-aged

adults, however an increase in younger age patients have been recently diagnosed due to an increase in obesity in the USA. Both genetics and environmental factors are thought to contribute to the development of type 2 diabetes.

Patients with T1DM shows an osteoporotic phenotype [10], having structurally weaker bones which puts them at higher risk for fractures; in many cases most individuals are unaware they have osteoporosis until suffering a fracture [11]. T1DM patients not only have osteoporosis and increased fracture risk, but also display impaired fracture healing [6, 12]. Similar to what is observed in T1DM humans, diabetic mice also develop an osteoporotic phenotype and delay fracture healing [13]. The osteoporotic phenotype in T1DM mice is due to decreased osteoblast activity [14], though some studies have also reported an elevated osteoclast activity [15, 16]. Diabetic mice show increasing bone loss beginning from the onset of diabetes [17] and children with early manifestation of diabetes may be at a higher risk for developing decreased cortical bone mineral density [18], indicating that the duration of diabetes may lead to the increase progression of bone loss and fracture risk later in adulthood.

Impaired or delayed fracture repair, observed in diabetic patients can be due to alterations during early stages of healing and/or during endochondral bone formation [19]. Previous studies observed an up-regulation of the levels of pro-inflammatory cytokine tumor necrosis factor alpha (TNF-alpha), and the osteoclast activity on chondrocytes during inflammation stage of fracture repair in diabetic mice [20]. The combination of elevated inflammation response and enhanced osteoclast activity may result in delayed chondrogenesis and maturation, angiogenesis, and elevated cartilage resorption [21] [19]. During the transition from cartilage to bone formation, enhanced cartilage resorption and decreased osteoblast activity can also lead to immature callus formation, contributing to delayed bridging and healing [22]. Due to their osteoporotic bone phenotype and impaired fracture healing, T1DM mice are an ideal model for evaluating potential therapeutic treatments for both osteoporosis and difficult to heal fractures.

Patients with T2DM have either a low bone mass, normal, or high bone mass phenotype, however independent of their bone parameters, they still have an increased fracture risk possibly contributed by one of more of the associated symptoms: retinopathy (visual impairment), muscle weakness, neuropathy (motor dysfunction, poor balance), and increased body weight (obesity). Increased fracture risk observed in T2DM patients suggests mechanically weak bone regardless of a high bone mass phenotype. Unstable bone in T2DM patients is primarily due to decreased osteoblasts and enhanced osteoclasts activity, although conflicting osteoclasts activity have been observed in rodents, possibly due to variation within species dependent or strain dependent T2DM models [15]. In addition to increased fracture risk, T2DM patients also have impaired fracture healing, however the mechanism may be different from T1DM patients as well as within T2DM patients due to variations in bone mass parameters. Variation of bone phenotypes in T2DM patients indicate that glucose levels and bone mineral density are not correlated, though this will not be discussed in this thesis.

1.3 Insulin Treatment in Type 1 Diabetes Mellitus and Bone Fracture

Many T1DM patients are administered insulin as a form of treatment to regulate their blood glucose levels. Unregulated blood glucose levels may lead to extreme high

or low levels which may result in coma or even death. Therefore, maintaining normal blood glucose levels may not only have contributing health benefits on glucose metabolism but may also have benefits on bone metabolism since the onset of diabetes is negatively correlated with bone loss and fracture risk in humans and rodents.

Insulin signaling involves insulin or insulin like growth factors (IGF) binding to either insulin receptors I and II or IGF-I/IGF-II receptors. Upon activation, ATP is recruited and auto-phosphorylation of the receptors occurs, which leads to a downstream signaling cascade and phosphorylation of other proteins to active other pathways [23]. One of the other downstream effects is to recruit glucose transporter (GLUT4) to the lipid membrane and facilitate in transporting glucose inside the cell. These receptors reside on the cell surface as a homodimer or heterodimer and auto-phosphorylate upon activation. Insulin receptors serve to regulate glucose levels by decreasing glucose *via* enhancing glycolysis, glycogen synthesis and amino acid uptake.

Insulin signaling activates phosphinositide-3-kinase/AKT/IKK and RAS/mitogen-activated protein (MAP) kinase (Fig. 1) [24, 25]. In the first downstream cascade (Fig. 1A), insulin receptor substrate 1 (IRS-1) and IRS-2 activates phosphatidylinositide-3-kinase (PI3K), which converts phosphatidylinositol 4,5-bisphosphate (PIP2) into phosphatidylinositol 3,4,5-trispohsphate (PIP3) and activate 3-phosphoinositide-dependent protein kinase 1 (PDK1) to recruit and activate Akt (also known as protein kinase B). Akt activation then leads to phosphorylation of various substrates and downstream factors, one of which is the deactivation of transcription factor, FOXO1, or glycogen synthase kinase 3 beta (GSK3 beta) via phosphorylation.

The second downstream cascade, RAS/mitogen-activated protein (MAP) kinase, involves activation of Ras, which leads to a signaling cascade activating MAP kinases (Fig.1 B). Upon insulin signaling, activated IRS or Src homology 2 domain containing (SHC) activates growth factor receptor bound protein 2 (GRB2), which binds to son of sevenless (SOS) and activate RAS. Activated Ras then initiates activation on the Raf-MEK-ERK pathway. This signaling cascade results in the activation of extracellular signal regulated kinase (ERK), which has multiple downstream target effects that is involved in cell proliferation, differentiation, gene expression regulation, as well as inhibiting FOXO1 via phosphorylation. Effects of phosphorylation of FOXO by ERK is still not well understood, therefore this will not be discussed in further detail.

The transcription factor FOXO is involved in regulating gluconeogenesis, cell cycle arrest, apoptosis as well as encouraging inflammation response [26]. Activated FOXO has multiple downstream effects, one which is promoting pro-apoptotic proteins to release cytochrome c from the mitochondria to activate caspase 9, leading to activated caspase 3 promoting cell apoptosis. Some other downstream effects of activated FOXO include promoting cell cycle arrest by targeting cell cycle inhibitors that represses cell cycle checkpoints [27], enhancing inflammatory genes expression, as well as cross-talking with Wnt signaling by preventing beta-catenin to interact with T cell factor/lymphoid enhancer factor (TCF1/LEF) transcription factor [28].

Upon insulin signaling, activated PI3K activates PDK1 which leads to Akt dependent phosphorylation and inhibition of FOXO and inhibiting FOXO (Fig.1 A). In the context of bone metabolism, deactivated FOXO would allow beta-catenin to interact with TCF1/LEF transcription factors and thus promote bone formation. For a type 1 diabetic patient with the lack of insulin, insulin signaling inactivation would result in FOXO activation and elevated inflammation, since FOXO allows expression of pro-inflammatory genes [26]. Elevated FOXO1 activity in chondrocytes was observed during impaired fracture healing in diabetic rodents, suggesting an enhanced inflammatory response and osteoclastogenesis [29]. FOXO1 may also regulate tumor necrosis factor (TNF alpha), which encourages cell death and inflammatory cytokines [30]. Therefore, elevated FOXO during fracture healing in diabetic patients may result in elevated inflammation, osteoclast activity, and chondrocyte apoptosis, possibly contributing to impaired healing.

Insulin knockout mice show no obvious developmental phenotypes but develop diabetes and die within 2 to 3 days of birth [31], while insulin receptor knockout mice are also postnatal lethal [31, 32] making it difficult to understand insulin's role in bone metabolism. However, insulin has been suggested to be a bone anabolic agent [33] and does improve the low bone mass phenotype and fracture repair in both T1DM humans and rodents [34]. Insulin administration during fracture repair has also shown to enhance healing via elevated osteogenesis in type 1 diabetic rats [34]. Insulin treatment during fracture repair in type 1 diabetic rats may be due to normalizing blood glucose rather than the signaling properties of insulin itself. This suggests that insulin is an indirect anabolic bone response, however the response is dependent on how well blood glucose is controlled since fracture healing in poorly control glucose diabetic rats is not significantly different than untreated diabetic rats [35]. Even though insulin treatment improves low bone parameters to a degree, this may not be mechanically stable as revealed in type 1 diabetic mellitus drug induced mice treated with insulin showing improved bone parameters, however were still mechanically weak [36]. This suggests that the high glucose environment may be a more contributing influence to the low bone mass phenotype more so than the low insulin levels.

Osteoporosis phenotype in T1DM mice reveals a decrease in osteoblast activity, suggesting that osteoblasts cells may be altered. Mice with insulin receptor knockout in osteoblasts are insulin resistant, hyperglycemic, and have a low bone mass phenotype due to decreased number of osteoblasts and activity [37]. This suggests that insulin treatment may not be an effective treatment strategy for impaired healing if insulin receptors are altered in osteoblasts.

1.4 High Glucose Environment & Bone

Both T1DM and T2DM patients suffer from a hyperglycemic environment, which can directly and indirectly influence osteoblasts and osteoclasts differentiation and activity [15]. Various effects due to hyperglycemia indirectly influence bone remodeling and structurally stability, such as an increased advanced glycation end products (AGE), often observed in T2DM patients and worsens as the disease progresses. AGEs occur when cross-linked products are formed by non-enzymatic reactions between glucose and proteins, also called non-enzymatic glycosylation of proteins [15]. Elevated amounts of AGEs can be detrimental since the covalent bonds between protein/lipids with glucose can inhibit proteins' normal functions. In the aspect of bone, elevated AGE

can disrupt bone collagen quality and structure within the bone matrix by interfering with normal hydroxyapatite crystals from binding to collagen matrix to provide mechanical strength, resulting in a bone structure that is more stiff and more likely susceptible to fracture risks [38, 39]. Increasing amount of AGEs can also have a detrimental effect on osteoblast by enhancing apoptosis and thus limiting osteoblast activity [40], as well as increasing osteoclast activity [41].

Increased AGEs can also create free radicals and oxidative stress, which can contribute to DNA damage and cell death. Diabetic mice display elevated levels of oxidation [deoxyguanosine, 8-hydroxydeoxyguanosine (8-OHdG)] within urinary samples and bone tissue [42]. Oxidative stress have also been shown to decrease osteoblast activity and differentiation [43] and increase osteoclast activity [44]. For example, hyperglycemia environment can influence osteoblast differentiation towards adipose differentiation via upregulating levels of peroxisome proliferator activated receptor-gamma (PPAR-gamma). Adipocytes and osteoblasts are derived from the same bone marrow stromal cells [45], thus under hyperglycemic environment, adipocyte differentiation is favored at the expense of osteoblast differentiation, as observed in T1DM humans and mice [15]. This may also be a contributing factor to the low bone mass phenotype associated with T1DM [15, 46]. The high glucose environment not only can influence osteoblast but can also alter osteoclast maturation and activity.

In T1DM patients, increased osteoclast activity [15] and decreased osteoclast activity [47] have been reported, revealing variability within the population possibly due to age and/or sex. Similarly, diabetic rodents also show a wide response range of decreased [48], increased [49], or normal osteoclast activity [50] possibly due to differences in diabetic model used. For example, previous reports using Streptozotocin (STZ), a drug induced diabetic model, have shown either elevated [49, 51], unaltered [46, 50], or decreased osteoclast activity [42]. The wide variation of osteoclast activity observed in diabetic rodents is due to the method of STZ administration used, since a single high dose or multiple low doses both results in hyperglycemia. In contrast, naturally developing diabetic mice models, the Akita mice [52] and non-obese diabetic (NOD) mice [46], show no changes in osteoclast activity. This indicates that different diabetic rodent models may serve as a representative of a subpopulation of T1DM patients for evaluating drug treatment studies. Altered osteoclast activity can be detrimental for bone repair since increased osteoclast activity may remove cartilage prematurely resulting in smaller callus size and impaired cartilage to bone transition [20, 49]. In contrasts, decreased osteoclast activity can also impair fracture repair since osteoclasts is valuable for removing damaged bone. Thus, decreased osteoclast activity may insufficiently remove damage bone and result in decreased bone turnover [15]. Therefore, alterations in osteoblast and/or osteoclast differentiation and activity due to a hyperglycemic environment may also be a contributing factor in low bone turnover and bone repair in diabetic mice.

1.5 Current Osteoporosis Therapy

Currently, several FDA approved drugs are prescribed to individuals suffering from osteoporosis, which are to either inhibit bone resorption or enhance bone formation. Bisphosphonates aim to inhibit bone resorption while only one treatment, parathyroid hormone, aims to enhance bone formation [53].

Bisphosphonates are analogues to pyrophosphate (PPi), and bind to hydroxyapatite crystals in the bone to inhibit osteoclast activity or reduce catabolic activity [54]. This treatment is used to decrease bone resorption and reduce fracture risk. While this treatment is highly effective for stopping bone loss, it does not benefit individuals who suffer from severe osteoporosis, since it lacks the ability to build bone *de novo*. Treatment with bisphosphonates does not directly enhance bone formation, since bisphosphonates dampens osteoclast activity, therefore allowing bone loss to continue if bone formation is also impaired. Since osteoporosis in T1DM mice is due to decreased osteoblast activity [13], bisphosphonates are an unlikely effective treatment for T1DM. In addition, bisphosphonate inhibits normal bone turnover and can delay bone repair [55].

Parathyroid hormone (PTH) is approved for clinical use for the treatment of osteoporosis. It is administered subcutaneously daily for severe osteoporotic patients for a maximum of two years due to increased risk of developing osteosarcoma (bone cancer), a risk found in long-term rat studies [56]. Unfortunately, the human response to PTH treatment is not universal and some patients have shown a bone catabolic effect (enhanced resorption) if too much PTH is administered or when treatment is stopped [57]. Enhanced osteoclast activity is also observed in constituently active PTH in osteocytes, in mice [58]. PTH targets osteoblast function to induce bone formation *via* the PTH type 1 receptor (PTH1R) which results in decreased *Sost* expression, increased WNT signaling, and increased bone formation, in wildtype mice [59]. PTH represses expression of Sost by inhibiting MEF2C transcription factor from binding to a distal enhancer region that transcribes Sost gene. T1DM patients have increased levels of both SOST and PTH even upon insulin treatment, suggesting that PTH-dependent down-regulation of *Sost* expression is impaired in T1DM [60]. In addition, STZ mice revealed decreased *PTH1R* osteoblast expression [61], suggesting that even with PTH treatment, T1DM patients would not benefit, due to impaired osteoblast response to PTH. A previous study using both PTH and bisphosphonates treatment on osteoporotic patients has also revealed a blunt response [62], confirming that another treatment is needed for treating osteoporosis in diabetic patients.

Although fracture healing in a T2DM setting is not discussed, medication commonly administered for T2DM may also contribute to fracture risk and bone fragility. For example, the use of thiazolidinediones (TZDs), which functions to lower blood glucose levels and improve insulin sensitivity via increasing the peroxisome proliferator activated receptor-gamma (PPAR-gamma) can be detrimental to bone. Increased PPAR-gamma, a gene transcription factor in adipocytes, can decrease bone turnover by inhibiting osteoblast differentiation in favor of mesenchymal stem cells differentiating into adipocyte cell fate. Alteration in favoring adipocyte cell fate and increase AGE's can result in decreased bone mineralization [63]. Since T2DM patients already have shown to have impaired fracture healing, those on TZD treatment may examine exacerbated impaired healing due to the effects from TZD treatment .

Thus, currently there are no available therapies for treating T1DM osteoporosis. Since we have a very elementary understanding of why fracture healing is delayed in diabetes, it is imperative to develop a new treatment for improving fracture healing in T1DM, which may also be globally beneficial for other situations where bones fractures fail to heal properly.

1.6 Type 1 Diabetic Mellitus Animal Models

Diabetic mice models are useful for studying fractures since mice are genetically similar to humans, have a shorter healing repair process, and are in large cohorts, which is useful for replication and reproducibility.

There are two main types of diabetic mellitus animal model: a drug induced diabetic mouse model and a naturally developing diabetes mouse model. The choice of drug induced or naturally developing diabetic model is often due to what is being studied. Naturally developing diabetes mouse models are used for studying autoimmune therapies and transplantation studies [64]. Inducible diabetes is ideal for observing drug or therapy effects and transplantation therapies, or where the primary focus is to lower hyperglycemia, such as a new insulin treatment in managing blood glucose levels [64].

The most common drug induced diabetic model uses alloxan or streptozotocin. Streptozotocin (STZ) (2-deoxy-2-(3-(methyl-3-nitrosoureido)-D-glucopyranose) is a nitrosourea compound that targets beta cells by entering *via* the glucose transporter, GLUT2, and is a widely used drug for inducing T1DM by inducing stress and DNA alkylation (cleaving) leading to cellular apoptosis [65, 66]. STZ can either be administered intraperiotoneally at a low dose (40-60 mg/g in 0.1M citrate buffer) continuously for 5 days or at a single high dosage (100-200 mg/kg), though the osteoporosis phenotype is dosage dependent [64]. High dose of STZ in rats is also toxic to T cells, inducing immunosuppression and making this an ideal model for transplantation studies [67]. STZ is predominately used to induce T1DM, however this can also be used induce T2DM in rats by administrating a single high dose of STZ (100 mg/kg) intraperiotoneally or intravenously to neonates. Neonates develop hyperglycemia 2 days post injection and maintain hyperglycemia after 6 weeks of age, revealing STZ as a multi-purpose drug model for diabetic studies [64].

Alloxan (2,4,5,6-tetraoxypyrimidine; 5,6-dioxyuracil) also enters the beta cells via glucose transporter (GLUT2) and induces oxidative stress via reactive oxygen species (ROS) that leads to cellular apoptosis similar to STZ. Both STZ and alloxan are similar in structure to glucose, thus these drugs are often administered in fasted animals to avoid competition with glucose [64]. Other tissues that express GLUT2, such as the liver and kidney, may also be vulnerable to STZ and alloxan effects, indicating a potential adverse or off target effects upon administering diabetic inducible drugs [68].

A well-known naturally developed diabetic mice models is the non-obese diabetic (NOD) mice. Non-obese diabetic (NOD) mice are a widely use model for studying T1DM and are useful for studying pharmaceutical studies since these mice spontaneously develop diabetes due to an autoimmune response, similar to humans. A disadvantage is that diabetes incidence varies between sexes and occurs at a low frequency, with only 30% of males developing diabetes by 30 weeks of age [64] [69]. Once diabetes become too severe, insulin treatment is required for these mice to prevent complications of diabetes and death. Due to the low frequency rate of NOD males developing diabetes and the non-synchronous onset of diabetes, this may lead to a wide range of responses, especially since the effects on bone proceeds to worsens due to the length time of hyperglycemia [17]. Both STZ mice and NOD mice have significant weight loss, hyperglycemia, and elevated adipocytes within the bone marrow, with NOD mice displaying a more severe phenotype than STZ mice. Bone loss in both trabecular and

cortical bone, decreased osteoblast activity and unaltered osteoclast activity are observed in STZ and NOD mice, supporting the conclusion that the STZ model is a comparable model to NOD for T1DM [46] [46].

Another common naturally developing diabetic model is the BB Wister rat, which is a model for juvenile T1DM, where an autoimmune response leads to the destruction of beta cells within the pancreas. These rats develop diabetes at 8-16 weeks of age with a 90% incidence in males and females [64]. After 7 days of glycosuria onset, all the beta cells are destroyed and death occurs at 5-10 days if untreated with insulin. BB rats have lymphopenia that is not observed in humans, and therefore may not accurately model diabetes in patients [70].

T1DM is due to a decrease in insulin secretion by beta cells within the pancreas and thus leads to hyperglycemia. Another T1DM model is the pancreas injury model, where the pancreas is surgically removed (pancreatectomy) or partial removal. Animals with pancreas injury are often used in studying beta cell regeneration. However, the pancreas injury model is an invasive surgery that is often done on larger animals, such as rats, rather than smaller animals, such as mice [64].

A naturally developing diabetic mouse model that hasn't been widely used is the Akita ($Ins2^{+/-}$) mice. Akita ($Ins2^{+/-}$; also known as MODY) mice have a mutation in the insulin 2 gene where alanine is replaced by guanine at nucleotide 1907, leading to a change in amino acid from cysteine to tyrosine at position 96, that causes misfolding of the insulin protein and prevents secretion. Upon prevention of insulin section, the beta cells undergo stress resulting in cellular apoptosis. Heterozygous mice spontaneously develop diabetes due to this dominant inheritance in both females and males at 4-5 weeks of age, while homozygous mice are post-neonatal lethal, rarely surviving more than 12 weeks of age [4]. Within each litter, the degree of hyperglycemia varies, thus this may alter a wide range of responses within a study. However, the advantage in using this diabetic mouse model is that the onset of diabetes occurs around the same time, serving as another diabetic model if the length of diabetes is considered, and are insulin sensitive, serving as a model for transplantation studies [71]. Additionally, since drug induced diabetic models, such as STZ, may have off target effects that may not accurately mimic T1DM in humans, Akita mice may serve as a preferred model that depicts diabetes and its systemic effects.

Both STZ and Akita mice have significant weight loss, hyperglycemia, low bone mass, increased adipocytes, and decreased osteoblast activity [52]. However, a previous study comparing the subtle differences between the two diabetic mice models revealed that STZ have a more severe bone loss phenotype that varies according to dosage, while the Akita have a milder low bone mass phenotype [52]. This suggests the possibility of having inaccurate data interpretation due to dosage dependent off target effects of STZ. Therefore, the advantage of using the Akita mouse model is that the onset of diabetes occurs around the same age, eliminating the wide response differences due to the length of onset diabetes, and may be a more representative of a similar human diabetic phenotype compared to STZ.

1.7 Wnt Signaling Role in Bone & Fracture

WNTs are secreted glycoproteins that are involved in embryonic and skeletal development. In canonical Wnt signaling, Wnt proteins bind to intracellular receptors, Frizzled (FZD) G-protein coupled receptors and low density lipoprotein receptor-related protein (LRP) LRP5 and 6 co-receptors (Fig. 2) [72]. Upon activation of Wnt signaling, this leads to a downstream cascade where Dishevelled (Dvl) inhibits the destruction complex, which consists of Axin, adenomatous polyposis coli (APC), and glycogen synthase kinase 3 beta (GSK-3 beta), from phosphorylating beta-catenin for ubiqutination by proteasomes. Accumulated stabilized beta-catenin in the cytoplasm is then translocated into the nucleus where it interacts with lymphoid enhancer-binding factor 1/T cell-specific transcription factor (LEF-1/TCF) to activate transcription of Wnt target genes, some of which are necessary for up-regulating osteoblast function and increasing bone formation [73, 74].

During fracture repair, Wnt signaling occurs during specific stages as observed in a reporter mice, where a LacZ gene under a c-Fos promoter is placed downstream of the T-cell factor (TCF) binding motif [75] [76]. Upon activation of beta-catenin dependent Wnt signaling, LacZ activity is transcribed and reveals where Wnt signaling is expressed during fracture healing. LacZ signal is apparent at 9 days post fracture in chondrocytes and osteoblasts while at 14 days post facture, LacZ is expressed in osteoblasts along the periosteum and woven bone. During the remodeling stage, 35 days post fracture, LacZ signal is predominately in osteoblasts located in the periosteum, revealing that Wnt signaling is involved throughout all stages of facture repair [75]. Stabilized beta-catenin in osteoblasts (collage type 1 promoter) reveals enhanced healing with increased bone formation, larger callus, and an absence of chondrogenesis during early fracture stage. In contrast, mice with null beta-catenin in osteoblast specific cells showed persistent cartilage and decrease bone formation at the site of injury, suggesting that altering canonical Wnt signaling during fracture repair may enhance healing [75].

Altering canonical Wnt signaling results in altered bone formation as observed in LRP5 co-receptor knockout mice having a low bone mass phenotype [77]. Co-receptor LRP6 knockout mice are embryonic lethal. However, heterozygous mice with one null LRP6 allele display an osteopaenia phenotype with decreased osteoblasts and elevated osteoblast apoptosis [78]. Wnt antagonist functions to inhibit Wnt binding to FZD receptor has been shown to negatively regulate bone formation. Some Wnt antagonists, such as secreted frizzled-related proteins (sFRPs), Cereberus, and Wnt inhibitory factor 1 (WIF-1), antagonize Wnt signaling by binding to Wnt proteins, while Dickkopf-related protein 1 (DKK1), Sclerostin (Sost), and Sostdc1 (Wise, Ectodin) binds to LRP 5/6 co-receptors. Overexpression of sFRPs [79], DKK1 [80], and Sost [81] results in an osteoporotic bone phenotype while null expression of Sost results in a high bone mass phenotype [82], suggesting that upregulation of Wnt signaling may enhance fracture healing.

Diabetic mice have altered Wnt signaling that results in decrease osteoblastogenesis [50] that may contribute to an osteoporotic phenotype and impaired fracture healing, suggesting that diabetic patients may also display altered Wnt signaling, though currently there is no studies to confirm this. As previously mentioned, the absence of insulin in insulin signaling can lead to elevated activated FOXO to translocate to the nucleus and bind to beta-catenin, preventing beta-catenin from binding

to LEF1/TCF transcription factors to modulate the transcription of genes involved in bone formation [26]. This reveals a possible contributing factor during impaired fracture healing in diabetes in which Wnt signaling is altered and leads to inhibited osteoblast activity as observed in decreased bone formation and delay bridging in T1DM mice [50].

1.8 Sost as a Wnt Antagonist & Sost Antibody

The Sclerostin (*SOST)* gene is located on human chromosome 17q12-q21, where its expression is regulated by myocyte enhancer factor 2 (MEF2C) transcription factor, which binds to the distal enhancer ECR5 in the 52kb noncoding region [83]. The Sost protein is a potent WNT antagonist secreted by osteocytes that normally functions to inhibit bone formation in osteoblasts by inhibiting WNT signaling through binding to the LRP5/6 co-receptors [72] [84] [74] with a preference in binding to LRP6 over LRP5 [85]. However, recently it has been discovered that Sost binds to the LRP4 co-receptor as well [86]. Normally, when Sost binds to the Wnt co-receptors (LRP 5, 6, 4), Sost gets internalized via the Clathrin dependent pathway and degraded in a proteasome manner [85].

In humans, the lack of SOST causes sclerosteosis, a generalized skeletal hyperostosis disorder that results from hyperactive WNT signaling/osteoblast activity [87]. Patients with sclerosteosis have a high bone mass phenotype that is structurally stronger and less likely to break, syndactyly of the fingers (digits 2 and 3), radial deviation, and abnormal nail development (Fig. 3, E). Similar to sclerosteosis, patients with van Buchem disease also display a high bone mass phenotype due to a deletion of a 52kb non-coding Sost enhancer region (ECR5) located 35 kb downstream of the Sost gene (Fig. 3, A) [88]. Van Buchem patients are often identified as having facial distortion along with facial palsy, deafness, and intracranial pressure, while high bone phenotype in sclerosteosis patients is more severe and often displays abnormal phalanges (Fig. 3). Consistent with the human *SOST* null phenotype, the high bone mass phenotype is recapitulated in *Sost* knockout mice ($Sost^{-/-}$) with 3-4 times more bone mineral density (BMD) [89]. In contrast, transgenic mice with elevated levels of human SOST develop osteopenia [81] and limb defects [90]. Additionally, removal of *Sost* in mice has been shown to enhance repair in a femoral fracture study [91], suggesting a potential therapy for treating impaired fracture healing.

SOST antibodies have been shown to increase bone formation, bone mass and strength in cynomolgus monkeys in a dose dependent manner [92]. In another study, murine Sost antibodies increase bone mineral density (BMD) in ovariectomized rats, and decrease fracture risk [93], revealing that SOST antibody may also be beneficial for those with osteoporosis. Sost antibody treatment on T2DM rats with a low bone mass phenotype has also revealed increased bone formation, however this effect has not been examined in T1DM mice [94]. Sost antibody have also shown an anabolic effect in fracture healing with enhanced bone formation and is mechanically stable [95]. Due to the positive effects of Sost antibody treatment on fracture healing [96], this may be the ideal treatment for impaired fracture in diabetic patients, as well as possibly serving a protective role against fracture risk for T1DM patients with osteoporosis.

Most often, osteoporotic patients are treated with bisphosphonates, to reduce osteoclast activity. As previously mentioned, the combination of PTH and bisphosphonates results in a blunted response [62]. This begs the question of whether

Sost antibody treatment in combination of bisphosphonate treatment would also result in a blunted response. A previous study has revealed that bisphosphonate pre-treatment or in combination with Sost antibody caused an increase in bone formation and strength just as effective with Sost antibody alone in ovariectomized rats [97], revealing that Sost antibody anabolic effect has no interference with bisphosphonate pre-treatment or in combination.

Sost antibody treatment compared to intermittent PTH treatment on rats revealed that Sost antibody have enhanced bone formation and strength in both cortical and trabecular bone (a systemic effect) in contrasts to PTH, which predominately enhanced bone formation in the trabecular bone [98]. Combining Sost and PTH would not be beneficial as a bone anabolic factor since PTH treatment is blunted in Sost knockout ($Sost^{-/-}$) mice, suggesting that Sost antibody treatment with PTH may not result in a greater anabolic response than with Sost antibody alone for impaired fracture healing [81].

Sost antibody also has a long presence within the circulating blood with a biphase half-life of 11-18 days and 6-7 days in humans that were administered a single dose of Sost antibody [99]. In addition, Sost antibody was still detected a month after the last Sost antibody administration in cynomologous monkeys, suggesting a potential long lasting effect post administration [100]. SOST antibody treatment on healthy men and postmenopausal women showed positive increased bone formation with no significant off target effects in phase 1 and 2 clinical trials, and is currently in phase 3 of clinical trials [101].

1.9 Sostdc1, a Paralog of Sost

Sostdc1, also known as *Wise*, *Ectodine*, *USAG1*, is located on human chromosome 7 and is a paralog of Sost with 55% protein sequence similarity to Sost. While Sost is a Wnt antagonist, Sostdc1 has been described as both a BMP and a Wnt antagonist. Sostdc1 is involved in tooth development as observed in Sostdc1 knockout mice with supernumerary incisors and fused molars [102] [103].

Since Sostdc1 is a paralog of Sost, there may be some functional redundancy. However, Sost knockout mice and Sostdc1 knockout mice, where a LacZ reporter gene replaces the entire Sost open reading frame or exon 1 and part of the intron in Sostdc1 locus, reveals Sost and Sostdc1 to be in non-overlapping expression patterns within the developing limb bud and skeletal organ, suggesting different roles involved in skeletal development [104]. The *Sost* knockout mice with LacZ reporter gene reveals Sost to be expressed predominately in osteocytes in both axial and appendicular skeleton, but also in osteoblasts, osteoclasts, articular cartilage, and aorta branches of the heart. LacZ reporter gene in Sostdc1 knockout mice showed *Sostdc1* to be expressed in the skin, hair follicles, pancreas, kidney, lungs, skeletal muscle, vasculature, teeth, and periosteum.

How the bone marrow and surrounding tissue of bone, which includes bone, fibrous tissue, and vasculature, communicate and are involved during fracture repair is not fully understood. Sostdc1 has been shown to be expressed in the periosteum shows a potential role of Sostdc1 involved during fracture repair. The periosteum, the tissue

between bone and surrounding tissue, is a reservoir of stem cells and progenitor cells involved in bone repair. Upon injury, stem cells from the periosteum migrate to the site of injury where chondrogenesis begins, initiating endochondral bone formation. Removal of the periosteum results in decreased bridging at the site of injury, emphasizing the important role of stem cells from the periosteum during healing [105]. Sostdc1 role in the periosteum during fracture repair will provide insight towards how the periosteum changes and communicates with local bone tissue will be discussed in this thesis.

1.10 Objective of Study and Hypothesis Tested:

Wnt signaling involvement in regulating bone formation has uncovered our understanding in how molecular changes can alter bone metabolism. However, altering Wnt signaling via changes in Wnt antagonists and how this regulates bone metabolism is not fully understood in fracture healing. The objective of my dissertation is to understand Sost and Sostdc1 contribution during fracture repair and to determine if the Akita mice can be another model for bone and impaired fracture repair studies.

In this dissertation, I aimed to study the role of Sost and Sostdc1 during fracture healing by completing the following objectives:

1. *Study the effects of Sost antibody treatment in diabetic mice during fracture healing.* I hypothesize that Sost antibody treatment will improve impaired fracture healing in diabetic mice by enhancing bone formation. I tested this by inducing a mid-femur fracture on diabetic mice, which were treated with Sost antibody twice per week. Fracture calluses were examined during endochondral and remodeling phases for fracture repair. These results are discussed in Chapter 2.
2. *Characterize fracture healing in Akita mice as another diabetic model for fracture healing studies.* I aimed to examine the bone phenotype and fracture healing in Akita mice, which I tested by analyzing bone parameters on uninjured and fracture calluses of Akita. These results are discussed in Chapter 3.
3. *Determine if Sostdc1$^{-/-}$ mice have altered fracture healing.* I tested this by examining fracture calluses throughout the complete stages of healing. Bone parameters were analyzed on uninjured and fracture callus as well as some mechanical testing on mature fracture calluses. These results are discussed in Chapter 4.

Figure 1: Insulin Signaling. A) During insulin binding to its receptors, autophosphorylation of the receptors lead to activation of IRS1/2 and PI3K. Activated PI3K converts PIP2 into PIP3 and activate PDK, which activates Akt. Akt activation then leads to phosphorylation of various substrates and downstream factors, such as inhibiting GSK-3 beta, aid in the recruitment of GLUT4 to allow glucose transport (not shown), and inhibiting FOXO. B) Upon insulin inactivation, activated IRS or SHC (not shown) activate GRB2, which binds to SOS to activate RAS. Activated RAS initiates the Raf-MEK-ERK pathway, resulting in activated ERK. ERK activation is involved in multiple downstream effects, one of which is inhibiting FOXO via phosphorylation.

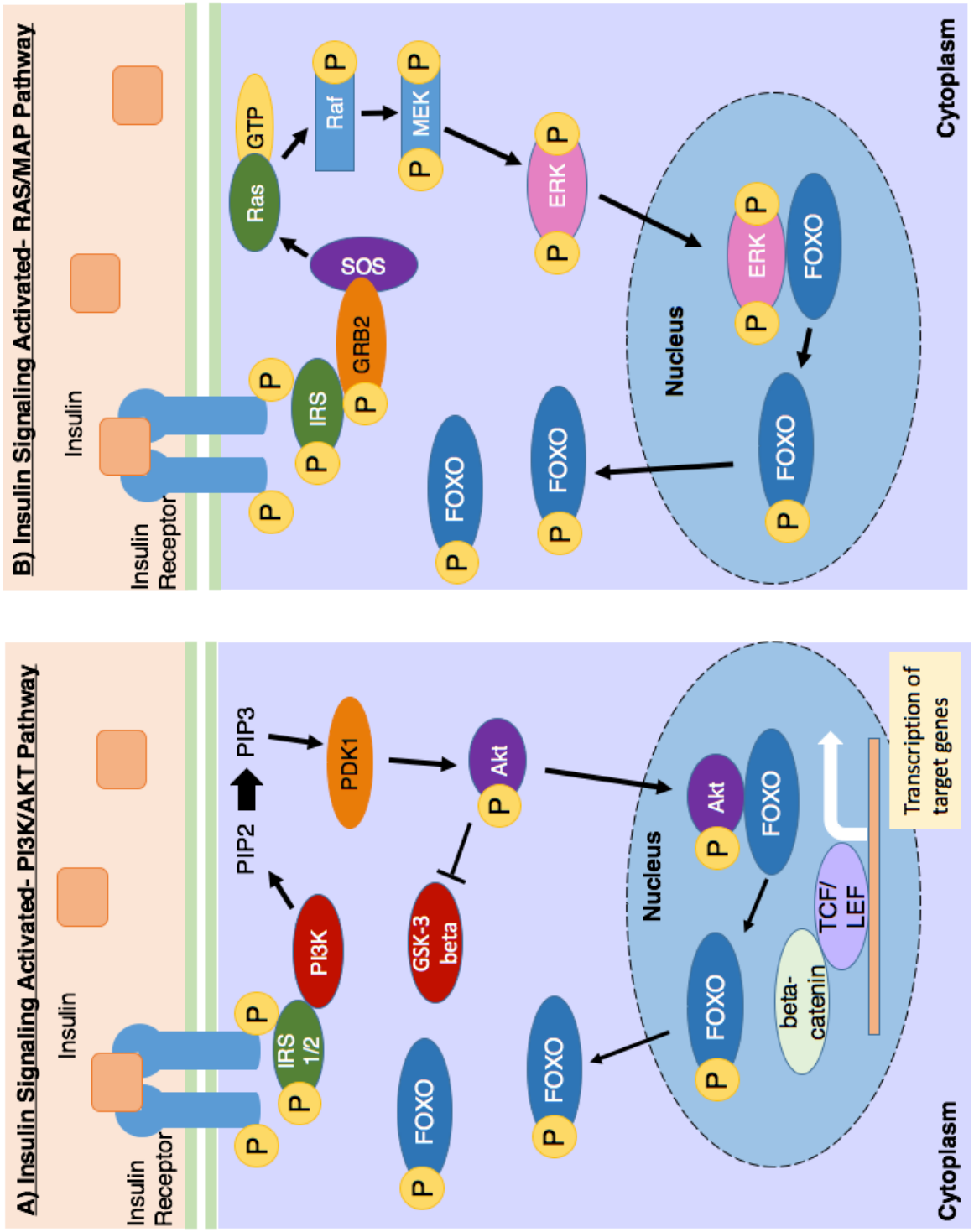
A) Insulin Signaling Activated- PI3K/AKT Pathway
Insulin
Insulin Receptor
P
IRS 1/2
PI3K
PIP2
PIP3
PDK1
Akt
GSK-3 beta
FOXO
Nucleus
beta-catenin
TCF/ LEF
Transcription of target genes
Cytoplasm
B) Insulin Signaling Activated- RAS/MAP Pathway
GRB2
SOS
Ras
GTP
Raf
MEK
ERK
Nucleus
Cytoplasm

Figure 2: Wnt Signaling. During activation of Wnt signaling, Wnt binds to FZD and LRP5/6 co-receptors. This leads to an accumulation of stabilized beta-catenin and translocation into the nucleus to interact with TCF/LEF to activate transcription of Wnt target genes. During inhibition of Wnt signaling, Wnt inhibitors (DKK, Sost, sFRPs, WIF1, Sostdc1), prevents Wnt from binding to FZD and LRP5/6 co-receptors. This results in the destruction complex, which consist of Axin, APC, and GSK-3 beta, phosphorylating beta-catenin for ubiquitination by proteasomes.

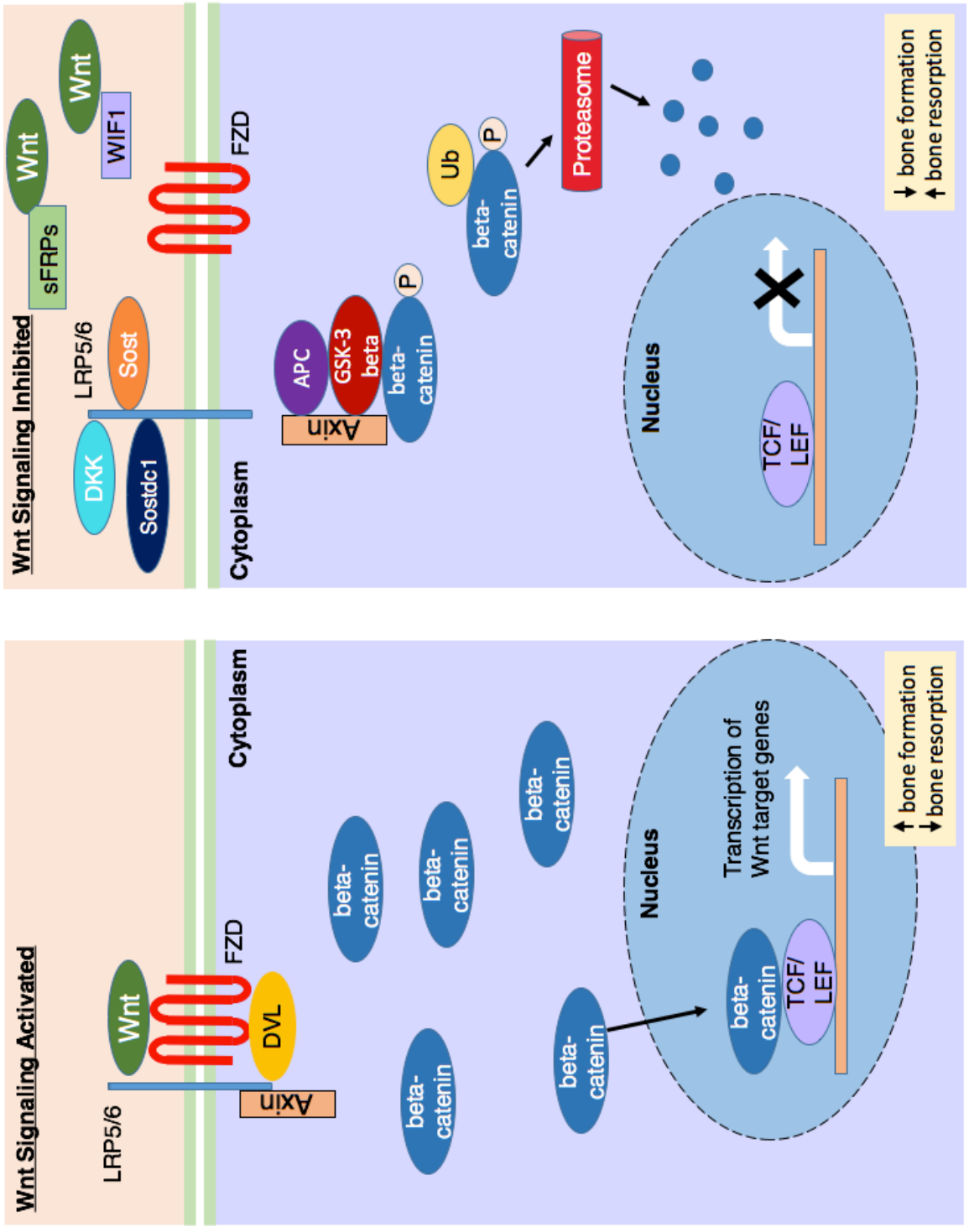
Wnt Signaling Inhibited
Wnt
sFRPs
Wnt
WIF1
LRP5/6
Sost
DKK
Sostdc1
FZD
Cytoplasm
APC
GSK-3 beta
beta-catenin
P
Axin
Ub
P
beta-catenin
Proteasome
Nucleus
TCF/ LEF
bone formation
bone resorption
Wnt Signaling Activated
LRP5/6
Wnt
FZD
DVL
Axin
beta-catenin
beta-catenin
beta-catenin
beta-catenin
beta-catenin
Nucleus
Transcription of Wnt target genes
beta-catenin
TCF/ LEF
bone formation
bone resorption

Figure 3: Phenotype of Sclerosteosis and Van Buchem Patients. A skull of a Van Buchem patient shows 4X more bone than a normal skull (A) [106]. Similarly, Sclerosteosis patients also have a high bone mass phenotype as shown in x-ray scans of a skull of a Sclerosteosis patient (D, right) compared to a normal individual (D, left) [107] Both Sclerosteosis (B) [108] and Van Buchem (C) [109] patients have facial distortion along with facial palsy and intracranial pressure. Sclerosteosis patients display digit syndactyly (E, black arrows), radial deviation (E, dashed line), and abnormal nail development (E, white arrow) [110].

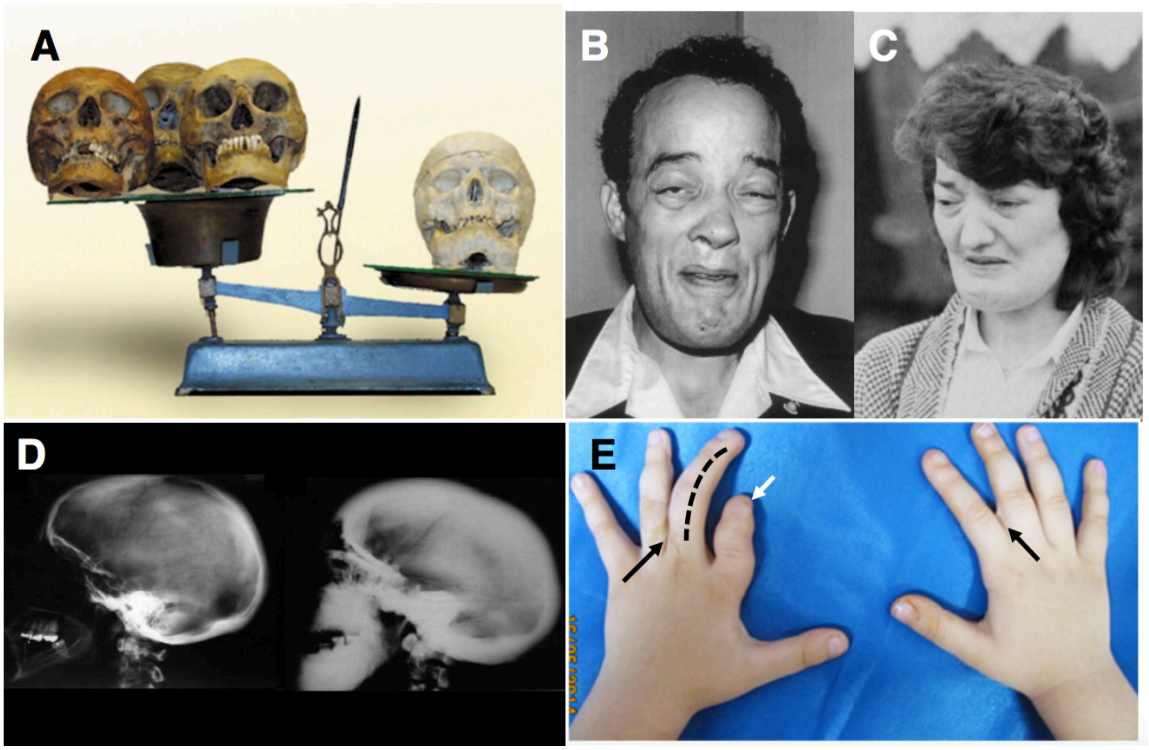

Chapter 2: Sclerostin Antibody Treatment Improves Fracture Outcomes in a Type I Diabetic Mouse Model

Abstract

Type 1 diabetes mellitus (T1DM) patients have osteopenia and impaired fracture healing due to decreased osteoblast activity. Further, no adequate treatments are currently available that can restore impaired healing in T1DM; hence a significant need exists to investigate new therapeutics for treatment of orthopedic complications. Sclerostin (SOST), a WNT antagonist, negatively regulates bone formation, and SostAb is a potent bone anabolic agent. To determine whether SOST antibody (SostAb) treatment improves fracture healing in streptozotocin (STZ) induced T1DM mice, we administered SostAb twice weekly for up to 21 days post-fracture, and examined bone quality and callus outcomes at 21 days and 42 days post fracture (11 and 14 weeks of age, respectively). Here we show that SostAb treatment improves bone parameters; these improvements persist after cessation of antibody treatment. Markers of osteoblast differentiation such as RUNX2, collagen I, osteocalcin, and DMP1 were reduced, while an abundant number of SP7/osterix-positive early osteoblasts were observed on the bone surface of STZ calluses. These results suggest that STZ calluses have poor osteogenesis resulting from failure of osteoblasts to fully differentiate and produce mineralized matrix, which produces a less mineralized callus. SostAb treatment enhanced fracture healing in both normal and STZ groups, and in STZ+SostAb mice, also reversed the lower mineralization seen in STZ calluses. Micro-CT analysis of calluses revealed improved bone parameters with SostAb treatment, and the mineralized bone was comparable to Controls. Additionally, we found sclerostin levels to be elevated in STZ mice and beta-catenin activity to be reduced. Consistent with its function as a WNT antagonist, SostAb treatment enhanced beta-catenin activity, but also increased the levels of SOST in the callus and in circulation. Our results indicate that SostAb treatment rescues the impaired osteogenesis seen in the STZ induced T1DM fracture model by facilitating osteoblast differentiation and mineralization of bone.

2.1 Introduction

Type 1 diabetes mellitus (T1DM) patients have osteopenia that increases fracture risk; additionally, fractures result in delayed or impaired fracture healing caused by reduced bone formation [19, 45, 111-114]. Fracture risk and the risk of osteoporosis increases with age, and with complications from diabetes, such as kidney disease, and length of time after diagnosis [115]. Recent studies revealed that the low bone mass phenotype is caused by reduced osteoblast activity [45, 116]. Although some studies show association of T1DM and increased osteoclast activity, many studies fail to show any changes in resorption [111]. In contrast to the osteopenia observed in T1DM patients, some type 2 diabetes mellitus (T2DM) patients have an increase in bone mineral density [117, 118]. However, similar to T1DM, T2DM patients are also more likely to develop fracture healing complications, suggesting a shared bone formation or remodeling defect in diabetic bone repair [117, 119].

Glucose control, although important for treatment, does not provide universal protection from downstream effects of diabetes. The attachment of glucose moieties (glycation) that interferes with protein and tissue structure and function can be reduced

but not prevented [120]. Glycation of type I collagen in bone reduces the ability of osteoblasts to adhere to the extracellular matrix and diminishes alkaline phosphatase (bone-forming) activity. In type I diabetic rats, closed fractures showed a delay in healing time in insulin-controlled and uncontrolled diabetes [35], which is also true for human patients [121]. It has also been suggested that oxidative stress leads to destructive cellular consequences in diabetic patients. Restoration of normal glucose levels does not prevent oxidative stress in the tissues examined [122]. Although insulin control of blood glucose levels is an integral part of T1DM treatment, it cannot completely correct the bone loss [123], nor the delayed fracture healing phenotypes in T1DM; an additional therapeutic intervention is needed.

Wnts are a family of secreted proteins that are involved in many aspects of embryonic development including primary axis formation [124], kidney organogenesis [125] and limb patterning and outgrowth [126]. Wnt ligand binding at the cell surface transduces a signal into the cytoplasm by binding to LRP5/6 and Frizzled co-receptors. β-catenin is activated and translocates to the nucleus where it binds to DNA, along with T cell factor/lymphoid enhancer factor (TCF/LEF) transcription factors, to activate downstream target genes [127]. During inactivation or inhibition of canonical Wnt signaling, GSK3β, a component of the destruction complex, phosphorylates β–catenin for degradation by proteasomes. Canonical Wnt signaling has been previously demonstrated to promote bone formation in genetically modified animals. For example, loss of function of LRP5 results in an osteopenic phenotype [128, 129], while other mutations in LRP5 result in a high bone mass phenotype in rodents and humans [130, 131] revealing the direct involvement of Wnts in bone formation. Genetic inhibition of GSK3β increases Wnt signaling through β-catenin, and enhances bone formation [132].

Canonical Wnt signaling, which relies on β-catenin activity, is involved during fracture repair [75, 132]. In TCF reporter mice, where a LacZ gene is placed downstream of tandem TCF binding sites, the reporter is only expressed upon activated β-catenin and TCF binding, thus providing a way to assess canonical Wnt signaling activity. After closed tibial fracture in mice, elevated β-catenin signaling is sustained during the entire time course of fracture repair [75]. β-catenin hyperactivity during fracture repair improved fracture healing even when increased in osteoblasts cells only [75]. In addition, β-catenin activation is a requirement for mesenchymal stem cell differentiation into osteoblasts; lack of β-catenin in mice results in decreased bone density [133]. Furthermore, the lack of β-catenin in osteoblastic cells results in inhibition of osteoblast differentiation. Type 1 diabetic rats showed a decrease in the Wnt downstream effectors phosphorylated glycogen synthase kinase 3β (GSK3β) and activated β-catenin, along with an increase in Sost protein level, resulting in decreased osteoblast activity [50]. This suggests that the high blood glucose environment alters osteoblast activity *via* Wnt signaling. Therefore, modulating Wnt signaling to enhance osteoblast activity during fracture repair may be a potential therapeutic target to improve impaired healing in T1DM patients.

A potent Wnt antagonist, sclerostin (Sost), is secreted by osteocytes (terminally-differentiated osteoblasts trapped within bone mineral matrix) and functions to inhibit bone formation [134]. In humans, lack of sclerostin causes sclerosteosis, a generalized skeletal hyperostosis disorder that results from elevated Wnt signaling/osteoblast activity

[108, 135], while non-coding deletions of gene regulatory regions that control SOST expression result in similar phenotypes [83, 88]. In animal models, overexpression of human *SOST* causes osteopenia and limb defects [136, 137], while lack of Sost in knockout mice causes 3-4 times more bone mass, consistent with human phenotypes [83]. Type 2 diabetic patients have elevated circulating SOST levels compared to non-diabetic patients [138], suggesting that Wnt signaling is altered in diabetic patients and may contribute to the observed osteopenia and delayed healing phenotype. Sost antibodies (SostAb) have been shown to enhance bone healing in ovariectomized rats [139, 140] by increasing bone formation and mass due to enhanced osteoblast function as determined by elevated levels of osteocalcin, a marker of osteoblast activitySostAb treatment in type 2 diabetic rats has also been shown to improve bone mass and strength [94].

In this study, we have administered Sost-neutralizing antibodies *in vivo* in a pharmacological model of T1DM in mice during fracture repair. By enhancing canonical Wnt signaling during fracture repair, we have shown improved fracture repair and rescued the osteopenic phenotypes in T1DM mice. The improved bone quality persisted at least three weeks after treatment had been discontinued, suggesting an extended benefit to bone quality and fracture repair in the absence of glucose control. In addition, T1DM in our model induced enhanced bone marrow adipogenesis, which was rescued in healing fractures by SostAb treatment. Herein we demonstrate for the first time that sclerostin antibodies counteract direct effects of high glucose-driven elevation of Sost levels in uncontrolled diabetes, indicating a positive therapeutic effect of modulating Wnt signaling in T1DM patients.

2.2 Methods

Animals and Fracture Model

Male C57BL6/J mice at six weeks of age were injected daily with Streptozotocin (*STZ)* (50mg/kg) or phosphate buffered saline (PBS) for 5 days. Prior to mid-femur fracture surgeries, blood glucose readings of $\geq$300 mg/dL, obtained one week after the last injection, confirmed diabetic status of *STZ*- treated mice. At eight weeks of age, mid-femoral fractures were generated using a closed Einohorn model, as previously described [141]. Briefly, a 27 gage (G) needle was surgically placed in the shaft of the femur and a dropped weight was used to induce a transverse fracture; fracture placement was confirmed by radiography. Sost antibody, a sclerostin-neutralizing monoclonal antibody suitable for *in vivo* use in mice, (SostAb) (25 mg/kg), or PBS was administered subcutaneously twice weekly up to 21 days post-fracture or 11 weeks of age, for a total of five injections, in *Control*, *STZ*, *SostAb*, and *STZ+SostAb* groups, each also with age-matched, uninjured cohorts. Antibody or PBS treatment was then discontinued for three weeks until 42 days post-fracture, or 14 weeks of age. At 21 days and 42 days post-fracture, bones were dissected and processed for microscale-computed tomography (μCT), RNA, histology and immunofluorescence (IF). A schematic diagram of the treatment regimen is shown in Figure 1A. All animal work was performed under an IACUC-approved Animal Use Protocol at an AAALAC-accredited facility.

Histology and Immunofluorescent Staining

Collected tissues were fixed in 10% neutral buffer formalin for 72 hours and then decalcified in 0.5M EDTA, pH 7.3, at 4°C until completion, as determined by weight-loss-weight gain and radiographic confirmation. Tissues were infiltrated and embedded into paraffin blocks and sectioned (6µm) on glass slides and baked at 42°C overnight. Alcian Blue and Nuclear Fast Red stain on histological slides were first de-waxed and stained with Alcian Blue pH 1.5 (stains cartilage) and counterstained with nuclear fast red and mounted with Permount. For osteoclasts analysis, Histological sections of injured (21 days) and uninjured controls (11 weeks of age) were de-waxed and stained with TRAP working solution for 1 hour at 37°C in the dark and counterstained with 0.02% Fast Green and mounted with 60% glycerol.

For immunohistochemistry, Uni-trieve (Innovex) was used for the antigen retrieval for 30 minutes at 65°C, unless stated otherwise. Primary antibodies against Runx2 (abcam, ab76956), SP7/Osterix (ab25522), Collagen Type 1 (calbiochem 234167), Osteocalcin (abcam, ab10911), active Caspase 3 (cellsig 9661), and cathepsin K (abcam, ab19027) were used. Anti-Sost (R&D, AF1589) required Trypsin/EDTA at 37°C for 25 minutes for antigen retrieval. Anti-Activated beta-catenin (Millipore, 8E7, 05-665) required Uni-trieve, Proteinase K (15µg/ml) for 15 minutes, and Rodent Block. Secondary antibodies (Alexa Fluor 488 (green) or 594 (red), Molecular Probes) were used or detection. Negative control slides included secondary antibody only, with the same antigen retrieval method used for the experimental samples (Fig.8) Stained slides were mounted with Prolong Gold with DAPI (Molecular Probes). ImagePro Plus V7.0 and CCD QIClick camera were used for imaging. Qualitative assessment of immunostains was performed by 2 blinded reviewers without knowledge of treatment group.

For histological analysis of adipocytes and osteoclasts, cells were counted on complete bone sagittal sections (n=12 sections per animal) for n=3 animals per group by two blinded reviewers. Counts by each reviewer were averaged on a per-section basis for analysis. Cells were counted by hand for adipocytes, as they are represented by clear round empty spaces on the slide. Data are expressed as mean number of cells per section ± standard deviation. Cathepsin K immunostains were quantified using the Analyze Particles tool in ImageJ. Data are expressed as mean % stained area± standard deviation.

Histological sections of injured (21 days) and uninjured controls (11 weeks of age) were de-waxed and stained with TRAP working solution for 10 minutes at 37°C in the dark and counterstained with 0.02% Fast Green and mounted with 60% glycerol. Fluorescent immunostains using primary antibody against cathepsin K (abcam, ab19027) required Unitrieve (Innovex) for the antigen retrieval, for 30 minutes at 65°C. Secondary antibodies (Alexa Fluor 488 (green) or 594 (red), Molecular Probes) against mouse, rabbit, or goat antigens/primary antibodies were used for detection and negative control slides. Stained slides were mounted with Prolong Gold with DAPI (Molecular Probes). ImagePro Plus V7.0 software and a QIClick CCD camera were used for imaging. Cathepsin K quantification was performed using the Analyze Particles tool in Image J, where percent area of stain was quantified.

Micro-CT

Specimens were stored in 70% EtOH at 4°C. Specimens were processed without knowledge of sex, age or treatment, as these data were provided only after all the scanning and image analyses were complete. L4 vertebrae, mid femoral cortical bone, and fracture callus were measured and analyzed for bone parameters (n=6-10 per group) (µCT 40, SCANCO, Brüttisellen, Switzerland) according to the guidelines for μCT analysis of rodent bone structure [142]: energy 55 kVp, intensity 114 mA, integration time 900 ms, 6 μm nominal voxel size. The threshold for "bone" was set at 375, which is approximately equal to 620 mg HA/cm^3. The trabecular bone region was identified manually by tracing the region of interest. Images were thresholded using an adaptive-iterative algorithm and morphometric variables were computed from the binarized images using direct, 3D techniques that do not rely on any prior assumptions about the underlying structure. L4 vertebrae were scanned axially in a cranio-caudal orientation and the region of interest was placed 0.3mm beneath the cranial and above the caudal growth plates [143]. Depending on the size of the vertebra, this ROI size ranged between 2220 and 2820 µm. 7 Images were segmented with the same algorithm and trabecular bone variables were assessed. To assess cortical bone parameters, 50 transverse μCT slices were obtained at the femoral mid-diaphysis using a 6 μm isotropic voxel size. Images were subjected to Gaussian filtration and segmented using a constant threshold. For fracture analysis, age-matched animals (11 or 14-weeks of age) were compared to 21 day or 42 day fractures for cortical measurements. Callus volume (TV) was measured including only callus tissue that excluded the native bone volume of the original cortical bone and marrow space. The whole callus was scanned, and we manually drew the contour line to define the region and volume of callus (TV). Then we used a unified threshold to segment mineralized callus from surrounding undermineralised callus, and only the callus that had similar BMD as native bone was counted into bone volume (BV).

Immunosorbent Assay

During dissections, serum was collected in serum collection tubes (BD microtainer). After separation, serum was stored in -20°C until use. A mouse sclerostin ELISA kit (ALPCO, 41-SCLMS-E01) was used according to the manufacturer's instructions to measure serum sclerostin levels. Data is represented as mean +/- standard deviation (n=5 per group).

Statistics

All data were expressed as the mean ± standard deviation. For uCT and quantitative histological analysis, two-way ANOVA was performed with Sidak's correction for multiple comparisons using PRISM 6 software. Significant results are presented as a diabetic effect, antibody treatment effect, or diabetic x antibody treatment interaction effect; $p<0.05$ was considered significant. For statistical analysis of SOST ELISA results, *Student's T-test* with a two-tailed distribution was used, with two-sample equal variance (homoscedastic test), for significance. All groups were compared to *Control*; $p<0.05$ was considered significant.

2.3 Results

SostAb improves the bone loss phenotype in uninjured STZ mice

The experimental design included two collection time points at 11 weeks and 14 weeks of age, for uninjured age-matched cohorts; SostAb was discontinued after 3 weeks of treatment or 11 weeks of age (Fig. *1A)*. At 11 weeks of age, *STZ*-treated mice *(STZ)* showed abnormal growth plates, with reduced trabecular bone and less organized cartilage matrix deposition in the growth plate (Fig. *1C*, yellow arrowheads), compared to *Controls* (Fig. *1B, C*). We also noted an increase in adipocytes in the bone marrow of *STZ*-treated mice, (Fig. *1C,G,* black arrowheads), as well as reduced trabecular bone (Fig. *1F, G*), supporting previous reports of bone loss in *STZ*-treated animals [42, 144]. All groups showed increased trabecular bone in the metaphysis, in comparison to *STZ*, which showed less trabecular bone (Fig. *1B-E*, and yellow arrowheads), *STZ+SostAb* also appeared to have a more organized growth plate (Fig. *1D,E*). *SostAb* treatment dramatically increased trabecular bone formation in the epiphysis (Fig. *1F,H,I*); however, it did not rescue the increased adipogenesis seen in the marrow of *STZ+SostAb* mice (Fig. *1E*, black arrowheads). Cortical bone was much thicker in *SostAb* treated groups (Fig.*1J-M*, arrows), and while *STZ* mice showed residual cartilage matrix in the cortical bone (Fig. *1K*, arrowhead) *SostAb* treatment of *STZ* mice resulted in less persistent cartilage (Fig. *1M*).

μCT analysis reveals that uninjured *STZ* mice had significantly reduced bone volume to total bone volume ratio (BV/TV), trabecular thickness (Tb. Th.), and Structural Model Index (SMI) in lumbar vertebrae (L4) as a result of the diabetic state (Table 1, see also Fig.*1N,P*). In cortical bone, bone area: total area (BA/TA) ($p<0.0001$), bone area (BA) ($p<0.0001$), and total area (TA) are reduced in uninjured *STZ* mice compared to *Control* (Table 1, see also Fig.*1R,S*). No changes were identified in connectivity density (Conn. Dens.), trabecular number (Tb. N.), trabecular separation (Tb. Sp.) or bone mineral density (BMD). *SostAb* treated mice, both with and without diabetes, had a significant improvement in all bone parameters except L4 BMD in L4 vertebrae (Table 1, see also Fig.*1N,P*). In cortical bone, *SostAb* treated mice, with or without diabetes, had significantly increased BA/TA ($p<0.0001$) and BA (Table 1, see also Fig. *1R,T*). In *STZ+SostAb* treated mice, BV/TV, SMI, and Tb. Th. (all $p<0.0001$), showed significant diabetes x antibody treatment interactions, suggesting that the effect of antibody treatment in diabetic animals may provide synergistic improvement for these parameters. Overall, our data from uninjured animals at 11 weeks of age indicates that SostAb improves diabetic osteopenia in the absence of fracture.

Improved bone parameters persist 3-weeks after discontinuation of SostAb treatment in uninjured STZ mice

To examine whether diabetic bone reverts to the osteopenic condition subsequent to *SostAb* treatment discontinuation, we examined bone parameters in 14-week old uninjured cohorts, or 3-weeks after cessation of *SostAb* treatment. We found no significant effect of diabetes on the variance in *STZ* mice, however, the means for all parameters in lumbar vertebrae were significantly different from *Control* mice ($p<0.0001$ for all parameters) (Table 2, see also Fig.*1N,O*). This indicated that although the diabetic state had a significant negative impact on bone, most of the variance in the data is contributed by antibody treatment. Statistically, we find a significant antibody effect for all

L4 bone parameters measured, with or without diabetes. At 14 weeks, different parameters show significant diabetes x antibody interaction effects (Conn. Dens., SMI, and Tb. N.) that at 11 weeks of age, suggesting that the synergistic benefits of antibody treatment on diabetic bone may change with age or growth status. In cortical bone, BA/TA, BA, and BMD did have a significant diabetic effect (Table 2). Antibody effects in *SostAb STZ+SostAb* mice increased BA/TA, BA, and BMD (all $p<0.001$), compared to *Control* and *STZ* groups (Table 2). Thus, at 14 weeks of age in uninjured animals, we saw continued bone quality improvement after discontinuation of SostAb treatment, in the absence of fracture.

SostAb treatment improves bone parameters in fracture callus of STZ-treated mice.

At 11 weeks of age, all groups had some amount of persistent cartilage in the mid-callus regions examined (Fig. 2A, *2B-E*). Both the *SostAb* and *STZ+SostAb* groups appeared to have more mineralized bone within the callus compared to *Control* and *STZ* groups (Fig. *2B-E*). At 14 weeks of age, bridging had occurred in all groups at the fracture site, and remodeling was evident by reduced trabecular bone in the callus region (Fig. *2F-I,* compared to *2B-E*). An enlarged marrow space at the bridging site was evident in *STZ* mice compared to *Control*, and abundant adipocytes persisted (Fig. *2F,G,* and arrowheads), while both *SostAb* groups displayed more bone at the site of fracture compared to *Control* and *STZ* respectively (Fig. *2H,I*).

Representative μCT reconstructions of calluses from 11 week old animals are shown in Fig. *2K-N*. Reconstructions were consistent with histology, indicating a more porous bone structure in the calluses of *STZ* mice compared to all other groups (Fig. *2L*). *SostAb*-treated groups (Fig. *2M,N*) appeared to have thicker trabecular structure in calluses compared to *Control* and especially *STZ* mice (Fig. *2L*). Quantitative callus analysis by μCT confirmed the histology (Table 3). Compared to *Controls*, *STZ* calluses at 11 weeks of age had decreased BV and TV, due to diabetic effects, indicating smaller fracture calluses, but this resulted in similar BV/TV between the two groups. Bone Mineral Content (BMC), the amount of mineralized bone per callus volume, had a significant diabetic effect, although the mean is unexpectedly higher than *Controls*; this may be due to the reduced volume of the callus in STZ animals. At 11 weeks of age, there was a significant antibody effect on all callus parameters except TV; and BMD had a significant diabetic x antibody interaction, which overall, reduced the BMD of the callus. Antibody effects on callus mineral suggested that *SostAb* treatment reduced BMD in the callus at relatively early healing stages.

By 14 weeks of age, the fracture calluses have matured. Diabetic effects on the callus at this stage are only seen in BMC and BMD (Table 3, lower half), which reveals the long-term negative effects of diabetes on callus mineralization ($p<0.0001$ for both parameters). Antibody effects on calluses at 14 weeks of age show significant improvements in BV/TV and BMC, indicating that *SostAb* treatment, regardless of diabetic state, enhances mineralization or maturation of the callus. Significant gains in callus quality in *STZ+SostAb* treated animals are retained at 14 weeks of age, and the mineralization of the callus had reached or exceeded the level of *Controls*.

Injured *STZ-treated mice have impaired osteogenesis during fracture repair*

SP7/osterix, an early osteoblast marker (Fig. *3A-D*), appeared dramatically elevated at 11 weeks of age, in *STZ* calluses (Fig. *3B, arrows*), with large numbers of positive cells aligned on the bone surface, suggesting that lineage commitment and early osteoblast differentiation was not inhibited in *STZ* mice. However, RUNX2, a pro-osteogenic transcription factor that is increased early in the osteogenic differentiation program (Fig. *3E-H*), appeared reduced in *STZ* mice compared to *Controls* (Fig. *3E,F*), consistent with published results [145]. In *STZ* mice, RUNX2 stain was less plentiful compared to *Controls*, (Fig. *3E,F*); Treatment with *SostAb* did not increase the level of RUNX2*(Fig. 3E,G)*; *STZ+SostAb* also did not appear to increase RUNX2 levels compared to *STZ* calluses (Fig. *3F,H*), Collagen I, a matrix protein secreted by osteoblasts (Fig. *3I-L*) was visibly reduced in *STZ* calluses (Fig. *3J*), which indicated a decrease in mineralized matrix production consistent with delayed or impaired osteogenesis (see also Table 3), while *SostAb* and *STZ+SostAb* calluses showed increased levels (Fig. *3K,L*), compared to *Controls* (Fig. *3I*). Osteocalcin (Fig. *3M-P*) and DMP1 (Fig. *3Q-T*), markers of osteoblast maturation and osteocyte differentiation, appeared to have dramatically reduced signal in *STZ* calluses (Fig. *3N,R*), which indicated delayed callus maturation in *STZ* calluses, while *Control* (Fig. *3M,Q*), *SostAb* (Fig. *3O,S*), and *STZ+SostAb* (Fig. *3P,T*) groups revealed abundant signal along the surface of the bone. To determine if there is an alteration of cell apoptosis, activated caspase 3 antibody, an apoptosis marker (Fig. *3U-X*), was stained on callus sections at 11 weeks of age, revealing no visible change in signal between any of the groups. Negative control stains for each antibody and antigen retrieval method are presented in Fig. 8. This suggests that cell apoptosis was not contributing to poor bone in *STZ* calluses at 11 weeks of age. At this time point, *STZ+SostAb* calluses appeared to show patterns for all markers similar to *Controls* or *SostAb* calluses, rather than *STZ* calluses, which indicated a return to normal or better than normal healing, based on marker representation of the healing process.

By 14 weeks of age, the callus had matured in injured *Control* animals, and SP7/osterix was still localized at the bone surface (Fig. *4A*). Collagen I appeared more abundant compared to 11 weeks of age (Fig. *3I,4E*), and DMP1 protein was plentiful in *Control* calluses (Fig. *4I*). Compared to *Controls*, *STZ* calluses continued to have an abundant number of SP7/osterix positive cells lining the bone surface (Fig. *4A, 4B*), although not as plentiful as at 11 weeks of age (Fig. *3B,4B). STZ* calluses continued to have visibly reduced signal for Collagen I compared to *Controls* (Fig. *4E,F*), which suggested a continued delay in mineralization of the callus (see also Table 3). However, by 14 weeks of age, cells that became embedded in bone matrix of *STZ* calluses produced DMP1, at similar apparent levels compared to the other groups (Fig. *4I-L*). Antibody-treated groups at this time point appeared to have more Collagen I in the callus relative to *Controls* or *STZ* calluses (Fig. *4E-H*), which indicated possible enhanced mineralization. There appeared to have been little impact of antibody treatment on the abundance of DMP1 in the bony calluses of *SostAb* or *STZ+ Sost Ab* groups, as all groups seemed to have similar levels (Fig. *4I-L)*.

While we did not see evidence of increased osteoblast apoptosis, we considered that enhanced osteoclast activity in *STZ* diabetic bones could contribute to fracture

callus instability and poor bone structure. We performed osteoclast-specific tartrate-resistant acid phosphatase (TRAP) stain on uninjured bones and fracture calluses of 11 week old animals, and did not find any evidence of increased osteoclast activity with this marker in the growth plate (Fig. *7A-D*), epiphyseal trabecular bone (Fig. *7E-H*), or fracture callus (Fig. *7I-L*) of *STZ* mice, nor did we see a change in TRAP activity with SostAb treatment. Additionally, we did not see a significant difference in cathepsin K when tested by two-way ANOVA, which was used to examine osteoclast maturity in epiphyseal bone and growth plate (Fig. *7M-Q*). These data indicated that there is no difference in osteoclast activity of *STZ* diabetic mice, 5 weeks after onset of diabetes (at 11 weeks of age), and are consistent with other reports of normal osteoclast activity in T1DM [45, 50, 146]. Our data indicated that osteoblast maturation markers were reduced in *STZ*-diabetes, while we found no evidence of osteoblast apoptosis or enhanced osteoclast activity to account for reduced bone mass; *SostAb* treatment of diabetic mice returned osteoblast marker levels to normal or enhanced levels.

Wnt signaling is diminished during diabetic fracture healing, and reversed with SostAb administration

To examine WNT signaling activity we assessed activated β-catenin protein levels. In calluses of 11 week old mice, very low levels of activated β-catenin were observed in *STZ* treated samples (Fig. *5B*). *Control* calluses showed modest levels of activated β-catenin, primarily localized to the bone-forming surface, with very few positive cells embedded in the bone matrix (Fig. *5A*). However, both *SostAb* treated groups appeared to have higher levels of activated β-catenin at the bone surface, along with several positive cells in the bone matrix (Fig. *5C,D*), suggesting enhanced β-catenin activity in osteocytes as well as in osteoblasts. By 14 weeks of age, in calluses, we found moderate levels of activated β-catenin in the bone of *Control* mice, and it was no longer confined to the bone-forming surface (Fig. *5I*). *STZ* mice appeared to have small patches of activated β-catenin, but the signal was primarily absent from osteocytes in the bone matrix (Fig. *5J*). In *SostAb* and *STZ+SostAb* treated mice, 42 day calluses showed robust activated β-catenin signal throughout the callus (Fig. *5K,L*), which seemed to be increased over the levels seen in either *Controls* or *STZ* calluses (Fig. *5I,L*). These data demonstrated that *SostAb* administration elevated β-catenin activity, consistent with SOST's role as a WNT antagonist [147].

When examining sclerostin levels in the callus at 21 days, we saw modestly increased sclerostin in matrix-embedded cells of *STZ* mice, compared to *Controls*, consistent with expression in osteocytes (Fig. *5E,F*). We did, however, observed dramatically increased sclerostin protein levels in the bone of *SostAb* treated groups (Fig. *5G,H*). We also observed increased activated β-catenin activity in these same groups (Fig. *5C,D*). By 42 days, we continued to find increased sclerostin signal in *STZ* calluses compared to *Controls* (Fig. *5M,N*). We also found further increased sclerostin localization in *SostAb* and *STZ+SostAb* treatment groups (Fig. *5O,P*). We questioned whether we may have detected the administered therapeutic SOST antibody, or whether we may have detected sclerostin that is inactivated, but still found in bone. Our negative control immunostains included secondary antibody stains against both the rabbit antibody that was used to examine SOST in tissues (Fig. 8, A-D), and the mouse monoclonal therapeutic antibody that was administered (Fig. 8, E-H), under the same

antigen retrieval conditions. We found no evidence of non-specific signal, or the ability to detect the therapeutically administered antibody. Thus, we presume that the high SOST signal detected in the tissue of antibody-treated mice is the combined protein accumulation of biologically active SOST, and SOST that is inactivated and bound to *SostAb* but still in tissues or circulation. These findings were supported by the detection of elevated levels of SOST in the serum. *STZ* mice had a 30% increase in circulating sclerostin, relative to *Controls* ($p<0.03$) (Fig. *5Q*). Circulating levels for sclerostin in *Controls* were within the reported range for the assay. However, we found 8 times the amount of circulating sclerostin in both antibody-treated groups compared to *Controls* (*SostAb* $p<5x10^{-9}$, *STZ+SostAb* $p<2x10^{-7}$). We find a pattern of elevated SOST and decreased β-catenin activity in the context of a high-glucose environment, while *SostAb* treatment enhances β-catenin activity despite high SOST levels.

Enhanced bone marrow adiposity in healing fractures of STZ mice is rescued by SostAb treatment

We saw some evidence that adipocytes are more abundant in the marrow compartment of *STZ* diabetic mice, as has been suggested by others, who have proposed that increased adipogenesis may be at the expense of precursor differentiation into osteoblasts, resulting in reduced bone formation [46]. We additionally observed an up-regulation of the number of adipocytes in the marrow after fracture, compared to intact bone. To quantify the effects of diabetes on bone marrow adiposity, we examined Masson's Trichrome-stained sections from uninjured age-matched bones, and fracture calluses at 11 weeks of age (Fig. 6). Total number of adipocytes per sagittal bone section were analyzed for both sets of samples and compared by two-way ANOVA. In uninjured bones we found a significant effect of diabetes on the adipocyte number ($p<0.001$) (Fig. *6I*), with no effect of antibody treatment (Fig. *6A-D*). However, in age-matched fracture calluses, we saw an increase in marrow adiposity in all groups, which was dramatically up-regulated in *STZ* diabetic mice (Fig. *6E-H*). Quantification of the differences by two-way ANOVA revealed a significant diabetic effect in *STZ* mice, a significant antibody treatment effect, and a significant diabetes x antibody interaction effect, suggesting that *SostAb* treatment mitigates the enhanced adiposity seen in healing fracture callus of *STZ* diabetic mice. *SostAb* treatment may in this way enhance fracture healing by directly or indirectly reducing marrow adiposity, independent of its effects on osteoblast maturation or activity.

2.4 Discussion

In this study, we treated fractured femurs in Type I diabetic mice with *SostAb* to improve fracture healing outcomes. We applied a clinically-relevant scenario to the administration of *SostAb*, to examine the effects on bone during fracture repair and after drug withdrawal, as it is unlikely that patients in a clinical setting would be treated indefinitely. We utilized a chemically-induced *STZ* diabetic model, to cause early-onset diabetes in growing mice. Consistent with previous reports, *STZ* treated mice lose bone mass and quality within 3 weeks of becoming diabetic [148, 149]. The loss of bone we report here is primarily based on reduced bone formation, as we saw reduced mineral deposition, which was confirmed by immunofluorescence for matrix markers and uCT, and we did not find evidence of enhanced osteoclast activity in either uninjured bones or fracture calluses in our model.

We found that *SostAb* treatment of *STZ* mice dramatically enhanced bone formation, but despite the dramatic increases in bone volume, mineral density did not increase compared to *Controls*. This suggested that *SostAb* in the diabetic setting may function to promote osteoblast differentiation or osteoblast activity, and allows mineralization to catch up to normal levels. This is evidenced by the fact that neither *SostAb* nor *STZ+SostAb* had bone mineral densities at the end of the study that exceed the levels of *Controls,* while densities of both groups were less than *Controls* after 3 weeks of treatment. However, *SostAb* appears to enhance mineralization of fracture calluses tand thus potentially improve the strength of newly repaired bone, as *SostAb* treatment resulted in dramatically enhanced bone mineral content of callus at 14 weeks of age in both normal and diabetic mice. Similarly, recent reports have demonstrated reduced mineral content of bone after Sost antibody treatment, or due to genetic loss of Sost, despite abundant bone formation [150, 151]. It is likely that reduction of Sost *via* antibody treatment increases osteoblast activity to produce abundant osteoid and undermineralized bone, which then mineralizes at a normal rate. At later time points, this leads to higher mineral content in the abundantly formed new bone, thereby potentially increasing mechanical stability. Furthermore, early reports that successfully used Sost antibody treatment to promote fracture healing relied heavily on models that primarily healed by intramembranous bone formation [94, 140, 152, 153]. This suggested that *SostAb* may be beneficial in problematic fracture healing that results from poor osteogenesis; however, Li et al (2011) [154] reported fracture repair in an endochondral model in *Sost*$^{-/-}$ mice, and Feng et al (2015) [155] reported similar results with Sost antibody treatment, suggesting that fracture repair may benefit from early intervention by reducing sclerostin levels, rather than only during osteogenesis. While we found a significant benefit in callus BV and BV/TV of *STZ+SostAb* mice, we also saw an increase in callus size, suggesting a benefit in early repair events prior to osteogenesis.

The large number of osteoblasts and precursors at the bone surface that express *Sp7/Osterix*, in the absence of significant mineral, suggests that the osteopenia in *STZ* diabetic mice may be due to a defect in osteoblasts maturation and mineral matrix synthesis. In another report, *STZ* mice had the same amount of immature mesenchymal tissue but decreased osteoblast differentiation. This was associated with decreased collagen type 1, and *Runx2* mRNA expression in an intramembraneous bone repair model [156], similar to our findings. Song et al (2012) [157] demonstrated that loss of β-catenin in osteoblast precursors results in a switch from osteogenesis to adipogenesis that causes low bone mass. As our *STZ* mice displayed increased adiposity in the marrow, this is a plausible explanation for impaired osteogenesis in our *STZ* mice. SOST is not known to regulate the cell fate of precursor cells; however, our study shows evidence that adipogenesis dramatically increases during callus formation. This suggested that a pool of precursors have recently differentiated, and *SostAb* mitigated this effect, leaving open the possibility that elevated Wnt signaling influences the fate of precursor cells.

Furthermore, *STZ* mice appear to have much less osteocalcin at the bone surface, indicative of immature osteoblasts. However, reduced osteocalcin has also recently been implicated in metabolic activity of osteoblasts, in which reduced insulin signaling in osteoblasts and reduced *Runx2* expression may fail to activate osteocalcin to promote

local and systemic metabolic homeostasis in *STZ* diabetes [158]. In *STZ* diabetic mice, osteoblasts are no longer able to depend on glucose as an energy source, but must rely on lipid metabolism to generate ATP [158]. LRP5, a Wnt co-receptor, has been implicated in this process, and mice lacking *Lrp5* develop metabolic imbalance with increased adiposity. We have shown that Sost primarily inhibits LRP5-dependent Wnt signaling [137], thus in the absence of insulin, *SostAb* may restore Wnt signaling through LRP5 to partially re-balance metabolic homeostasis, independent of glucose metabolism. In this way, metabolic stress on the osteoblasts is relieved, and differentiation and metabolism can proceed more normally.

Another *STZ* diabetic model showed that in T1DM, insulin and IGF-1 deficiency decreases osteogensis due to negative regulation of Wnt signaling activity [50]. It was demonstrated that the decreased bone formation was caused by reduced levels of activated β-catenin, precipitated by a loss of phosphorylated GSK3β, and phosphorylated Akt/PKB, targeting β-catenin for degradation. They also observed a dramatic increase in Wnt inhibitor (Sost and Dkk1) levels. Loss of phosphorylated Akt/PKB can occur from a cycle of reduced Wnt signaling, as in the presence of high Sost levels, or in the event of oxidative damage. As a result, cells (such as osteoblast precursors and early osteoblasts) in a low insulin, high Sost, high glucose (oxidative) environment may be subject to cell cycle arrest [159]. Furthermore, we confirmed that short-term treatment of cultured osteoblasts with high glucose results in an increase in *Sost* expression, indicating that high glucose alone may contribute to elevated sclerostin levels in T1DM, consistent with another study that examined *Sost* expression in osteocytes treated with high glucose [160]. Another study observed a decrease in cyclin D mRNA expression in osteoblasts cells treated in a high glucose environment [161], which correlated with increased apoptosis and reduced cell proliferation. Taken together, these findings may account for the reduced number of Runx2-positive cells, and/or the apparent inhibition of differentiation of Osterix-positive cells seen in our *STZ* mice. While we did not observe enhanced activated caspase-3-driven apoptosis in calluses at 21 days, it is possible that early osteoblast or precursor death at another time point may contribute to reduced osteognesis in our T1DM model.

Reports are conflicting on whether T1DM induces changes in osteoclast activity, with some studies reporting enhanced, unchanged, or even reduced osteoclast activity in the context of T1DM. Reports of osteopenia compared to osteoporosis in T1DM are difficult to deconvolute, and are likely due to differences in age of animals or patients, time since diagnosis, diabetic complications (such as vascular or kidney disease), and body condition [45, 112, 115]. We found no change in osteoclast activity, which is consistent with the recent diagnosis and young age of our study groups.

Oxidative stress in tissues leads to much of the destructive sequelae in diabetic patients, causing pancreatic beta-cell death, kidney disease, cardiovascular disease, and may contribute to the effects of diabetes seen in the skeleton [122]. Reduced Wnt signaling and increased Wnt antagonism have been associated with increased oxidative stress, and reduced osteoblast activity [50, 162, 163]. Oxidative stress activates FOXO signaling, which competes for β-catenin in the cell, to reduce activation of Wnt target genes. Activation of Wnt signaling activates the Akt/PKB pathway; PKB then

phosphorylates and sequesters FOXO in the cytoplasm, and prevents it from competing with β-catenin [164]. As Sost is an antagonist of β-catenin-mediated Wnt signaling, reduction of bioactive SOST through SostAb treatment activates β-catenin signaling, potentially mitigating the effects of oxidative stress and competition by activated FOXO [162]. Thus, Wnt signaling may be suppressed by a mechanism that is independent of Sost, but can be mitigated by promoting Wnt signaling through inhibition of Sost. In this way, *SostAb* can alleviate the effects on diabetic bone that cannot be overcome by treatment with insulin.

We examined sclerostin and β-catenin levels in our mice, to demonstrate that *SostAb* is effective at suppressing sclerostin activity and elevating Wnt signaling activity through activation of β-catenin. We found elevated sclerostin in serum, and decreased activated β-catenin in *STZ* mice, consistent with other reports of diabetic animals and patients with elevated Sclerostin levels [50, 51, 138, 162]. While we did find elevated β-catenin in antibody-treated groups, consistent with elevated Wnt signaling and promotion of osteogenesis, we also saw an unexpected and very highly elevated level of sclerostin protein in the bone and blood of antibody-treated animals. This finding was unexpected, but there has been a recent report of sclerostin-antibody treatment associated with elevated expression of sclerostin [165]. At these extreme levels of Sost protein we find in the serum and bone, however, it is likely that the majority of the protein is inactivated by antibody bound to it. Sost antibody has been reported to have a very long lifespan in circulation; Ominsky et al (2010) reported Sost antibody levels in circulation of Cynomolgus monkeys and found that a single dose can be detected in circulation up to nearly a month post-dose [100], while Padhi et al. (2011) reported a single dose detected in serum up to an amazing 85 days after a single dose [99]. These results pose some questions that remain unanswered: *SostAb* bound to sclerostin may have a very long lifespan in tissues; are high therapeutic doses of antibody needed to combat elevated expression and protein levels in response to treatment? Furthermore, sclerostin bound to *SostAb* may prevent degradation of either molecule, revealing a need to study downstream effects of this protein construct which appears to be in circulation for extended periods of time. Future experiments are needed that examine the long-term effects of *SostAb* treatment on osteoblast metabolism; these experiments can be conducted in *Ins2(Akita)* mice, as they become diabetic by a nearly identical mechanism to *STZ*-induced diabetes, and have a much longer lifespan in the diabetic state. These studies have the potential to uncover more mechanistic insight into the interaction between the diabetic state and Lrp5-dependent/Sost-mediated osteoblast metabolism, and the contribution to whole body metabolic homeostasis. The phenotype of these mice is penetrant in both genders, which will facilitate much-needed studies in female animals.

Our study has revealed that anabolic doses of *SostAb* enhance bone formation and quality in an early-onset Type I diabetic fracture healing model. We provide evidence that *SostAb* alleviates inhibition on osteoblast differentiation caused by the diabetic state. We further demonstrated that the effects of *SostAb* treatment may extend well beyond the end of the dosing regimen, since our result show continued improvement of bone parameters in STZ diabetic mice treated with antibody, even three weeks after treatment had stopped. We observed *SostAb*-mediated reduction of marrow

adiposity during callus formation, which may be of significant therapeutic benefit in diabetic fracture healing. We also uncovered an as yet undocumented phenomenon of apparent accumulation of sclerostin and/or sclerostin-antibody complexes as a result of treatment, which is worth further exploration. In summary, *SostAb* is an effective treatment to counteract the low osteogenesis that occurs in T1DM bone environments, and may provide extended benefits beyond the treatment span.

Figure 1. SostAb treatment Improves Low Bone Mass in STZ mice.
Experimental design (A). Histological sections and stain with Alcian Blue and Nuclear Fast Red (B-M). The growth plate (B-E), Epiphysis (F-I), and Cortex (J-M) represents the location of the cartilage, trabecular bone, and cortical bone respectively. Alcian Blue stains the cartilage in blue- see also yellow arrows (C, D, E). *STZ* mice showed some cartilage present also in the cortical bone (K, black arrow). White circles, indicated by black arrows (C, G, E) show adipocytes in the bone marrow. The cortical bone (J-M) shows degrees of cortical bone thickness (vertical arrows) in each group. Uninjured 11 week old mice were euthanized and the L4 vertebrae (N-Q) and distal femurs (R-U) were scanned for μCT. L4 vertebrae μCT scans reveals a visualized amount of trabecular bone is present within each group. A trasverse plan on the distal uninjured femurs visually provides the differences of relative cortical bone thickness among each treated group. Calibration scale: bar = 100 μm.

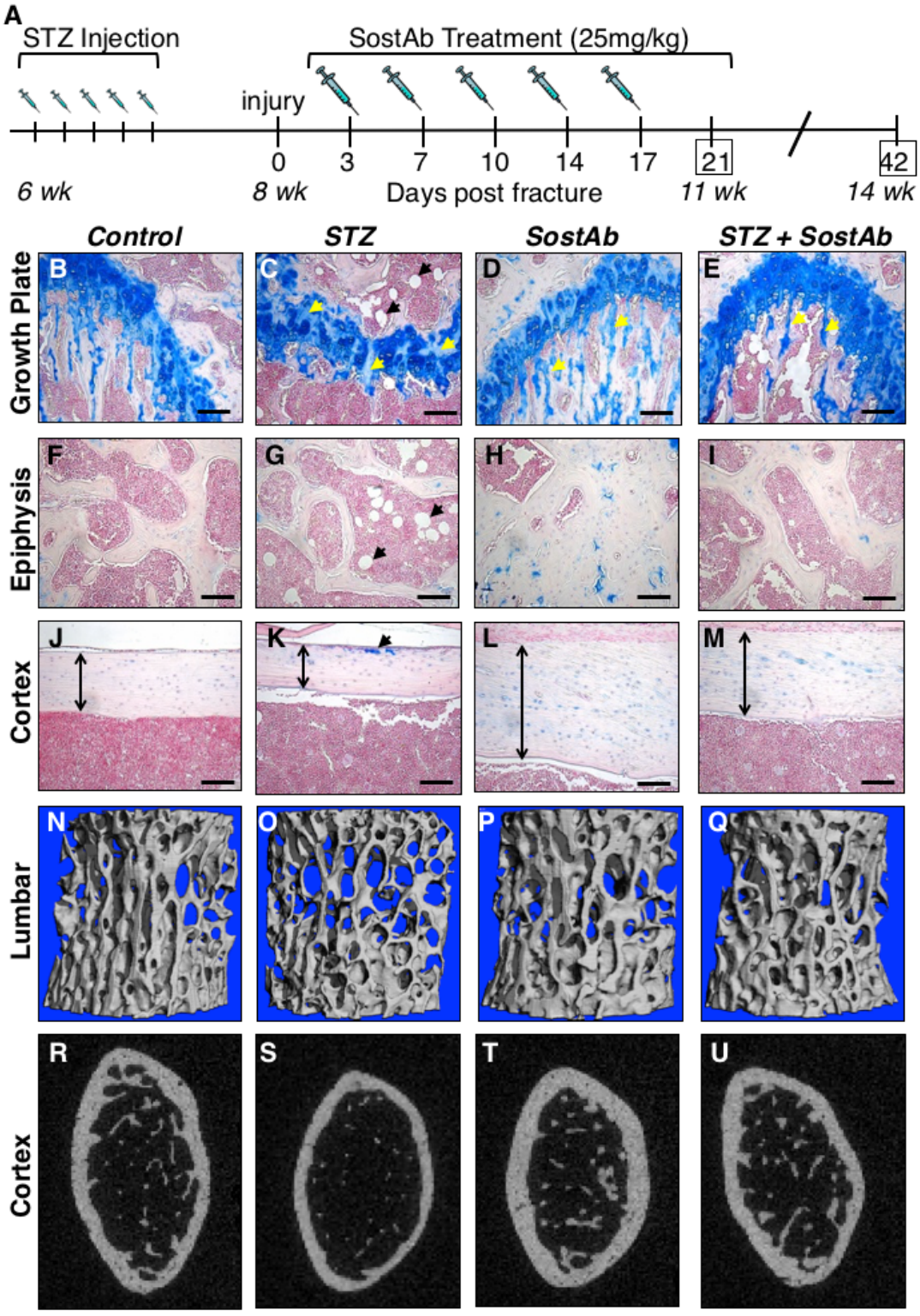
A
STZ Injection
SostAb Treatment (25mg/kg)
injury
0
3
7
10
14
17
21
42
6 wk
8 wk
Days post fracture
11 wk
14 wk
Control
STZ
SostAb
STZ + SostAb
Growth Plate
Epiphysis
Cortex
Lumbar
Cortex
B
C
D
E
F
G
H
I
J
K
L
M
N
O
P
Q
R
S
T
U

Figure 2. Histology and MicroCT reveals SostAb Enhances Endochondral Healing. Histological sections on post fracture (dpf) callus at 11 and 14 weeks of age were all analyzed and observed at the mid regions (diagrams, A). Calluses at 11 weks of age (B-E) and 14 weeks of age (F-I) were sectioned and stained with Alcian Blue and Nuclear Fast Red. Alcian Blue stains the cartilage blue, easily observed in 11 weeks old mice (B-D). Adipocytes, indicated by black arrows (G, I) were observed in the bone marrow, easily seen in calluses of 14 week old mice. Calluses at 11 weeks of age were also scanned for uCT, providing a visual illustration of the amount of woven bone present in the callus (K-N). Calibration scale: bar = 100 μm

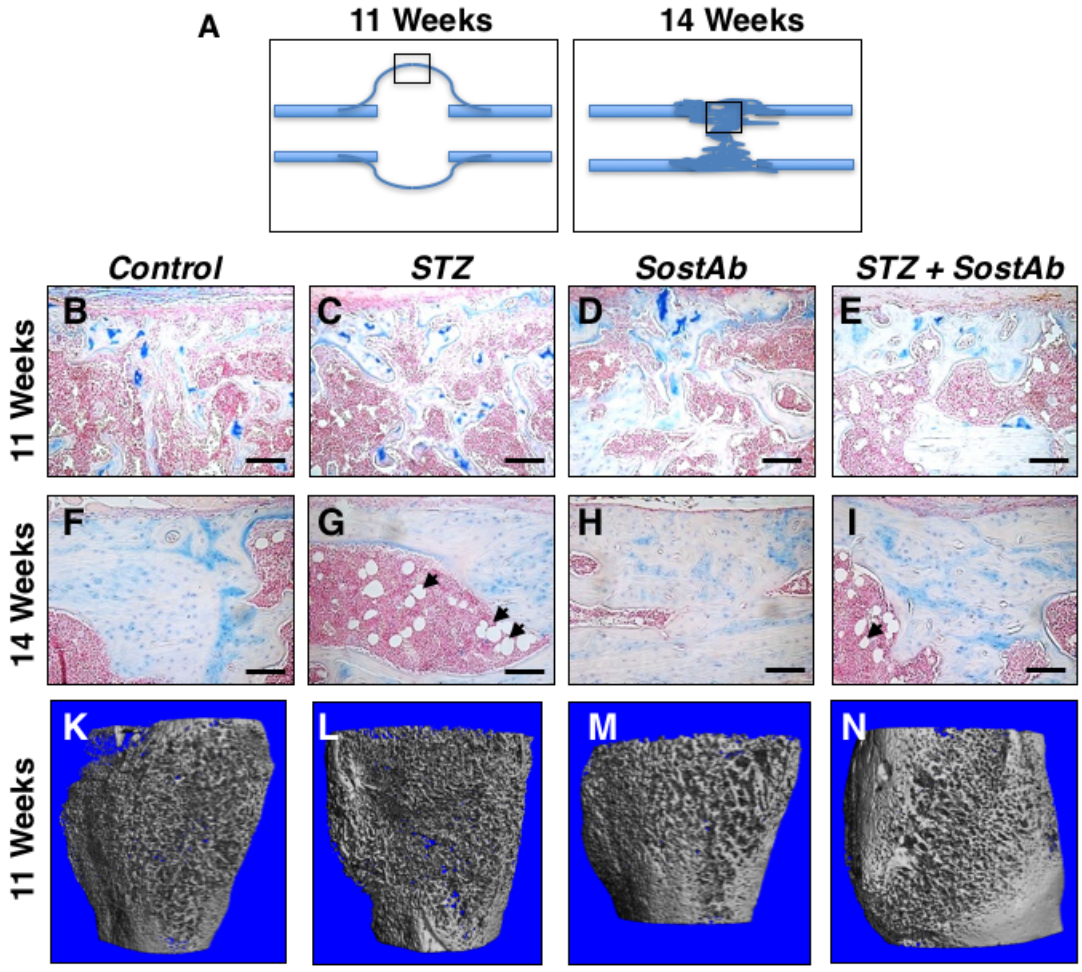

Figure 3. SostAb Rescues Abnormal Osteoblast Maturation in STZ Observed by Immunofluorescence. Fluorescent immunostains callus sections of 11 week old mice were completed with the markers of interest. Secondary antibodies of either green (Alexa Fluor 488) or red (Alexa Fluor 594) were used for detection and DAPI stains the nuclei of cells blue. An early osteoblast marker, osterix, showed osteoblast residing along the surface of the woven bone as indicated by white arrows (A-D). An early osteoblast transcription factor, RUNX2, is shown in panel E-H. Collagen type 1, a protein secreted by osteoblasts, was shown in green within woven bone in panel I-L. A late osteoblast differentiation marker, osteocalcin, and osteocyte marker, DMP1, are represented in panels M-P and Q-T, respectively. Apoptosis marker, activated caspase 3, is shown along the woven bone and in the bone marrow in panel U-X. Negative control slides, see Fig. 8. Calibration scale: bar = 100 μm.

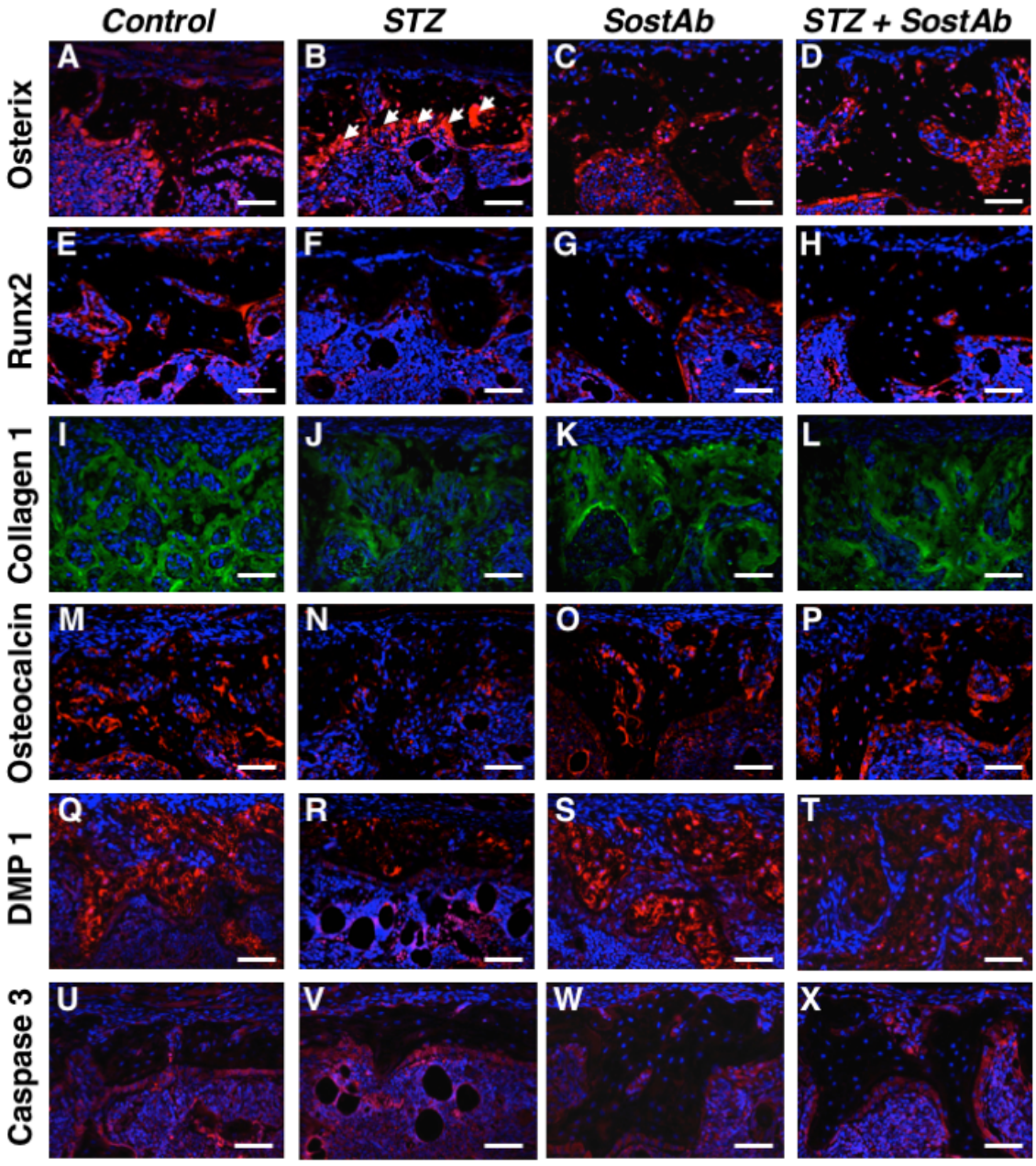
Control
STZ
SostAb
STZ + SostAb
Osterix
Runx2
Collagen 1
Osteocalcin
DMP 1
Caspase 3
A
B
C
D
E
F
G
H
I
J
K
L
M
N
O
P
Q
R
S
T
U
V
W
X

Figure 4. SostAb Anabolic Effect During Repair Continued After Treatment Termination. Calluses in mice at 14 weeks of age were stained with markers of interest by fluorescent immunostaining. Secondary antibodies of Alexa Fluor 488 (green) or Alexa Fluor 594 (red) were used for detection and DAPI stained the nuclei of cells blue. Osterix, an early osteoblast marker, signal was along the surface of the bone in panels A-D. STZ calluses displayed abundant Osterix positive cells residing on the surface of the bone as indicated by the white arrows (B) compared to *Controls* (A). Collagen 1, a protein secreted by osteoblasts, appeared within the bone in panels E-H. DMP1, an osteocyte marker, also appeared within the remodeling bone in panels I-L. Negative control slides, see Fig. 8. Calibration scale: bar = 100 μm.

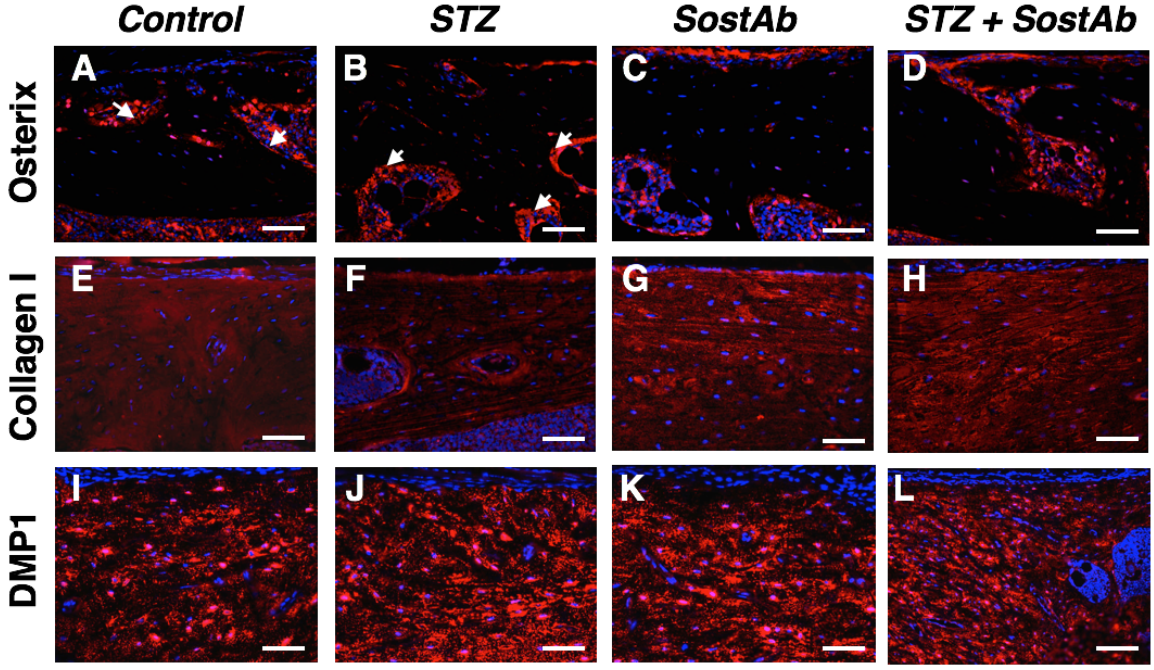

Figure 5. Immunohistochemistry Reveals Altered Wnt Signaling in Treated Groups. Fluorescent immunostains for β-catenin were stained on calluses at 11 (A-D) and 14 weeks of age (I-L). Alexa Fluor 594 (red) was used as a secondary antibody while the cells nuclei was stained with DAPI. Beta-catenin signal is initially expressed along the surface of the bone (A-D) and later within osteocytes during the remodeling stage (I-L). Sost antibody immunohistochemistry on calluses at 11 weeks of age (E-H) and 14 weeks of age (M-P) is expressed with the woven bone and osteocytes during the later stages of healing. Sost serum levels in each treated groups was measured using an ELISA kit for mouse Sost (Q) and represented in ng/ml. p-values <0.05 are statistically significant (asterisks) compared to *Controls*. Negative control slides, see Fig.8. Calibration scale: bar = 100 μm.

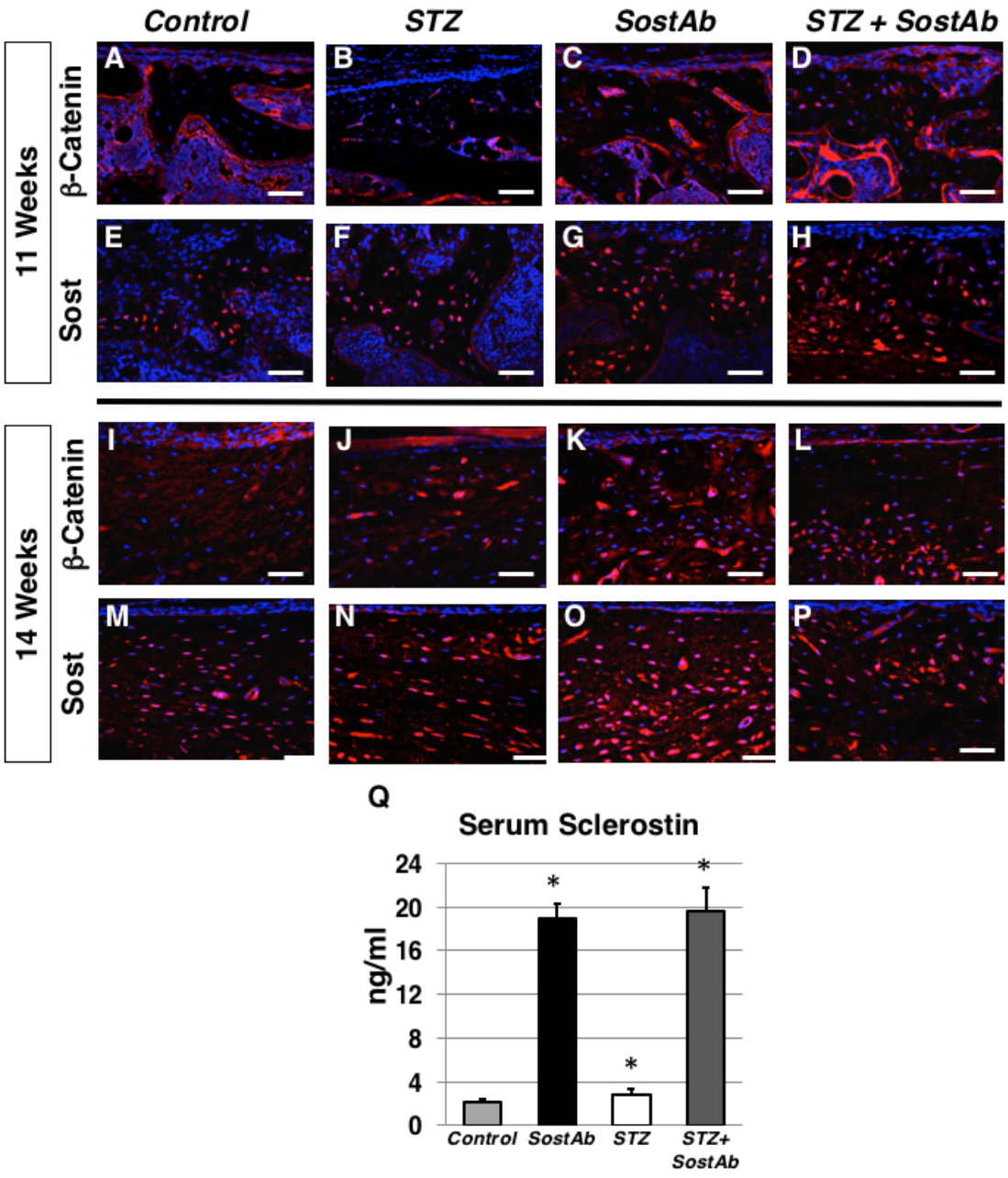
Control
STZ
SostAb
STZ + SostAb
11 Weeks
β-Catenin
Sost
14 Weeks
A
B
C
D
E
F
G
H
I
J
K
L
M
N
O
P
Q
Serum Sclerostin
ng/ml
24
20
16
12
8
4
0
*
*
*
Control
SostAb
STZ
STZ+ SostAb

Figure 6. ***Histology Reveals increased Adipogenesis in STZ mice that is Reversed with SostAb Treatment.*** Masson Trichroms stain (collagen, red; nuclei, black; bone, blue; cartilage, white; adipocytes, empty circles) on uninjured bone sections and fracture callus at 11 weeks of age indicated increased marrow adiposity in STZ mice without injury (A-D, I). During fracture healing, adipogenesis increased in the marrow of all groups, but substantially in *STZ* calluses (E-J). Two-way ANOVA demostrated a diabetic effect in uninjured animals (I), and in fracture calluses, there was a diabetic effect, an antibody effect, and a diabetes x antibody interaction effect. *$p<0.05$, diabetic effect. § $p<0.05$, antibody effect. ❖ $p<0.05$, diabetes x antibody interaction. Calibration scale: bar = 500 μm.

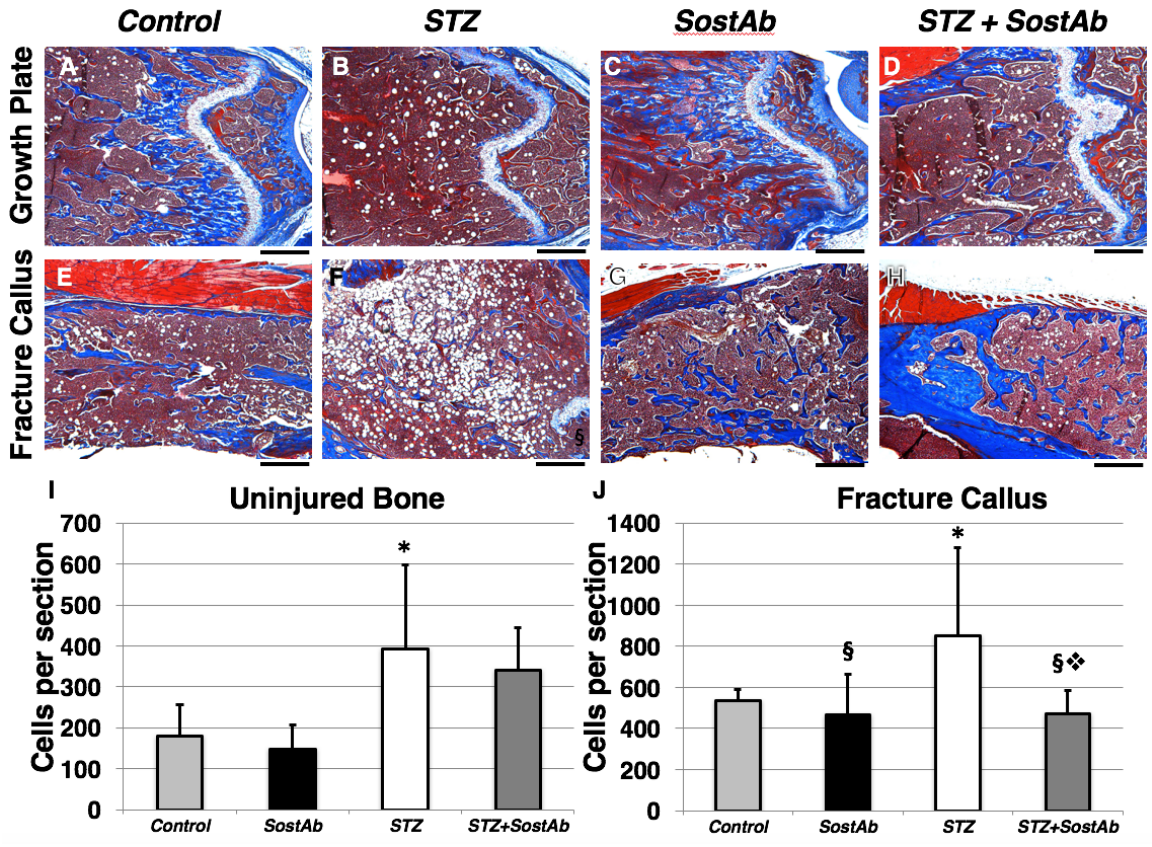

Figure 7. Osteoclast Activity was Unchanged in Treated Groups. Histological sections on uninjured femora of 11 week old mice were stained with TRAP, staining (osteoclasts, red) and counterstained with Fast Green,(bone, blue-green); calibration scale: bar = 500 μm. (A-H). Analysis on osteoclast activity was analyzed at the growth plate (A-D) and epiphysis (E-H), representing the regions of natural osteogenesis and trabecular bone, respectively. No alterations in osteoclast activity was observed, which was confirmed from fluorescence immunohistochemistry on cathepsin K; calibration scale: bar=40 μm (I-L). Trabecular regions just below the growth plate were analyzed. Expression was shown by secondary antibody Alexa 594 (red) along the surface of trabecular bone. Two-way ANOVA was used to quantify Cathepsin K-positive area of growth plate and trabecular bone. Statistical analysis revealed no differences between groups (p>0.05).

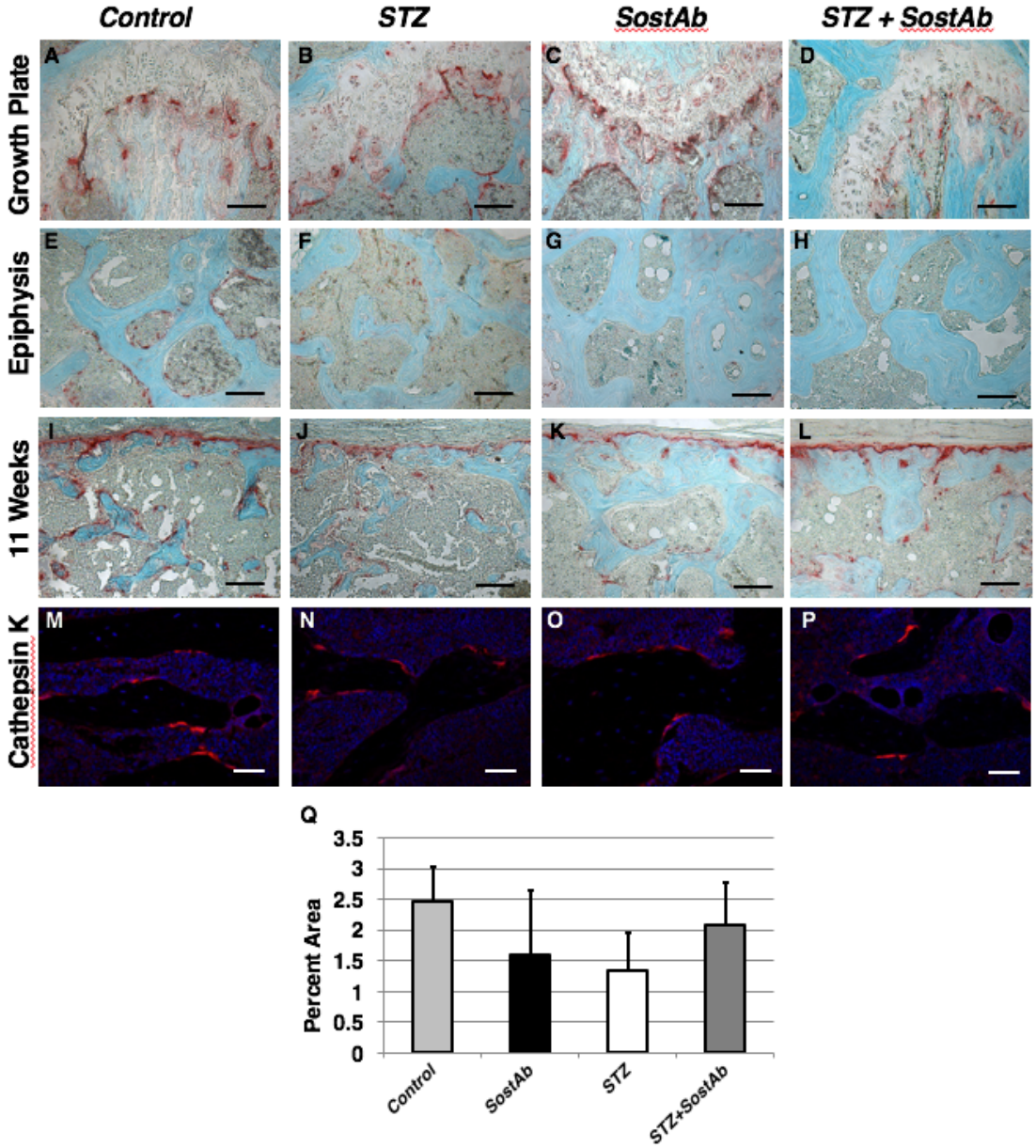

Figure 8. ***Negative Antibody Control Stains Show No Evidence of Cross-reactivity or Non-specific Signal.*** Histological sections on fracture calluses of 11 week old animals were stained with secondary antibodies corresponding to the primary antibodies used in this study. These stains utilized the antigen retrieval methods used for individual antibodies and are as follows: Donkey anti-goat 594 was used with trypsin/EDTA as a negative control for –Sost protein detection (A-D). Goat anti-mouse 594 was used with trypsin/EDTA as a negative control to detect administered mouse monoclonal SOST-neutralizing antibody (*SostAb*) (E-H). Goat anti-rabbit 594 was used with trypsin/EDTA as a negative control for active caspase 3 and osteocalcin (I-L). Goat anti-rabbit 488 was used with Unitrieve as a negative control for Collagen type I (M-P). Goat anti-rabbit 594 was used with Unitrieve as a negative control for SP7/Osterix, DMP1, and Cathepsin K (Q-T). Goat anti-mouse 594 was used with Unitrieve and Proteinase K as a negative control for activated b-catenin and Runx2. Calibration scale: bar = 100 μm.

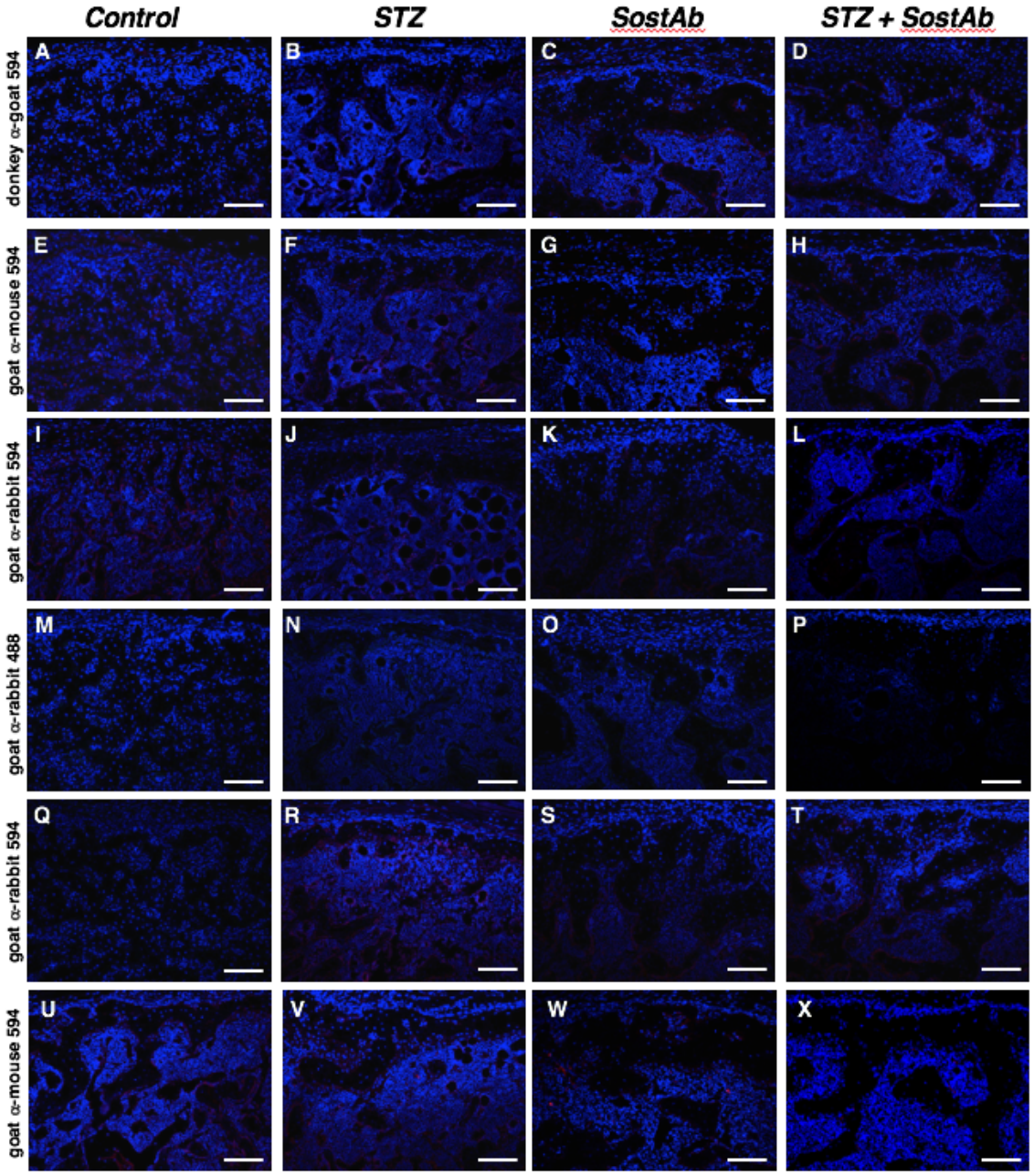
Control
STZ
SostAb
STZ + SostAb
donkey α-goat 594
goat α-mouse 594
goat α-rabbit 594
goat α-rabbit 488
goat α-rabbit 594
goat α-mouse 594
A
B
C
D
E
F
G
H
I
J
K
L
M
N
O
P
Q
R
S
T
U
V
W
X

Table 1. Bone Phenotyping Based on uCT Parameters in the Cancellous Bone Compartment of the L4 Vertebrae and Cortical Bone of uninjured 11-week old Male Mice Compared to Controls.

Index	*Control (n=6)*	*SostAb (n=6)*	*STZ (n=8)*	*STZ + SostAb (n=8)*
BV/TV (%)	0.235±0.038	0.299±0.006§	0.177± 0.010*	0.333± 0.028§⋄
Conn. Dens. (1/mm³)	326.203±22.476	294.848±23.435§	288.401±33.059	272.996±22.562§
SMI (index [1])	0.395±0.219	0.32695±0.030§	0.8251±0.101*	-0.114875± 0.214§⋄
Tb.N (1/mm)	5.490±0.339	5.572±0.165§	5.191±0.219	5.743±0.319§
Tb.Th (mm)	0.042±0.004	0.055±0.000§	0.0350±0.001*	0.057± 0.003§⋄
Tb.Sp (mm)	0.172±0.013	0.165±0.007§	0.183±0.009	0.160±0.011§
BMD (μg HA/cm³)	970.109±14.809	963.635±8.277	951.211±18.037	967.104±7.427
BA/TA (%)	0.393±0.023	0.464±0.020§	0.308±0.035*	0.408±0.026§
BA (mm²)	0.927±0.131	1.143±0.107§	0.635±0.123*	0.909±0.067§
TA (mm²)	2.349±0.235	2.463±0.184§	2.052±0.197*	2.232±0.123§
BMD (μgHA/cm³)	1062.294±9.606	1067.389±12.429§	1049.428±11.972	1069.487±15.893§

Data represents mean ± standard deviation for parameters measured. BV=Bone Volume; TV= Total Volume; Conn. Dens.= Connectivity Density; SMI= Structural Model Index; Tb. N= Trabecular Number; Tb.Th= Trabecular Thickness; Tb.Sp= Trabecular Separation; BMD= Bone Mineral Density; TA= Total Area; BA= Bone Area. §*p*-values <0.05, antibody effect; **p*-values < 0.05, diabetic effect;⋄*p*-values <0.05, diabetic x antibody interaction.

Table 2. Bone Phenotyping Based on uCT Parameters in the Cancellous Bone Compartment of the L4 Vertebrae and Cortical Bone of uninjured 14-week old Male Mice Compared to Controls

Index	*Control (n=9)*	*SostAb (n=9)*	*STZ (n=9)*	*STZ + SostAb (n=8)*
BV/TV (%)	0.223±0.025	0.399±0.025§	0.191±0.027	0.403±0.053§
Conn. Dens. (1/mm³)	317.424±32.066	335.117±34.703§	282.650±23.429	362.147±55.315§⋄
SMI (index [1])	0.392±0.193	-0.653±0.208§	0.601±0.149	-0.844±0.424§⋄
Tb.N (1/mm)	5.417±0.274	6.265±0.255§	5.073±0.263	6.350±0.372§⋄
Tb.Th (mm)	0.041±0.003	0.067±0.004§	0.037±0.003	0.065±0.008§
Tb.Sp (mm)	0.177±0.009	0.148±0.006§	0.188±0.011	0.149±0.009§
BMD (μg HA/cm³)	969.230±11.598	977.497±12.198§	955.274±15.103	976.473±20.533§
BA/TA (%)	0.465±0.015	0.565±0.0127§	0.521±0.034*	0.439±0.020§
BA (mm²)	0.945±0.094	1.084±0.067§	1.030±0.138*	0.771±0.069§
TA (mm²)	2.030±0.190	1.920±0.133	1.971±0.155	1.757±0.117⋄
BMD (μgHA/cm³)	1121.596±16.381	1146.834±11.915§	1123.519±16.748*	1117.314±17.243§

Data represents mean ± standard deviation for parameters measured. BV=Bone Volume; TV= Total Volume; Conn. Dens.= Connectivity Density; SMI= Structural Model Index; Tb. N= Trabecular Number; Tb.Th= Trabecular Thickness; Tb.Sp= Trabecular Separation; BMD= Bone Mineral Density; TA= Total Area; BA= Bone Area. §*p*-values <0.05, antibody effect; **p*-values < 0.05, diabetic effect;⋄*p*-values <0.05, diabetic x antibody interaction.

Table 3. Bone Phenotyping Based on uCT Parameters in the Cancellous Bone Compartment of 21-day and 42-day fracture calluses of Male Mice Compared to Controls

Index	*Control (n=6)*	*SostAb (n=6)*	*STZ (n=6)*	*STZ + SostAb (n=6)*
BV/TV (%)	0.121±0.014	0.206±0.034§	0.132±0.0174	0.199±0.039§
BV (mm^2)	2.814±0.496	4.368±1.543§	1.841±0.414*	3.333±1.258§
TV (mm^2)	23.447±4.642	21.473±7.424	14.429±5.038*	16.458±3.638
BMC (μgHA/cm^3)	172.312±5.433	253.603±25.708§	204.106±17.506*	265.681±33.555§
BMD (μgHA/cm^3)	945.376±15.143	905.870±23.073§	917.758±4.496	908.803±13.723§+
Index	***Control (n=6)***	***SostAb (n=8)***	***STZ (n=7)***	***STZ + SostAb (n=8)***
BV/TV (%)	0.286±0.096	0.388±0.072§	0.234±0.037	0.366±0.056§
BV (mm^2)	1.797±0.31	2.923±0.738	0.952±0.349	2.75±0.474
TV (mm^2)	6.831±2.275	7.747±2.67	4.088±1.516	7.717±1.516
BMC(μgHA/cm^3)	373.075±100.387	425.818±70.307§	279.438±66.801*	412.253±53.769§
BMD (μgHA/cm^3)	1033.059±32.891	1033.101±22.847	1004.713±31.445*	1010.653±14.439

Data represents mean ± standard deviation for parameters measured. 11-week old mouse fracture callus data are presented in the top half of the table, 14 week-old mouse data are presented in the bottom half. BV=Bone Volume; TV= Total Volume; BMC= Bone Mineral Content; BMD= Bone Mineral Density. §*p*-values <0.05, antibody effect; *p-values < 0.05, diabetic effect;+p-values <0.05, diabetic x antibody interaction.

Chapter 3: Akita Mice Fracture Healing Characterization

Abstract

The Akita, a naturally developing diabetic mouse model, has not yet been fully characterized and may represent an alternative diabetic model for future studies in bone metabolism. In this study, I aimed to characterize bone phenotype and fracture healing in Akita mice. Femurs and lumbar vertebrae of 14 week old uninjured Akita and C57BL6 (Control) mice were analyzed using histology and microscale computed tomography (uCT), revealing unchanged bone parameters in both the lumbar vertebrae and the trabecular region of the distal femur. However, Akita mice showed significant decreased bone mineral density and maximum inertia in the cortical region of femurs, indicating increased fracture risk. During fracture repair, smaller calluses and decreased woven bone were observed in Akita mice at 21 days post fracture, while during bone formation at 42 days post fracture, calluses of Akita were less mature and had less bridging formation at the fracture site. The Akita mice can provide another model of diabetes with increase fracture risk and delay fracture healing.

3.1 Introduction

Insulin is a secreted hormone produced by the beta cells of the pancreas and functions to shuttle glucose into cells. Type 1 diabetic mellitus (T1DM), also known as insulin dependent diabetes, occurs when insulin is not adequately produced and causes hyperglycemia. T1DM patients have osteoporotic bones, increased fracture risk, and impaired fracture healing, suggesting that several factors contribute to bone metabolism. Patients with T1DM are treated with insulin, which regulates blood glucose levels, and have shown to improve the osteoporotic and impaired fracture healing observed in T1DM patients and rodents. However, insulin treatment may be an indirect anabolic bone response as the hyperglycemia environment may be a greater contributing factor in impaired fracture healing.

Using a naturally developing diabetic mouse model, such as the Akita mice, may better accurately recapitulate type 1 diabetes in humans. Akita ($Ins2^{+/-}$) mice naturally develop diabetes due to a single point mutation in the Insulin (Ins2) gene that disrupts proper folding for insulin secretion. Heterozygous mice results in naturally developing type 1 diabetes at 4-5 weeks of age, while homozygous mice are post-neonatally lethal [4]. Akita mice are hyperglycemic with a bone loss skeletal phenotype being more severe in male offsprings of diabetic fathers [166]. Previous studies also revealed that Akita mice have decreased anabolic response in bone formation upon mechanical loading, revealing altered osteoblast response in bone reponse to loading [167], as well as having chalky white incisors with decreased enamel mineralization [168]. The Akita mice have an osteoporotic bone phenotype similar to patients with T1DM, and in comparison have a less severe osteoporotic bone phenotype compared to the drug induced diabetic mouse model, Streptozotocin (STZ) mice [52].

Although the Akita bone phenotype have been previously described, characterization of fracture healing in the Akita mice has yet to be investigated. Since T1DM humans and rodent models have shown impaired healing, using the Akita mice in fracture studies may aid in separating out factors involved in impaired healing due to hyperglycemia or to adverse effects of drug iduced diabetic model such as STZ mice.

Understanding impaired healing in the Akita model would provide a diabetic model for testing potential treatement that may improve impaired healing that can more accurately depict treatment effects in diabetic patients. In this study, we aim to characterize impaired fracture healing in Akita mice.

3.2 Materials and Methods

Experimental Animals and Fracture Model

Mice with C57BL6 background were used in this study. Akita (Ins2+/-) mice were purchased from The Jackson Laboratory and were maintained by mating Akita heterozygous males with C57BL6 females. Akita males were confirmed by a blood glucose reading of $\geq$300 mg/dL at 6 weeks of age in addition to genotyping completed by PCR. At 8 weeks of age, mid-femur fractures were completed using a closed Einhorn model, as previously described [141]. Fracture calluses were collected at 21 days and 42 days post-fracture, fixed, and processed for microscale computed tomography (uCT) and histology. Aged matched uninjured mice were dissected and processed for uCT and histology. All animal work was IACUC- approved and performed at the Lawrence Livermore National Laboratory in an AAALAC-accredited facility.

Histology

Uninjured C57BL6 and Akita male bone tissues were dissected, fixed, and processed for histology as previously mentioned in chapter 2 [169]. Briefly, bones were fixed, decalcified, dehydrated, embedded in paraffin blocks, and sectioned. Sectioned femurs were then stained with Alcian Blue and Nuclear Fast Red stain. Photographs were imaged using ImagePro Plus V7.0 software and a QIClick CCD camera.

Micro-CT

Uninjured age-matched femurs, fracture calluses, and L4 vertebraes were fixed and stored in 70% EtOH at 4°C and processed for uCT scans as previously described [169]. Briefly, L4 vertebraes, mid femur cortical bones, distal femur trabecular bones, and fracture calluses were measured and analyzed for bone parameters (uCT 40, SCANCO, Bruttisellen, Switzerland) according to the guidelines for uCT analysis for rodent bone structure [142]: energy 55 kVp, intensity 114 mA, integration time 900 ms, 6 micrometer nominal voxel size. The threshold for “bone” was set at 395 for femur and 421 for L4. To evaluate bone parameters in the distal femur trabecular bone, 240 transverse uCT slices was obtained starting 60 slices below the growth plate, and 20 transverse uCT slices was obtained to evaluate mid femur cortical bone. Bone parameters for the L4 vertebrae was obtained by obtaining transverse uCT slices of the L4 vertebrae. Callus volume (TV) was measured only including the callus tissue and excluding the native bone volume of the original cortical bone and marrow space.

Statistics

All data were expressed as the mean $\pm$ standard deviation. For μCT results, statistical analysis was done using Student’s T-test with a two-tailed distribution, with two-sample equal variance (homoscedastic test). All groups were compared with aged-matched uninjured or fractured C57BL6 male mice; $p \leq 0.05$ was considered significant. Statistical analysis due to limitation of the 21 days post fracture callus Control group was not completed.

3.3 Results

Akita Mice are Hyperglycemic

To confirm the Akita mice are diabetic, blood glucose levels of aged matched C57BL6 and Akita mice were measured (Fig. 1, Table 1). Male C57BL6 mice will be referred to as the Control group and had an average blood glucose level of 200 mg/dl. Akita male mice had a significant increase in blood glucose levels with readings over 500 mg/dl glucose levels, indicating development of diabetes as observed with hyperglycemia, consistent with previous reports [52].

Bone Parameters are Unchanged in Uninjured Akita Mice

Histological sections of 11 week old femurs were stained with Alcian Blue and Nuclear Fast Red, where the cartilage is stained blue. Mid-femur region, examining the cortical bone, and growth plate (Fig.2 A-D) showed a decrease in cortical thickness in the Akita mice and unchanged cartilage proliferation, maturation and trabecular bone along the growth plate. Micro-CT analysis was used to quantify bone parameters of the cortical bone in the femur, trabecular bone in the distal femur region, and trabecular bone in the L4 vertebrae of 11 week and 14 week old Akita and control mice. All bone parameters showed no significant changes between both 11 week and 14 week old Control and Akita mice in the trabecular and cortical bone of the distal femur of 11 week old mice (Table 2). Significant decrease of bone mineral density (BMD), cortical area (Ct.Ar), and maximum inertia (Imax) of the femur cortical bone were apparent in only 14 week old Akita mice compared to age matched Controls (Table 2, Fig. 2 B), suggesting a decrease in bone formation affecting predominately in the cortical bone that is mechanically weak and becomes more severe in mature mice.

Micro-CT scans of the L4 vertebrae in the transverse (Fig.1 E,F) and frontal plan (Fig.1 G,H) showed no obvious changes in trabecular formation. When examining bone parameters of 11 week old L4 vertebrae, there was no changes in bone mineral content (BMC), bone volume/total volume (BV/TV) ratio, and trabecular thickness (Tb. Th.), revealing no changes in trabecular bone formation (Table 3). Although, a significant increase in trabecular number (Tb. N.) and decreased trabecular separation (Tb.Sp.) were observed in 11 week old Akita mice compared to Controls, this was not observed in 14 week old mice. All bone parameters of the L4 vertebrae in 14 week old mice showed no significant changes in the axial skeleton.

Fracture Repair is Modestly Altered in the Akita Mice

Micro-CT scans of fractured calluses at 21 and 42 days post-fracture (dpf) of whole calluses of Control (Fig.3 A,E) and Akita (Fig.3 C,G) and sagittal sections of Control (Fig.3 B,F) and Akita (Fig.3 D,H) reveals progression during fracture healing. At 21dpf, Akita mice appeared to have an overall smaller callus and less woven bone (Fig.3 E,F) compared to Controls (Fig.3 A,B). Bone parameters shows an overall decrease in TV, BV, BMC, and BMD, in Akita 21dpf calluses compared to Controls (Table 4), revealing decreased woven bone within the fracture site. At 42dpf, calluses of Akita mice have more persistent woven bone and less bridging at the site of injury (Fig.3 G,H) compared to Controls (Fig.3 C,D). Akita calluses at 42dpf also have a significant larger TV and decreased BV/TV (Table 4), suggesting a less mature and delayed fracture healing.

3.4 Discussion

Impaired fracture healing observed in diabetic mouse models shows variations in contributing factors during bone remodeling. We observed bone parameters and fracture healing in Akita mice that may be a better representative of what is occurring in bone metabolism and healing in type 1 diabetic humans.

Akita mice were confirmed to be diabetic with a significant increase in hyperglycemia in blood glucose levels compared to C57BL6 (Control) group. This hyperglycemia condition was consistent with a previous report on the high glucose levels compared to C57BL6 mice and STZ [52]. Since Akita mice are a type 1 diabetic mouse model, which have been shown to have an osteoporotic bone phenotype, we first examined uninjured bone parameters in Akita compared to Control group. Contrary to a previous report of Akita mice having a significant decrease in trabecular bone in the femur [52], our uninjured Akita femurs of 11 and 14 week old mice showed no significant bone loss compared to Controls. However, a significant decrease in bone formation in the mid-femur cortical bone region of 14 week old Akita mice was observed, revealing differences in bone metabolism within the regions of the femur. There are several possibilities for the differences observed in the bone parameters of the Akita mice in our colony and those examined by Coe et al., 2013 [52], that could be either technical or environmental. One possible contributor to the observed differences could be a result of μCT instrument settings employed to obtain the μCT measurements. Another possibility could be due to animal care facility conditions. Each facility carries its own set of pathogens which in turn could alter the gut microbiota of the colony. Differences in the gut microbiota could have a dramatic impact on bone metabolism, as previously described where germ free mice have higher bone mass than mice grown in a conventional facility [170]. Uninjured Akita mice also displayed a significant decrease in bone mineral density and maximum inertia (Imax) in the cortical mid-femur region only at 14 weeks of age. This reveals a mechanically weak bone structure and increase fracture risk, which appears to worsen as the disease progresses.

Since fracture healing may reveal differences in bone parameters between Akita and Control mice that were not observed in uninjured femurs, we characterized 21dpf and 42 dpf calluses to determine if Akita mice have impaired fracture healing based upon uCT analysis. During endochondral bone formation, where woven bone is formed within the callus, the Akita mice displayed an overall smaller callus size and decreased formation of woven bone, an indication of delayed fracture healing. Previous studies on fracture repair in diabetic mice have also shown smaller callus size and less bone formation that can contribute to impaired healing [169]. At 42 dpf, Akita have less mature calluses as observed with persistent woven bone and less bridging at the site of injury, suggesting that delay healing persists during the later bone remodeling stage. Decrease bone formation is further supported in uCT analysis, however bone mineral density and bone mineral content is unaltered, indicating that mineralization is not altered. It is currently understood that the hyperglycemic environment can decrease osteoblast differentiation and activity [15] resulting in altered bone remodeling; which is likely what is occurring in delayed fracture repair observed in Akita mice.

The Akita bone phenotype having an unaltered trabecular bone and decreased cortical bone that is mechanically weak may accurately represent the bone phenotype of a young human with type 1 diabetes since bone loss increase/worsens as the duration of diabetes progresses [18]. Additionally, bone phenotype of children upon a 5-year duration of diabetes reveals unaltered changes in bone phenotype [171], suggesting that the bone phenotype in Akita at 11 and 14 weeks of age may represent an early onset of diabetes in adolescences since C57BL6 mice reaches peak bone mass at 4-6 months of age [172]. This may accurately portray a recently diagnosed diabetic child with unaltered bone mineral density but have increased fracture risk due to mechanically weak bones and can be beneficial in long-term disease progression studies on bone metabolism and fracture healing.

Figure 1. Blood Glucose Levels of Akita Mice. Blood glucose levels were measured at 6 weeks of age to confirm hyperglycemia with a of ≥300 mg/dL. p-value of ≤0.05 were considered significantly different (asterix).

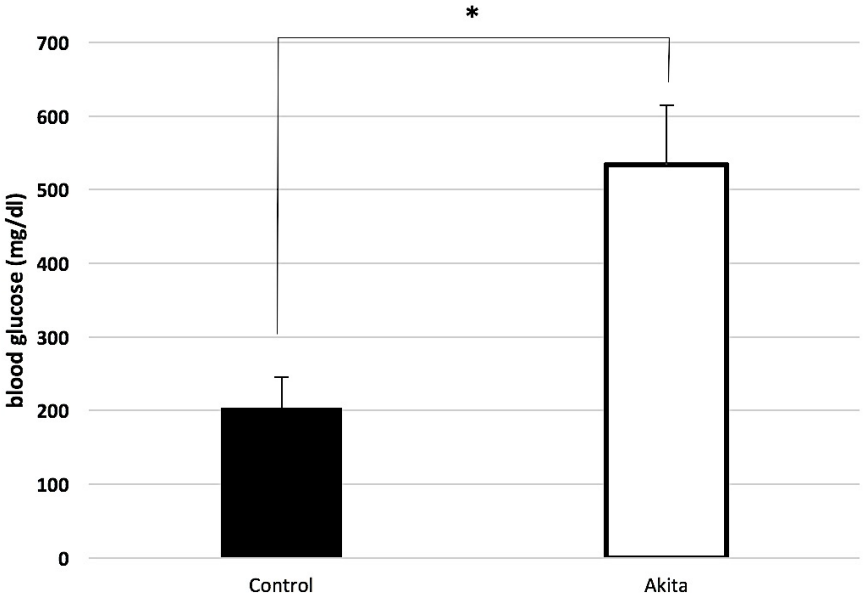

Figure 2. Akita Mice has Insignificant Changes Compared to Controls. Histological sections on 11 week old uninjured Control and Akita were stained with Alcian Blue and Nuclear Fast Red with cartilage and unmineralized bone stained blue. Histology stains were analyzed and observed at the mid-femur regions (A,B) and growth plate (C,D). White circles (indicated by black arrows) show adipocytes in the bone marrow. MicroCT scans of the transverse (E,F) and frontal (G,H) plan of the L4 vertebrae show visualized trabecular bone within each group.

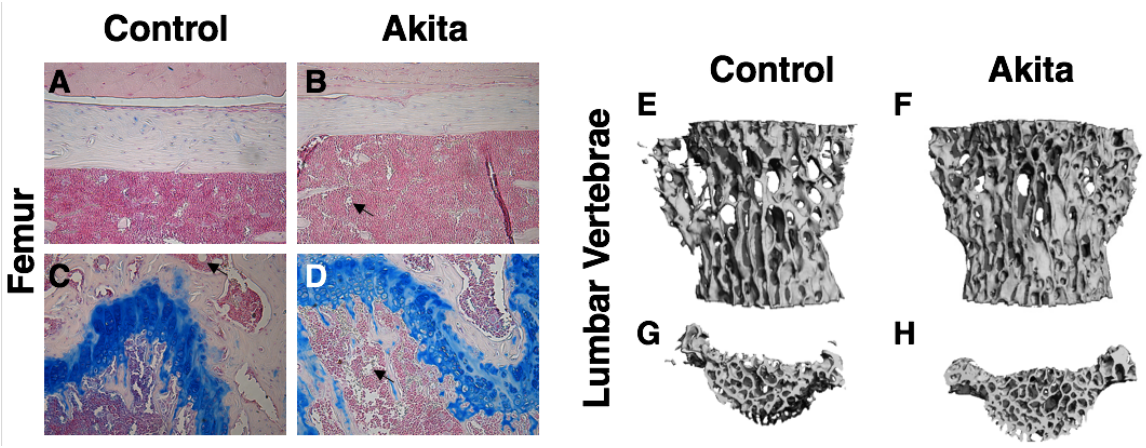

Figure 3. Akita Mice Have Delayed Fracture Healing. MicroCT scans of fracture calluses at 21 days post fracture (A,B,E,F) and 42 days post fracture (C,D,G,H) show fracture sizes within each group. Whole callus sections (A,E,C,G) and sagittal microCT scans (B,F,D,H) show visualized amount of woven bone present.

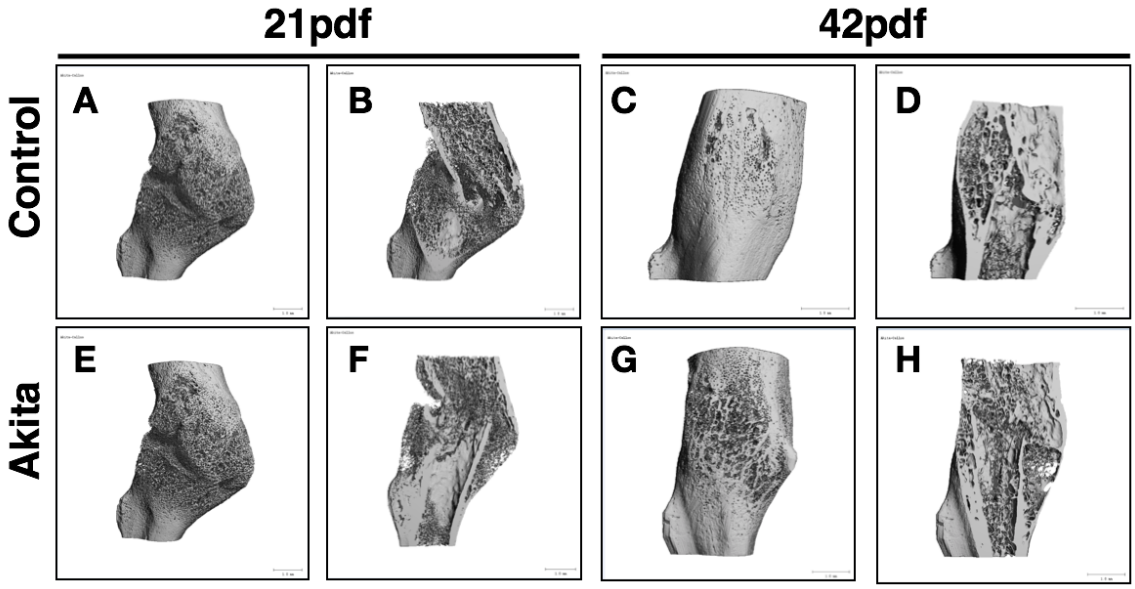

Table 1. Blood Glucose Levels in Control and Akita Male Mice at 6 Weeks of Age

	Control (n=165)	*Ins2+/- (n=142)*
Glucose (mg/dl)	203.572±41.494	533.818±80.320*

Data represents mean ± standard deviation for blood glucose levels.
*p-value ≤ 0.05 compared to control.

Table 2. Bone Phenotyping Based on Micro-CT Parameters data on Trabecular Bone Compartment of the Distal Femur Region and Cortical Bone of Uninjured 11 and 14 Week Old Akita Male Mice Compared to Controls

Trabecular				
	11-week old		**14-week old**	
	Control (n=10)	*Akita (n=11*	*Control (n=8)*	*Akita (n=5)*
BMC	143.90±41.53	142.24±44.59	142.9±36.82	130.30±24.94
BMD	933.17±14.17	939.02±17.9	942.85±16.23	951.9±10.11
BV/TV	0.12±0.038	0.123±0.040	0.121±0.035	0.109±0.024
Tb.Th.	0.038±0.004	0.037±0.008	0.038±0.006	0.037±0.005
Tb.N.	4.86±0.411	4.891±0.541	4.72±0.280	4.464±0.288
Tb.Sp	0.197±0.017	0.198±0.026	0.201±0.013	0.214±0.015
Cortical				
	11-week old		**14-week old**	
	Control (n=10)	*Akita (n=11)*	*Control (n=8)*	*Akita (n=5)*
Imax	0.303±0.063	0.289±0.077	0.344±0.057	0.284±0.020*
Ma. Ar	1.16±0.055	1.182±0.070	1.245±0.091	1.118±0.062
Ct Ar	0.848±0.12	0.811±0.162	0.907±0.104	0.858±0.029*
Tt. Ar	2.01±0.131	1.993±0.198	2.15±0.173	1.976±0.086
Ct. Ar/Tt. At	0.42±0.034	0.403±0.052	0.42±0.022	0.434±0.010*
BMD	1116.1±31.15	1133.1±29.16	1163.29±23.68	1152.26±14.05*

Data represents mean ± standard deviation for parameters measured. BMC= Bone Mineral Content; BMD= Bone Mineral Density; BV= Bone Volume; TV= Total Volume; Tb. Th.= Trabecular Thickness; Tb. N.= Trabecular Number; Tb. Sp. = Trabecular Separation; Imax= Maxium Inertia; Ma. Ar= Marrow Area; Ct. Ar= Cotrical Area; Tt. Ar= Total Area. *p-value ≤ 0.05 compare to controls.

Table 3. Bone Phenotyping Based on Micro-CT Parameters in the Trabecular Bone Compartment of the L4 Vertebrae of Uninjured 11 and 14 Week old Akita Male Mice Compared to Controls

Trabecular				
	11-week old		**14-week old**	
	Control (n=10)	*Akita (n=11)*	*Control (n=8)*	*Akita (n=5)*
BMC	236.98±36.59	231.85±40.55	240.497±26.525	236.11±17.804
BMD	964.58±14.72	968.20±15.48	976.558±12.345	976.62±12.75
BV/TV	0.205±0.033	0.202±0.035	0.207±0.024	0.203±0.016
Tb.Th.	0.038±0.003	0.035±0.004	0.0383±0.004	0.036±0.002
Tb.N.	5.23±0.372	5.612±0.413*	5.244±0.305	5.300±0.206
Tb.Sp	0.184±0.014	0.171±0.0146*	0.183±0.016	0.180±0.009

Data represents mean ± standard deviation for parameters measured. BMC= Bone Mineral Content; BMD= Bone Mineral Density; BV= Bone Volume; TV= Total Volume; Tb. Th.= Trabecular Thickness; Tb. N.= Trabecular Number; Tb. Sp.= Trabecular Separation. *p-value ≤ 0.05 compared to control.

Table 4. Bone Phenotyping Based on Micro-CT Parameters in 21 and 42 days post fracture calluses of Akita Male Mice Compared to Controls

	21dpf		42 dpf	
	Control (n=1)	***Akita (n=7)***	***Control (n=4)***	***Akita (n=9)***
TV	50.65± n/a	32.36±8.20	10.33±3.50	16.78±4.44*
BV	7.68± n/a	5.78±1.19	3.31±0.31	3.72±0.72
BV/TV	0.15± n/a	0.18±0.03	0.35±0.12	0.23±0.05*
BMC	7.52± n/a	5.62±1.25	3.24±0.44	3.72±0.81
BMD	982.40± n/a	968.96±25.91	976.25±62.69	996.19±33.28

Data represents mean ± standard deviation for parameters measured. TV= Total Volume; BV= Bone Volume; BMC= Bone Mineral Content; BMD= Bone Mineral Density. *p-value $\leq$ 0.05 compared to control.

Chapter 4: *Sostdc1* Deficiency Accelerates Fracture Healing by Promoting the Expansion of Periosteal Mesenchymal Stem Cells

Abstract

Loss of *Sostdc1*, a growth factor paralogous to *Sost*, causes the formation of ectopic incisors, fused molars, abnormal hair follicles, and resistance to kidney disease. *Sostdc1* is expressed in the periosteum, a source of osteoblasts, fibroblasts and mesenchymal progenitor cells, which are critically important for fracture repair. Here, we investigated the role of *Sostdc1* in bone metabolism and fracture repair. Mice lacking *Sostdc1* (*Sostdc1*$^{-/-}$) had a low bone mass phenotype associated with loss of trabecular bone in both lumbar vertebrae and in the appendicular skeleton. In contrast, *Sostdc1*$^{-/-}$ cortical bone measurements revealed larger bones with higher BMD, suggesting that Sostdc1 exerts differential effects on cortical and trabecular bone. Mid-diaphyseal femoral fractures induced in *Sostdc1*$^{-/-}$ mice showed that the periosteal population normally positive for *Sostdc1* rapidly expands during periosteal thickening and these cells migrate into the fracture callus at 3 days post fracture. Quantitative analysis of mesenchymal stem cell (MSC) and osteoblast populations determined that MSCs express *Sostdc1,* and that *Sostdc1*$^{-/-}$ 5 day calluses harbor >2-fold more MSCs than fractured wildtype controls. Histologically a fraction of *Sostdc1*-positive cells also expressed nestin and α-smooth muscle actin, suggesting that *Sostdc1* marks a population of osteochondral progenitor cells that actively participate in callus formation and bone repair. Elevated numbers of MSCs in D5 calluses resulted in a larger, more vascularized cartilage callus at day 7, and a more rapid turnover of cartilage with significantly more remodeled bone and a thicker cortical shell at 21 days post fracture. These data support accelerated or enhanced bone formation/remodeling of the callus in *Sostdc1*$^{-/-}$ mice, suggesting that *Sostdc1* may promote and maintain mesenchymal stem cell quiescence in the periosteum.

4.1 Introduction

Optimal fracture repair requires contribution from surrounding tissues, yet we know very little about the interactions between bone, muscle, vasculature, and the periosteum [173-175]. In particular the periosteum, a thin tissue that covers the outer cortical bone surface, contains a reservoir of progenitor cells that contribute to bone repair; further, periosteal grafts and alpha-smooth muscle actin (α-SMA)-positive cells integrate into the callus after fracture [105, 175]. Other *in vivo* studies have shown that periosteal and perivascular cells migrate into developing bone and bone undergoing repair, and differentiate into osteoblasts [105, 176].

Sostdc1, a paralog of *Sost* also known by several other names including *Sost-Like*, *Wise*, *Ectodin* and *Usag-1* arose by segmental gene duplication and was previously studied in the context of tooth development, kidney disease, cancer progression, hair follicle formation, and embryo implantation [103, 177-181]. Recently, we have shown that *Sostdc1* also contributes to limb morphogenesis [104], and its expression in the periosteum suggests that it may also play a role in bone maintenance and repair. However, the role of Sostdc1 in fracture healing has not been investigated. Sostdc1 has been described as both a Bmp and a Wnt antagonist in a context-dependent manner [182], and it interacts with Lpr4, 5, and 6 Wnt co-receptors and with

Bmp ligands [3, 103, 182-184], *in vivo*. While Sostdc1 shares 55% protein sequence homology to its paralog Sost, it reportedly displays higher specificity for the Lrp4 co-receptor [183], in contrast to the preferred binding to the Lrp5 and 6 co-receptors by Sost [85, 137]. Mesenchyme-derived Sostdc1 inhibits Wnt signaling in the epithelium through the activation of Hedgehog signaling, which in turn suppresses Wnt signaling *via* Sostdc1 up-regulation in the mesenchyme [185, 186].

To determine the contribution of Sostdc1 to bone metabolism and repair, we characterized trabecular and cortical bone structure and fracture healing program in *Sostdc1*$^{-/-}$ mice. Herein we show data in support of *Sostdc1* as both an anabolic and a catabolic agent, with distinct compartmental contributions to bone metabolism, wherein *Sostdc1* deficiency results in a substantial loss of trabecular bone and a significant gain in cortical bone. We find that *Sostdc1* marks a population of progenitor stem cells of mesenchymal origin that rapidly expands after injury and populates the callus up to 7 days post-fracture. In addition, we show that in the early stages of fracture repair, *Sostdc1*$^{-/-}$ cells increase β-catenin-dependent Wnt signaling and promote callus formation *via* enhanced progenitor cell migration and differentiation. At early stages post-fracture (3 and 7 days post fracture), *Sostdc1*$^{-/-}$ mice show enhanced intramembranous bone formation and neovascularization compared to controls, along with dramatically elevated numbers of cells expressing nestin, α-SMA, and SP7/Osterix. Although the genetic loss of *Sostdc1* results in trabecular bone loss, *Sostdc1* may represent a novel therapeutic target for bone formation defects that require rapid intramembranous bone formation to stabilize structural integrity.

4.2 Material and Methods

Animals and Femoral Fracture Model

Sostdc1$^{-/-}$ mice have been previously described [186]. Stabilized femoral fractures were produced in *Sostdc1*$^{-/-}$, *Sostdc1*$^{+/-}$ and *C57B/L6* wildtype control male mice at 8-weeks of age using an Einhorn closed fracture model, as previously described in chapter 2 [141]. Fractures were confirmed radiologically (CareStream *in vivo* MS-FX) at the time of surgery and femora were harvested at days 3, 5, 7, 10, 14, 21 and 28 post-fracture for subsequent analysis. Animal studies were approved by the Institutional Animal Care and Use Committee of Lawrence Livermore National Laboratory (Livermore, CA, USA).

LacZ and Immunohistological Staining

The *Sostdc1* knockout allele was generated by replacing both *Sostdc1* exons with an in-frame *LacZ* reporter [177]. *LacZ* stains were performed on fixed tissues (fractured and intact femora at days 3, 7, 10, 14, and 21 post-fracture, n=3 per group, per time point, male mice) of *Sostdc1*$^{+/-}$ and *Sostdc1*$^{-/-}$ mice as previously described [187] with minor modifications. Tissues were fixed and then decalcified in 0.5M EDTA until endpoint confirmation by radiotranslucency. *LacZ* stain was followed by fixation, dehydration, and paraffin embedding for sectioning (6μm) and histology. Sections were counterstained with alcoholic eosin. For immunostains, femora from *Sostdc1*$^{-/-}$ or *Sostdc1*$^{+/-}$ mice, with or without fractures (n=3 per group of male mice, per time point), were fixed for 72 hours in 10% neutral buffered formalin at 4^{o}C, followed by decalcification and sectioning as above. Antigen retrieval was conducted using Uni-

trieve (Innovex) for 30 minutes at 65°C unless otherwise stated. Antigen retrieval for activated β-catenin (Millipore, 05-665) included digestion with Proteinase K (15μg/ml) for 20 minutes at 37°C followed by Rodent Block M (Biocare Medical, 50-832-64). Primary antibodies for α-Smooth Muscle Actin (α-SMA) (abcam, ab5694), β-galactosidase (abcam, ab9361), nestin, (abcam, ab6142) and SP7/osterix (abcam, ab22552) were incubated on slides overnight at RT followed by secondary antibody conjugated with Alexa Fluor 488 or 596 (Molecular Probes) for green and red stains, respectively. Immunostained slides were mounted with Prolong Gold with DAPI (Molecular Probes) for imaging. Images were obtained with a color CCD QIClick camera and ImagePro Plus V7.0 imaging software. Quantification of immunostains was performed using Image J software, utilizing the Analyze Particles tool, to determine the total area of stem cell marker-positive cells. A minimum of 50 images of similar callus regions from n=3 animals per group per time point were used. This quantification was not absolute, but provided an estimate for the magnitude of the observed differences seen between genotypes.

Micro-Computed Tomography (μCT) of intact and fracture calluses

Sostdc1$^{-/-}$ and *C57B/L6* wildtype control male mice at 5.5 months of age were analyzed by μCT at the distal femoral metaphysis, femoral mid-diaphysis, and L4 vertebral body to determine bone micro-structure parameters (n=6-10 per group) (μCT 35, SCANCO, Brüttisellen, Switzerland) according to the guidelines for μCT analysis of rodent bone structure [142]: energy 55 kVp, intensity 114 mA, integration time 900 ms, 6 μm nominal voxel size. For fracture analysis, callus measurements were compared at 28 days post fracture between *Sostdc1*$^{-/-}$ and *WT,* 3 month old, age-matched animals. Intact femora of *Sostdc1*$^{-/-}$ and *C57B/L6* animals were also measured at 12 weeks of age. The threshold for "bone" was set at 350 (35% of maximum value), which is approximately equal to 567 mg HA/cm^3. Callus volume measurements (CV) excluded the native bone volume.

Bone Histomorphometry Measurements

Dynamic bone histomorphometry measurements were obtained from femoral mid-diaphyses of 12 weeks and 5.5 month old male mice. Mice were injected with 30 mg/kg alizarin red and 10 mg/kg calcein 10- and 3- days before euthanasia. Femora were dissected and fixed in 10% neutral phosphate-buffered formaldehyde for 24 hours. Bone histomorphometry was performed using semiautomatic image analysis as described [188, 189]. Briefly, histomorphometry is a method that measures the bone architecture and provides a quantitative analysis of the bone cellular activity. Fluorochrome labels, alizarin red and calcein, are incorporated into newly calcified bone upon administration in mice at 10- and 3- days before euthanasia. The fluorochrome labels that are incorporated into mineralized bone is measured under fluorescent light to obtain dynamic parameters of bone turnover.

Bone Strength Measurements

Fractured and uninjured contralateral femora of male mice were mechanically tested in torsion to quantify biomechanical properties of bone (n=8-10 per group). Femora were rehydrated in isotonic saline for 5-10 minutes prior to testing, and were kept hydrated throughout testing. Both ends of each femur were embedded in Wood's

metal alloy blocks with a testing length of 6 mm, then mounted in a materials testing system (Bose ELF 3200, Eden Prairie, MN) with torsion motor (Exlar SLM Series). An axial load of 3-4 N was applied, then 10 preconditioning torsion cycles were applied to +/- 5° at 0.1 Hz, followed by a single cycle to failure in external rotation at 1°/s. Torque and rotational displacement data were collected at 50 Hz. The failure cycle was used to calculate torsional stiffness, ultimate torque, and rotation at ultimate torque.

Analysis of Stromal Bone Cells

Unfractured and fractured femora at 8-10 weeks of age male mice were dissected and placed in 1x Hank's Balanced Salt Solution (HBSS) pH7.2 without serum. Bone digestion was performed as described [190]. Briefly, bones were crushed in 1x HBSS using a mortar and pestle and bone marrow cells were washed away from the bone chips. The bone chips were then transferred to a 50 ml conical tube with 2.0 ml of 3.0 mg/ml Type I Collagenase (Worthington, Lakewood, NJ) and digested in a shaker at 110 rpm at 37ºC for 1 hour. The supernatant from the digest was transferred through a 70 micron filter into a fresh conical tube, the remaining bone chips were rinsed with additional 1x HBSS containing 2% FCS, which was added to the supernatant. Cells were then pelleted at 1200 rpm for 5 minutes at 4ºC. Live cell yield was counted using a hemocytometer and Trypan blue staining. Cells were then prepared for flow cytometric analysis. Cells were transferred to 96 well V-bottom plates and stained with an antibody cocktail containing anti CD16/32 (clone 93), and PE-Cy7 conjugated anti-CD3 (2C11), CD4 (GK1.5), CD8 (53.6.7), CD11b (M1/70), CD19 (6D5), NK1.1 (PK136), Ter119 (TER119), and Gr1 (RB6-8C3) in 50 μl volume of FACS Buffer for at least 15 minutes at 4ºC. Cells were then washed and pelleted for 5 minutes at 2000 rpm, and stained with a second antibody cocktail containing CD45-eFluor 450 (30F11), Sca1-FITC (D7), CD31-APC (390), and either CD51-biotin (RMV-7) or isotype-matched biotin control Ab. Cells were incubated at 4ºC for 15 minutes, washed, and pelleted. Lastly, cells were stained with streptavidin-PE for 5 minutes, washed, pelleted and resuspended in FACS buffer for analysis. Propidium iodide was added to the samples before analysis as a viability stain. Live cells were analyzed on a BD LSR II flow cytometric analyzer and data analysis was performed using FlowJo software. Antibodies were purchased from BioLegend and eBioscience.

Gene Expression Analysis

Bone derived mesenchymal stem cells (MSCs) cells were stained as above, except that Sca1-Brilliant Violet 510 (BioLegend) was used. MSCs, OBs and endothelial cells were isolated using the BD FACS Aria II flow cytometry sorter, and then pelleted and resuspended in Trizol (Qiagen). Total RNA was purified using RNeasy mini Kit (Qiagen) according to manufacturer's protocol. Samples were analyzed for purity and concentration using a NanoDrop 2000c (Thermo Scientific). Superscript III First-Strand Synthesis System (Invitrogen) was used with oligo dT primers for reverse transcription according to manufacturer's protocol. Real-time quantitative PCR was then performed with SYBR Select Master Mix (Applied Biosystems) using an Applied Biosystems 7900HT Fast Real-Time PCR System with the following cycling conditions: 50°C for 2 min for Sybr then 95°C for 3 min (2 min for SYBR), followed by 40 cycles of 95°C for 3s (10s for SYBR) and 30s at 60°C. Reactions were run on a 2% agarose gel then DNA fragments imaged under UV light. Primers: β-galactosidase forward

ACGGCCAGGACAGTCGTTTG and reverse CCGCTCATCCGCCACATATC; GAPDH forward CCAATGTGTCCGTCGTGGATCT and reverse CCTCAGTGTAGCCCAAGATGC.

Statistics

Data are expressed as the mean ± standard deviation. For statistical analysis, we used *Student's t-test* with a two-tailed distribution, and two-sample equal variance (homoscedastic), for significance. $p < 0.05$ was considered significant.

4.3 Results

Sostdc1 deletion decreases trabecular and increases cortical bone volume

Sostdc1$^{-/-}$ mice displayed 31% lower trabecular bone volume fraction (BV/TV) in the distal femoral metaphysis and 35% less in the L4 vertebral body compared to controls ($p<0.05$). Connectivity density ($p<0.005$), and trabecular number ($p<0.0005$) were also reduced 30% and 18%, respectively in the distal femur. Trabecular separation ($p<0.005$) was increased 28% in the femur and 31% in L4, consistent with a lower trabecular bone volume phenotype. However, bone tissue BMD (mg HA/cm^3) was increased in the cortical bone, relative to *WT* ($p \leq 0.05$) (Table 1). In contrast to the trabecular compartments, the cortical compartment indicated that the bones (total area, TA) were larger (TA 2.02 vs 2.35, $p<0.05$). The cortical total area was increased by 16%, and the marrow area was enlarged by 21% ($p<0.01$) (Table 1). These data show that Sostdc1 modulates bone metabolism differently in the cortical than in the trabecular compartments of bone.

Sostdc1*$^{-/-}$ *mice exhibit enhanced cortical bone formation

Histomorphometric analysis of mid-femur regions of 5.5 month old mice on the periosteal and endocortical surfaces indicated enhanced bone formation in *Sostdc1*$^{-/-}$ mice, with a significant increase in mineralized surface (MS/BS) and 78% increase on the periosteal surface ($p<0.035$). An 8% increase on the endocortical surface was also observed, but this change was not statistically significant. We also observed a 30% increase in the bone formation rate (BFS/BS) on the periosteal surface of *Sostdc1*$^{-/-}$ mice compared to *WT* controls, indicating significantly more active bone formation on the periosteal surface compared to the endocortical surface. There was a significant 32% decrease in BFR/BS ($p=0.0497$) and 42% decrease in mineral apposition rate (MAR) ($p<0.00013$) on the endocortical surface and no change on the periosteal surface in *Sostdc1*$^{-/-}$ mice compared to *WT* controls (Table 2). The decreased change in both MAR and BFR/BS suggests that the endocortical region of *Sostdc1*$^{-/-}$ femora has a reduced remodeling rate, which, combined with the more active bone formation rate on the periosteal surface, contributes to the high bone mass phenotype and larger bone morphology observed in the cortices of *Sostdc1*$^{-/-}$ femora. In addition, we compared intact mid-diaphyseal µCT data of 5.5 months to 12 weeks of age data (Fig. 7A). None of the parameters measured (Table 1) changed statistically as a function of age or genotype. Furthermore, cortical reconstruction images do not indicate cortical thinning or enlargement indicative of premature aging in *Sostdc1*$^{-/-}$ mice (Fig. 7B,C). These data show that lack of *Sostdc1* promotes periosteal cortical bone formation, suggesting that Sostdc1, similarly to Sost, acts as a negative regulator of bone formation, although its function is regionally restricted to the diaphysis due to its periosteal expression [104].

We examined osteoclast differentiation in these mice as well, and scored hematopoietic progenitors by flow cytometry (Fig. 8A, B). We found no significant differences ($p<0.05$) in numbers of osteoclast progenitors of the types indicated. In addition, TRAP stains on 12-week old mice (Fig. 8C) indicate that there are no gross differences in mature osteoclast number. These data corroborate evidence by histomorphometry that do not suggest increased resorption in *Sostdc1*$^{-/-}$ compared to mice *WT*.

Sostdc1-positive cells participate in early fracture repair

Sostdc1 expression *in vivo* was examined by tracking the *LacZ* reporter from the *Sostdc1* knock-in allele [178]. In neonatal *Sostdc1*$^{+/-}$ mice, *LacZ* expression was observed in tissues adjacent or near the bone, including the adipose and periarticular cartilage (Fig. 9F-J). We also noted *LacZ* expression in the proliferating chondrocytes of the neonatal epiphysis [186] (Fig. 9F, J); this expression did not persist into the adult growth plate or articular cartilage (Fig. 9A, E). In intact adult *Sostdc1*$^{+/-}$ femora, *LacZ* was observed in the periosteum, muscle, and vasculature (Fig. 9A-E).

To examine the functional consequence of losing *Sostdc1* expression in adult mice, we performed transverse femoral fractures in *Sostdc1*$^{-/-}$ mice, and tracked the *Sostdc1*-deficient cells using *LacZ*. In unfractured *Sostdc1*$^{-/-}$ femora, LacZ was expressed in the same pattern as the LacZ determined for *Sostdc1*$^{+/-}$ femora, primarily in the periosteum (Fig. 1A), muscle and vasculature (Fig. 1E). At 3 days post fracture (D3), the rapidly expanded periosteum contained primarily *LacZ*-positive cells (Fig. 1B). Furthermore, *LacZ*-positive cells appeared to migrate from the interstitial space of the adjacent injured skeletal muscle and the vasculature (Fig. 1B-C,F-G,I-J). The elevated density of *LacZ*-positive cells was confined to the fractured limb (B, F, I), in regions adjacent to the injury site, and was not observed in the contralateral limb (Fig. 1A, E). We found no expression LacZ-positive cells in the chondrocytes of uninjured animals, including in the growth plate (Fig. 10A). However, patellar chondrocytes distal to the injury site on the broken limb activated *LacZ* expression shortly after injury (Fig. 10B). This suggests that *Sostdc1* transcriptional activation is mediated locally by the traumatic injury.

At 7 days post injury (D7) many *LacZ*-positive cells remained in the periphery of the developing callus (Fig. 1C, G, J). Migratory cells remained present in the soft tissue surrounding the bone injury (Fig. 1G, J). Fewer *LacZ*-positive cells were observed in the vasculature (Fig. 1J). By 10 days post fracture (D10), weak *LacZ* expression emerged in the developing cartilage callus (Fig. 1K), and *LacZ*-positive cells had embedded into the newly formed bone surface (Fig. 1D, K; arrows). Histologically, we observed bone formation as cells with mesenchymal morphology, yet surrounded by abundant matrix, increasing their cell-to-cell spacing (Fig. 1D, K), in contrast to the tightly packed mesenchymal cells observed in the D3 and D7 callus (Fig. 1B-C; F-G, I-J). At this stage of repair, *LacZ* expression decreased in the fracture callus and in the surrounding tissues. *LacZ* expression primarily marked the boundary between muscle and bone at the edge of the callus and the soft tissue near the skin (Fig. 1D, H, K). Immature chondrocytes near the callus edge continued to show weak *LacZ* expression, yet no

LacZ expression was observed in the hypertrophic chondrocytes of the callus, consistent with the lack of expression in uninjured adult bones (Fig. 10C,D).

LacZ-positive cells were confined to the periosteal and soft tissue compartments of the *Sostdc1*$^{-/-}$ limb, at all time points examined. No *LacZ*-positive cells were found on the endosteal surfaces or in the marrow cavity of contralateral, uninjured limbs, nor was *LacZ* activated in these regions of the injured limb, in response to injury. No *LacZ*-positive cells were seen in the metaphyseal trabecular niche of the uninjured bones, or in the injured bones in response to injury at any time point examined (Fig. 9A, F, I). During fracture repair, we conclude that *LacZ*-positive cells in *Sostdc1*$^{-/-}$ injured femora, and hence *Sostdc1*-positive cells in injured *WT* femora, appear to migrate from the soft tissues surrounding the injury, including periosteum, vasculature, and/or muscle, and participate in early fracture repair events. Participation of these *LacZ*-positive cells diminished at later milestones of healing, and was not present in the mature cartilage or in bone cells, suggesting that *Sostdc1* may mark a population of periosteal osteochondral progenitor cells needed for fracture repair.

Fracture healing program is altered in Sostdc1*$^{-/-}$ *mice

Histological analysis of *Sostdc1*$^{-/-}$ calluses revealed several differences between *Sostdc1*$^{-/-}$ mice and *WT* or *Sostdc1*$^{-/+}$ controls throughout the 28-day fracture healing interval examined (Fig. 2). Starting at D3, *Sostdc1*$^{-/-}$ mice had an enhanced periosteal reaction, as characterized by a thicker layer of undifferentiated cells in the periosteal areas adjacent to the injury (Fig. 2A, F). By D7, the cartilage callus was larger in *Sostdc1*$^{-/-}$ mice and intramembranous bone formation was more robust (Fig. 2G), with pronounced vascular invasion, as indicated by the presence of red blood cells in vessels (Fig. 2G; arrow). In contrast, *WT* calluses displayed insignificant intramembranous bone formation or neovascularization (Fig. 2B). At D14, while vascular invasion was occurring only at the periphery of the cartilage callus of *WT* animals (Fig. 2C), *Sostdc1*$^{-/-}$ mice had evident neovasculature deeper within the interior of the callus (Fig. 2H). By D21, the calluses of each genotype looked distinctly different, with *Sostdc1*$^{-/-}$ calluses showing a thick cortical shell surrounding the callus, very little woven bone in the interior of the callus, and original cortical bone that was remodeling, compared to *WT* (Fig. 2D, I). These mature calluses in *Sostdc1*$^{-/-}$ mice showed no evidence of persistent cartilage in the callus relative to matched controls. These data suggest that the absence of Sostdc1 accelerates and/or enhances intramembranous bone formation and neovascularization in the callus.

Sostdc1*$^{-/-}$ *mice have larger, more mineralized fracture calluses with normal mechanical strength

Sostdc1$^{-/-}$ fractured limbs had a significantly increased callus size (60%, $p<0.05$) and increased apparent bone mineral density (3%; $p<0.0005$) at D28, compared to *WT* calluses (Fig. 2E*,* J; Table 3). While bone volume was increased ($p<0.01$), BV/TV was increased by 36%, but this value was not significantly different between *Sostdc1*$^{-/-}$ and *WT* controls, due to large animal to animal variation. Mechanical testing of intact bones and calluses revealed that *Sostdc1*$^{-/-}$ femora and calluses were not mechanically different from *WT* controls (Table 3), as determined by torsional stiffness, ultimate torque at failure and rotation at ultimate failure quantification. Larger calluses (Fig. 2*E, J*), with

an increased mineral content indicated they were structurally mature. These data suggest that *Sostdc1*$^{-/-}$ fractured femora have an expedited healing program compared to *WT* controls, and that the healed calluses may yield stronger repaired bones.

Sostdc1 marks a population of osteochondral progenitor cells

Since Sostdc1-positive cells display migratory, proliferative, and differentiation capabilities consistent with those of mesenchymal stem cells (MSCs), we next examined co-localization of stem cell markers nestin and alpha smooth muscle actin (α-SMA) with *LacZ* as a surrogate of Sostdc1 expression, in D3 and D7 calluses (Fig. 3). We compared *LacZ* expression in *Sostdc1*$^{-/-}$ and *Sostdc1*$^{-/+}$ calluses using an antibody specific for its gene product, β-galactosidase. Nestin is a mesenchymal cell marker used in flow cytometry to identify mesenchymal stem cell populations [191] and α-SMA marks progenitor cells that can differentiate into chondrocytes and osteoblasts [174]. β-galactosidase antibody stain (Fig. 3G-R; red) closely resembled the β-galactosidase enzymatic activity (Fig. 3D-F). While nestin and β-galactosidase co-localized in only a few periosteal cells in *Sostdc1*$^{-/-}$ intact femora (Fig. 3G, J), at D3 there was a discernable increase in the population of nestin - LacZ double positive cells, in the expanded periosteal region of *Sostdc1*$^{-/-}$ fractures (Fig. 3H, K). By D7, a large fraction of the *Sostdc1*$^{-/-}$ callus harbored nestin - LacZ double positive cells (Fig. 3I), and now a smaller such population emerged in the *Sostdc1*$^{-/+}$ callus (Fig. 3L), suggesting that Sostdc1 may mark a unique population of periosteal derived stem cells. In contrast, at D3, α-SMA - LacZ marked mostly cells resembling well-developed blood vessels at the muscle-bone interface of *Sostdc1*$^{-/-}$ calluses (Fig. 3N, Q), with insignificant evidence of neovascularization at this time-point in *Sostdc1*$^{-/+}$ controls. By D7, the population of α-SMA – LacZ-positive increased in *Sostdc1*$^{-/-}$ calluses without a correspondent increase in the *Sostdc1*$^{-/+}$ control calluses (Fig. 3O, R). The overlapping expression of β-galactosidase with either nestin or α-SMA initiated at ~D3 and showed similar elevated levels near the site of injury at D7, suggesting that they mark a small population of rapidly dividing cells that are migrating from the periosteum and/or vasculature into the injured site.

Quantitative analysis of nestin and α-SMA-positive cells, revealed a significant increase in the number of stem cell marker positive cells in *Sostdc1*$^{-/-}$ mice, compared to controls (Fig. 3S, T) which suggests that lack of *Sostdc1* promotes or accelerates progenitor or stem cell response to injury and supports a role for *Sostdc1* in stem cell maintenance. Protein expression of Osterix (Sp7/Osx), a transcription factor essential for the differentiation of pre-osteoblasts into mature osteoblasts [192], was similarly analyzed. Significant differences were observed in intact femora, where *Sostdc1*$^{-/-}$ periosteal cells expressed higher levels of Osx than controls (Fig. 4A, D). At D3, the periosteal region closest to the cortical bone showed increased expression of Osx in *Sostdc1*$^{-/-}$ mice (Fig. 4B, E). Significantly more Osx-positive cells remained near the periosteal surface of *Sostdc1*$^{-/-}$ D7 calluses, compared to *Sostdc1*$^{+/-}$ controls (Fig. 4C, F, G) suggesting that lack of Sostdc1 promotes differentiation towards the osteoblast lineage.

Sostdc1$^{-/-}$ hastens the expansion and differentiation of mesenchymal cells during fracture repair

Using cell surface signatures established for mesenchymal stem cells (MSC) [190] and mature osteoblasts (OB)[190] we quantified MSC and OB populations in *Sostdc1$^{-/-}$* and *WT* femora in intact contralateral limbs and 5, 6, 7 days post fracture. No significant differences were observed in the frequency of MSCs or OBs in *Sostdc1$^{-/-}$* and *WT* intact femora or at D7 (Table 4). At D5, while the MSC and OB populations remained at baseline levels in *WT* femora, the *Sostdc1$^{-/-}$* injured bones had significantly more MSCs (>2-fold; $p<0.0105$) and OBs (>3-fold; $p<0.00246$). At D6, the *WT* MSC population reached 8-fold above baseline; whereas the MSC population in the *Sostdc1$^{-/-}$* was significantly lower than *WT* (Table 4, Fig. 5C). The *Sostdc1$^{-/-}$* OB population tended to outpace the magnitude observed in the *WT*, at D6, but was stabilized between the genotypes by D7, with significant differences only observed at D5 (Table 4). We also quantified the populations of endothelial cells and found no significant differences between *WT* and *Sostdc1$^{-/-}$,* at all time points examined. Furthermore, we found *LacZ* expression only within MSCs, consistent with Sostdc1 marking a subpopulation of osteochondral progenitor cells (Fig. 5A).

We next questioned whether loss of *Sostdc1* enhances fracture repair by enhancing the differentiation of MSCs in a cell autonomous fashion, or whether the enhanced fracture repair resulted from increased number of both MSCs and OBs in *Sostdc1$^{-/-}$* mice. To discriminate between the two potential scenarios, we plotted frequency of each cell type as a function of days *post* fracture. The resulting curve for MSCs exhibited a left shift in *Sostdc1$^{-/-}$* compared to *WT* mice (Fig. 5C), as did the curve of OBs (Fig. 5B), however, computing the area under the curve generated highly similar values for *Sostdc1$^{-/-}$* and *WT* MSC profiles (Table 4). This temporal shift in MSC expansion can also be visually observed in the nestin and α-SMA immunostains where the double positive population is always higher in the *Sostdc1$^{-/-}$* (Fig. 3H, I, K, L, N, O, R) than in the *Sostdc1$^{-/+}$* calluses. However, the immunostain quantification indicates both significantly more nestin^{+} cells and α-SMA^{+} cells (indicators of stem cells) in *Sostdc1$^{-/-}$* at D7 compared to *Sostdc1$^{-/+}$* (Fig. 3). This difference may be due to the use of whole broken bones for the flow cytometry analysis, compared to fracture-callus-only for immunostain quantification. In addition, the immunostain quantification used single markers, and both nestin and α-SMA may also indicate the presence of endothelial cells [193] while the cell surface markers define endothelial cells as a separate population, and could contribute to the differences seen at D7 between the two analyses. The temporal shift in MSCs populating the callus is consistent with a rapid shift in cellular identity which contributes to the accelerated differentiation into OB in the *Sostdc1$^{-/-}$* calluses (see also Fig. 4) and is reconciled as a greater area under the curve for *Sostdc1$^{-/-}$* OBs (Fig. 5, Table 4). As later time points did not have osteoblast quantification by flow cytometry, it is not possible to determine whether there is a greater absolute number of osteoblasts throughout fracture healing in *Sostdc1$^{-/-}$* compared to *WT*, or if there is simply an early shift toward differentiation in the *Sostdc1$^{-/-}$* calluses. However, at late time points during repair, *Sostdc1$^{-/-}$* mice show enhanced callus volume, BV, and mineral density (Table 3) suggesting that increased osteoblast differentiation, or relative number early in repair, translates to more bone formation (Table 3).

Loss of Sostdc1 activates Wnt signaling during fracture repair

Sostdc1 had been described as both a BMP and a Wnt antagonist [184], and we have previously shown that Sostdc1 does not behave as a canonical Wnt antagonist in the context of limb development [186]. We examined the expression pattern of activated β-catenin in the fracture callus at D3 and D7 to determine whether Sostdc1 behaves similarly in the context of fracture repair. In contrast to our limb analyses, we found dramatically increased levels of activated β-catenin in *Sostdc1*$^{-/-}$ mice, compared to controls (Fig. 6). In unbroken bones, we found increased signal at the periosteal surface and in the metaphyseal niche of *Sostdc1*$^{-/-}$ mice, compared to controls (Fig. 6A, B, F, G). At D3 post-fracture, higher levels of activated β-catenin were observed in the periosteum as well as in the cortical bone of *Sostdc1*$^{-/-}$ femora (Fig. 6C*,* H). By D7, increased levels of activated β-catenin were observed in the periphery of the developing cartilaginous callus (excluding chondrocytes), and the expression intensified in regions resembling blood vessels in the callus (Fig 6D*,* I*;* brackets/arrows). Furthermore, the developing neovascular network in the callus consisted of larger diameter vessels compared to controls. Woven bone present in the marrow space of D7 injured femurs also contained elevated levels of activated β-catenin in *Sostdc1*$^{-/-}$ mice (Fig. 6E*, J*). The increase in activated β-catenin levels in the metaphysis and cortical bone suggests that Sostdc1 affects canonical Wnt signaling in a non-cell-autonomous manner, and it implies that the increase in cortical bone is due to elevated Wnt signaling.

4.4 Discussion

Sost is a potent negative regulator of bone formation and Sost deficiency contributes to high bone mass and enhanced fracture healing phenotypes; yet its paralog Sostdc1, which is expressed in the periosteum, has not yet been examined for its potential contribution to bone repair despite the established role of periosteal cells in fracture healing [105, 194]. Here we report that global loss of Sostdc1 results in a complex skeletal phenotype characterized by an increase in femoral cortical bone structure and BMD, but with reduced trabecular bone mass. Since periosteal osteoblasts are responsible for outward expansion of long bones, our results suggest that lack of Sostdc1 increases the osteoblast activity locally in the periosteum, resulting in larger, thicker bone cortices. The increased moment of inertia (pMOI) in *Sostdc1*$^{-/-}$ femurs suggested that the increase in periosteal activity among *Sostdc1*$^{-/-}$ mice might translate into improved bending properties for the diaphysis. These findings are consistent with results published by He *et al*., who correlated a polymorphism in *Sostdc1* with low lumbar BMD but not with femoral neck or total hip BMD, in Chinese women [195]. Since lumbar vertebrae are primarily composed of trabecular bone, this human association study suggests that mutations that interfere with Sostdc1 function may negatively influence trabecular BMD to a greater extent than cortical BMD.

Previous studies have shown that both Sostdc1 and Sost inhibit Wnt signaling by binding to multiple Lrp co-receptors (Lrp1, Lrp4, Lrp5 and Lrp6) [134, 147, 196], and that Sost primarily functions in a cell non-autonomous manner wherein it is secreted by osteocytes and binds to receptors on the osteoblast surface. The loss of Sost results in a robust response in trabecular bone, contributing to strengthening and replenishment of trabeculae in the case of osteoporosis. Loss of Sost, as with Sclerostin-neutralizing antibody treatment, also directs fracture calluses and stem cells toward enhanced bone

formation, although it is not yet clear by what mechanism [169, 197]. Thus, we speculated that due to its expression in periosteum, Sostdc1 may exert its effects on periosteal osteoblasts in a similar fashion, where it is secreted by periosteal cells and binds to Lrp co-receptors on the neighboring osteoblasts residing on the periosteal bone surface. Since osteoblasts residing on the periosteal surface of cortical bones are likely to be exposed to both Sostdc1 from the periosteum and to Sost from the underlying osteocytes, the periosteal osteoblasts may be more sensitive to levels of Wnt antagonists, and therefore may be more likely to upregulate β-catenin-dependent Wnt signaling in the absence of Sostdc1 than osteoblasts residing on the trabecular surfaces. Immunohistological analysis of activated β-catenin expression supports this hypothesis, where we observe greater levels of activated β-catenin on the periosteal surface of *Sostdc1*$^{-/-}$ than in *Sostdc1*$^{+/-}$ controls (Fig. 6A, F).

Since the cambium layer of the periosteum is also a major source of osteoblast and chondrocyte progenitors during fracture healing, we also examined whether Sostdc1-deficient periosteal cells interfere with normal fracture healing. After injury, a typical periosteal thickening was observed accompanied by a rapid expansion of *Sostdc1-LacZ* positive cells with mesenchymal morphology that populated most of the callus forming region at D3. Beyond D7, these *LacZ* positive cells became restricted to regions closer to the periosteum, suggesting that the *Sostdc1*-expressing cells rapidly expand during periosteal reaction and are subsequently recruited into the fracture site where they participate in the soft callus formation. FACS analysis of MSCs in combination with histological staining with stem cell markers nestin and α-SMA indicate that *Sostdc1*-positive cells in the early fracture callus mark a subpopulation of multipotent mesenchymal stem cells that migrate into the callus from the periosteum. The behavior of Sostdc1-positive cells is similar to osteochondroprogenitor cells in the periosteum that, using lineage tracing, make a major contribution to the soft callus [194]. The role of *Sostdc1* as a WNT antagonist, and the known role of WNT/β-catenin signaling to promote osteogenic[198] and chondrogenic [199, 200] differentiation and maturation, suggests that Sostdc1 may act as the rate-limiting inhibitor of the differentiation of pluripotent periosteal cells during fracture repair. Indeed, we observe a temporal shift in the frequency of MSC and OB subpopulations during fracture repair in *Sostdc1*$^{-/-}$ mice, as well as greater area-under-curve of OBs, but not of MSCs, indicating more rapid activation of migration, proliferation and differentiation of MSCs and OBs, and further supporting the role of Sostdc1 as an osteochondral progenitor gatekeeper. Further exploration of Sostdc1 may define it as a morphogen that functions to maintain stem cells in a progenitor state [201].

This work describes Sostdc1 activity in a new context, highlighting its potential role in the metabolism and repair of the skeleton. In addition, for the first time we have linked *Sostdc1* to the behavior of mesenchymal stem cells, which is consistent with, and mechanistically may explain *Sostdc1*-related phenotypes noted by other published studies, such as in cancer prognosis, tooth development, kidney injury resistance, and diet-induced obesity resistance. We have shown that *Sostdc1*^{LacZ} is expressed in Sostdc1$^{-/-}$ MSCs, therefore, Sostdc1 expression marks a subpopulation of osteochondral progenitor cells, and have shown that stem cell response is enhanced in the absence of *Sostdc1* after injury, accelerating bone repair. We have demonstrated that *Sostdc1* is

important for trabecular bone maintenance, bone formation, early fracture repair events, and the lack of *Sostdc1* influences mesenchymal stem cell behavior in response to injury, *in vivo*. Future work may show a synergy between the loss of *Sost* and *Sostdc1* to combine enhanced trabecular bone and enhanced cortical bone in the treatment of fractures and osteoporosis.

Figure. 1. Histological Characterization of Early Time Points in Fracture Repair of Sostdc1$^{-/-}$ Mice. Sostdc1-/- mice shows *LacZ* expression [as a surrogate for Sostdc1 expression] in and around the early fracture callus. Schematics are shown for unfractured, and the fractured femora at 3, 7, and 10 days post-fracture; boxes within this schematic indicate regions visualized for each time point. Deep orange- soft tissue outside bone; blue- periosteum and undifferentiated cells; red- clot or vasculature; light orange- cartilage callus; yellow- bone. Control unfractured *Sost*$^{-/-}$ limb (A, E) shows *LacZ* expression in the periosteum (A), and in intermittent cells in muscle tissue and peripheral vascular tissue (E). Images taken at D3 post-fracture show *LacZ* expression in the expanded periosteum (B) and evidence of cell migration into the callus (I). Cells within muscle and periosteum distal to the fracture site are also strongly *LacZ*-positive at this early time point (F). In nearby muscle, *LacZ*-positive cells appear to occupy the interstitial space, and appear to migrate out from the vasculature (B, F, I). At D7 *LacZ* expression begins to fade (C, G, J). The outside of the callus is marked by *LacZ*-positive cells (C). Undifferentiated cells continue to be found near the periphery of the callus in undefined tissue (G). At the edges of the muscle, positive cells are located in distinct cluster near connective tissue surrounding muscle bundles (G, J). By D10 post-fracture, *LacZ* expression is reduced both in terms of numbers and intensity (D, H, K). Newly formed periosteum, embedding osteoblasts, and nearby developing muscle show cells around the boundaries that express *LacZ* (arrows) (D, H). Undifferentiated cells near the periphery of the callus retain *LacZ* expression (K). *LacZ* expression is also found in the healing muscle tissue outside the callus proper (D). Images are shown at 40X magnification. m muscle; v blood vessel; p periosteum; pa patella; cb cortical bone; hc hypertrophic chondrocytes; bm bone marrow; b newly formed bone; ch chondrocytes.

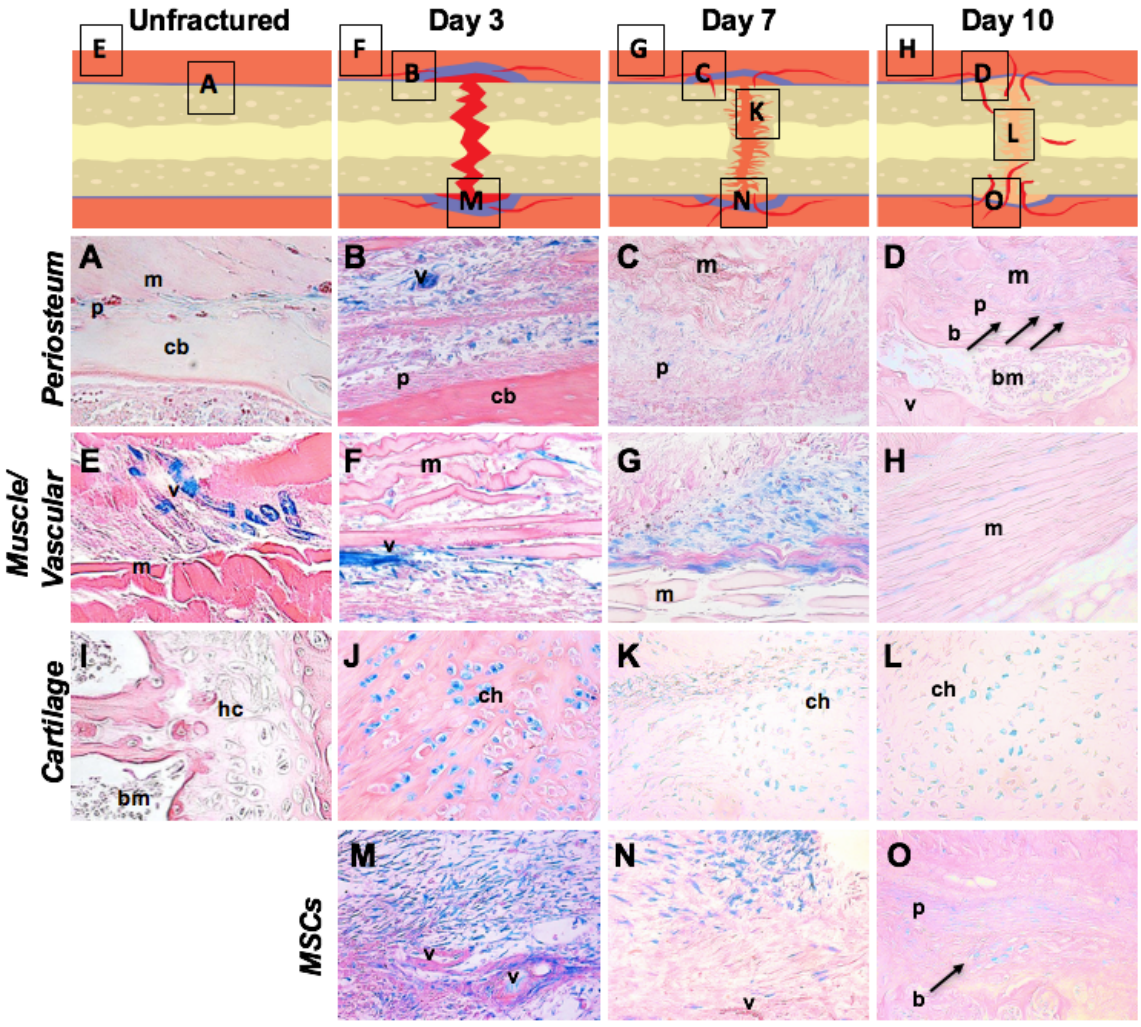
Unfractured
Day 3
Day 7
Day 10
E
A
F
B
G
C
K
H
D
L
M
N
O
Periosteum
Muscle/
Vascular
Cartilage
MSCs
m
p
cb
v
b
bm
hc
ch

Figure. 2. Fracture Healing Observed in Calluses of Sostdc1$^{-/-}$ Mice. Fracture callus is larger at 28 days post-fracture in *Sostdc1*$^{-/-}$ mice and H&E stains indicate differential progress during healing milestones. Periosteal reaction is more extensive in *Sostdc1*$^{-/-}$ compared to *WT* controls at D3 post-fracture (A, F). Chondrogenesis during early callus formation (D7) shows increased vascular invasion (arrow) in *Sostdc1*$^{-/-}$ mice compared to controls (B, G). Vascular invasion at D14 progresses to the middle of the cartilaginous callus in *Sostdc1*$^{-/-}$ mice, while neovascularization is occurring in the peripheral callus in *WTs* (arrows) (C, H). At D21, a thick cortical shell around the callus is evident in *Sostdc1*$^{-/-}$ mice, a reduced amount of trabecular bone formation in the interior of the callus is also present, and the original cortical bone is remodeling while in *WTs* there is more trabecular bone, thinner cortical shell, and the original cortex remains unremodeled (D, I). Micro-CT analysis of 28-day calluses shows a greater callus volume in *Sostdc1*$^{-/-}$ ($p<0.005$) (E, J) (See also Table 2). p periosteum; cb cortical bone; chondrocytes; v blood vessel.

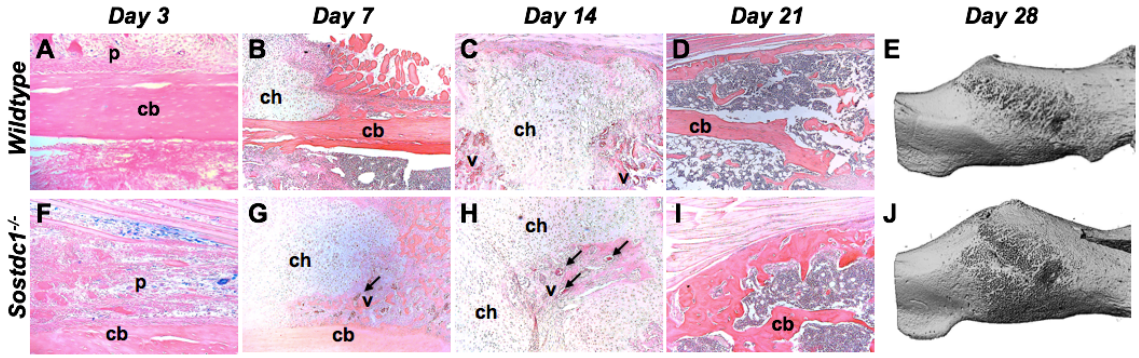

Figure. 3. Stem Cells Co-localize with Sosdc1 During Fracture Healing. Nestin and α-smooth muscle actin co-localize with Sostdc1 [using LacZ from the knocked in allele]. *LacZ*-stained bones show positive cells on the periosteal surface of the unbroken bone (D). *LacZ*–positive cells participate in the periosteal expansion at (E). This population of *LacZ* -positive cells expands into the undifferentiated callus tissue at D7 (F). *LacZ* expression in *Sostdc1*$^{+/-}$ mice is qualitatively reduced in intact periosteum, D3 and D7 fracture calluses, suggesting the pool of *LacZ*-positive cells is expanded in *Sostdc1*$^{-/-}$ mice (A-C). Dual marker immunofluorescent staining indicates the presence of both *LacZ* and Nestin at the periosteal surface in unfractured femora, while there are fewer Nestin(+) cells in *Sostdc1*$^{+/-}$ (G, J). During the periosteal reaction, some cells expressing Nestin also show *LacZ* expression (H, K), while the two groups of cells are mutually exclusive in *Sostdc1*$^{+/-}$. By D7, many cells in the undifferentiated callus region of *Sostdc1*$^{-/-}$ are positive for both markers, while substantially fewer double-labeled cells are present in *Sostdc1*$^{+/-}$ samples (I, L). [red β-galactosidase (*LacZ*); green Nestin (G-L); green α-Smooth muscle actin (α-SMA) (M-R)]. α-SMA is also shown in periosteum of unfractured femora of *Sostdc1*$^{+/-}$ and *Sostdc1*$^{-/-}$ mice (M, P). Cells and vessels positive for α-SMA are much more abundant, have more dual label, and vessel are of a larger diameter in *Sostdc1*$^{-/-}$ mice at D3 post-fracture (N,Q). There is significant dual-labeling of undifferentiated cells in the D7 fracture callus of *Sostdc1*$^{-/-}$ mice, while there is very little overlap and very few α-SMA-positive cells in *Sostdc1*$^{+/-}$ calluses (O, R). Quantitation of Nestin signal in D3 and D7 calluses of *Sostdc1*$^{-/-}$ mice revealed a significantly higher percentage of image area covered by Nestin(+) cells compared to *Sostdc1*$^{-/-}$ calluses at both time points (S). Quantitation of α-SMA signal in D3 and D7 calluses of *Sostdc1*$^{-/-}$ mice revealed a significantly higher percentage of image area covered by α-SMA -positive cells compared to *Sostdc1*$^{-/+}$ calluses at both time points (T). [p periosteum; cb cortical Bone; mc mesenchyme.]

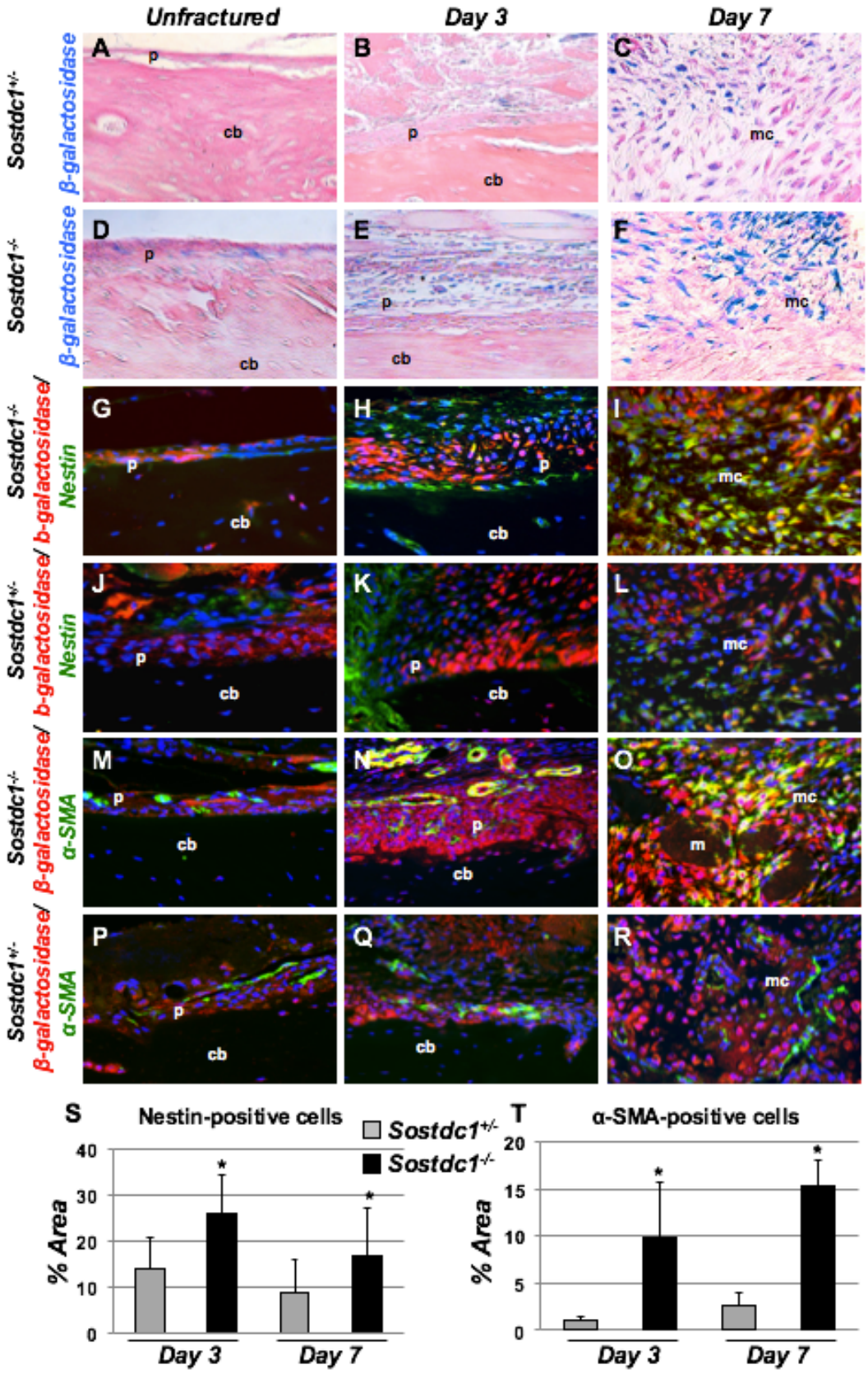
Unfractured
Day 3
Day 7
Sostdc1+/- β-galactosidase
Sostdc1-/- β-galactosidase
Sostdc1+/- Nestin β-galactosidase/
Sostdc1+/- Nestin b-galactosidase/
Sostdc1-/- α-SMA β-galactosidase/
Sostdc1+/- α-SMA β-galactosidase/
A
B
C
D
E
F
G
H
I
J
K
L
M
N
O
P
Q
R
p
cb
mc
m
S
Nestin-positive cells
Sostdc1+/-
Sostdc1-/-
% Area
40
30
20
10
0
Day 3
Day 7
T
α-SMA-positive cells
% Area
20
15
10
5
0
Day 3
Day 7

Figure. 4. Elevated Osteoblast Precursors During Fracture Repair in Sostdc1$^{-/-}$ Mice. *SP7/Osterix (Osx*) osteoblast precursor levels are dramatically increased in *Sostdc1*$^{-/-}$ mice during fracture repair. Immunostains for Osx in *Sostdc1*$^{-/-}$ mice show an increased number of positive cells at the resting periosteal bone surface of unbroken bones compared to *WT* controls (A,D). The layer of cells that participate in the periosteal reaction at D3 post fracture is thicker and has more Osx-positive cells, especially at the periosteal surface, compared to controls (B,E). At D7 post-fracture, Osx levels are activated in developing intramembranous callus, which is larger and contains more positive cells in *Sostdc1*$^{-/-}$ mice, especially at the periosteal surface (C,F). Quantitation of signal area at D3 and D7 revealed an increased area of Osx-positive cells in *Sostdc1*$^{-/-}$ mice at both time points examined (G).

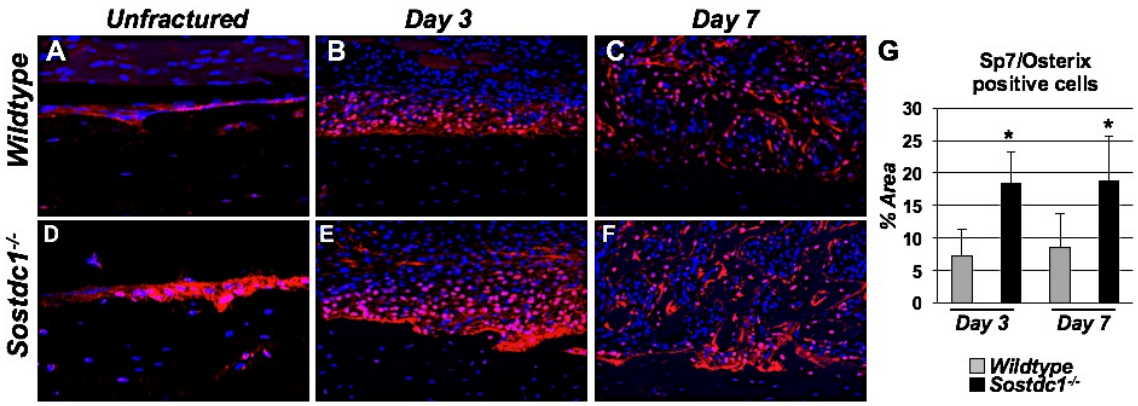

Figure. 5. Quantification of Mesenchymal Stem Cells and Osteoblasts Population During Fracture Repair. Quantification of mesenchymal stem cells (MSC) and osteoblasts (OB) populations during fracture repair. Purified MSCs from *Sostdc1*$^{-/-}$ femurs were found to express β-galactosidase, but no expression was detected in OB or endothelial (ENDO) cells, suggesting that *Sostdc1* is expressed in MSCs only (A). A time course quantification of MSCs (C) and OBs (B) determined that both MSC and OB expansion curves are shifted to the left, suggestive of earlier expansion of MSCs during fracture repair.

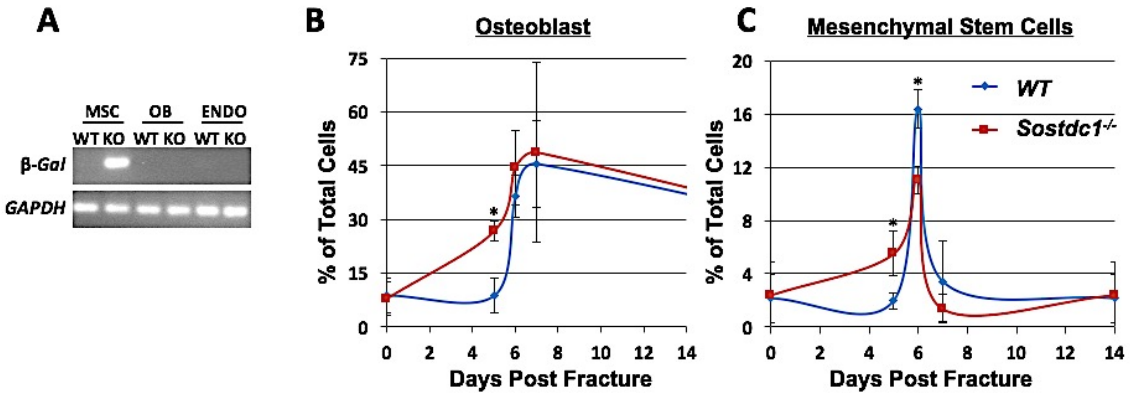

Figure. 6. Elevated Beta-Catenin During Fracutre Repair in Sostdc1-/- Mice. Higher Levels of Activated β-catenin are detected in *Sostdc1*$^{-/-}$ mice during fracture repair. Immunostains for activate β-catenin in *Sostdc1*$^{-/-}$ and *WT* mice show increased β-catenin levels at the resting periosteal and metaphyseal bone surfaces in unbroken bones compared to *WT* controls (A,B,F,G). The layer of cells that participate in the periosteal reaction at D3 post-fracture is thicker and has more robust activated β-catenin compared to controls (brackets) (C,H). At D7 post-fracture, β-catenin is activated in the developing neovasculature, which is larger and more plentiful in *Sostdc1*$^{-/-}$ calluses compared to *WT* (brackets, arrows). Chondrocytes are negative for activated β –catenin (D,I). *Sostdc1*$^{-/-}$ show more activated β-catenin in woven bone at D7 post-fracture compared to controls (E,J). [p periosteum; cb cortical bone; ch chondrocytes; v blood vessel; vb woven bone.]

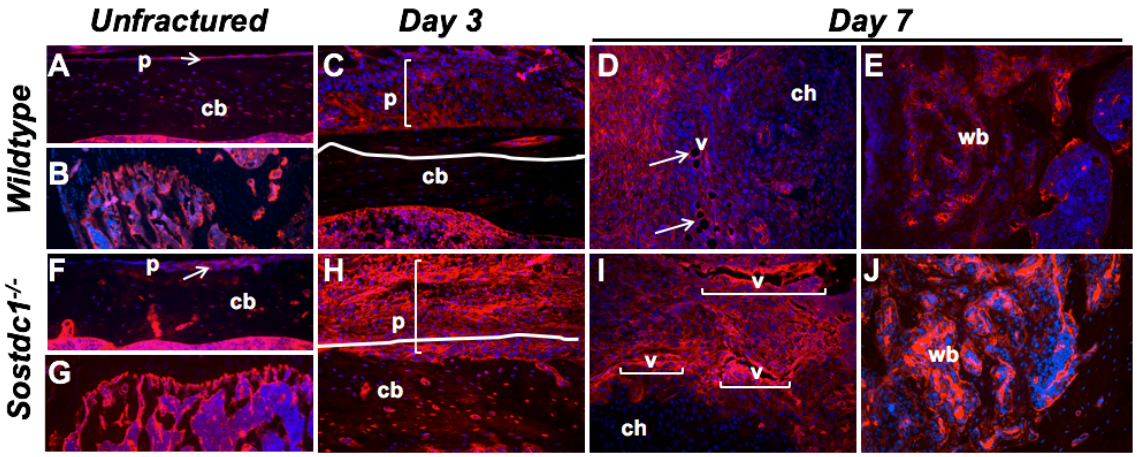

Figure 7. Micro-CT parameters for intact cortical bone in WT and Sostdc1$^{-/-}$ mice at 12 weeks of age. (B) Reconstructed outline of *WT* cortical bone, and (C), *Sostdc1$^{-/-}$* cortical bone. (A) No differences were observed in any parameters except Marrow Area (* indicates p=0.029). Values shown are mean +/- standard deviation. Bar represents 100mm.

A	*WT*	*Sostdc1$^{-/-}$*
Bone Area (mm^2)	0.889+/- 0.075	0.929+/-0.143
Marrow Area (mm^2)	1.12+/-0.115	1.29+/-0.138*
Total Area (mm^2)	2.013+/-0.160	2.220+/-0.269
Bone Area/Total Area (%)	44.18+/-2.42	41.65+/-2.41
Cortical Thickness (mm)	0.182+/-0.013	0.186+/-0.019
BMD (mg HA/cm^3)	1221.25+/-25.77	1122.40+/-17.15

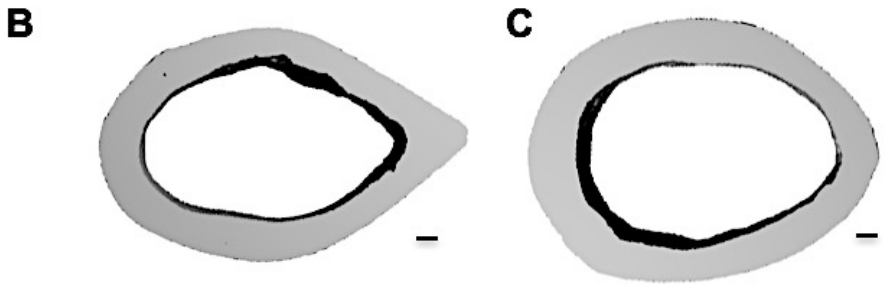

Figure 8. Quantification of osteoclast development in WT and Sostdc1$^{-/-}$ mice. Osteoclast progenitors and precursors indicating the progenitor pool were scored by flow cytometry using the indicated cell-surface markers (A). Percent of each type of progenitor cell were scored and statistically compared; no parameters were statistically different by genotype ($p<0.05$) (B). TRAP (Tartrate-Resistant Alkaline Phosphatase, red) and Fast Green counterstain (green) of growth plate/trabecular bone, cortical bone, and trabecular bone are indicated for both Sostdc1$^{-/-}$ mice and WT mice, in which no differences in osteoclast number are indicated (C).

A

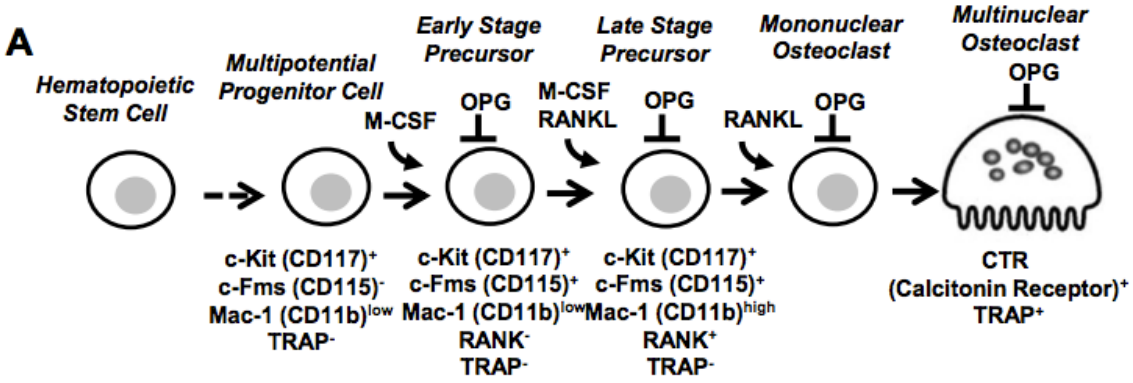

B

	Hematopoietic Stem Cell	Multipotential Progenitor Cell	Early Stage Precursor	Late Stage Precursor
Sostdc1$^{-/-}$	42.31 ± 6.39	16.82 ± 1.75	0.025 ± 0.021	91.49 ± 0.37
WT	48.47 ± 2.72	11.99 ± 1.51	0.050 ± 0.001	88.10 ± 0.37

C

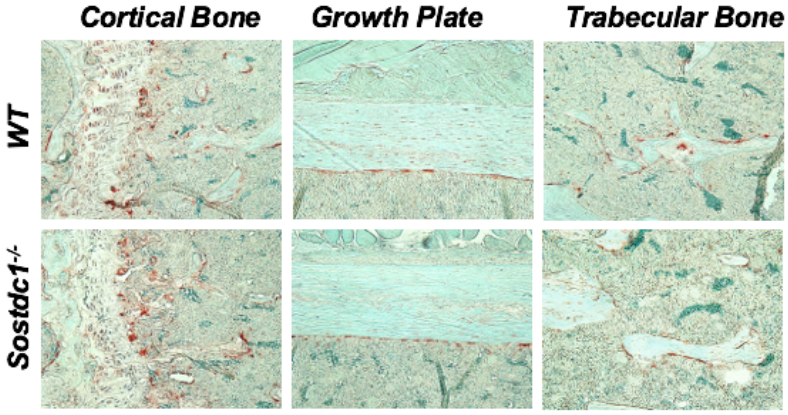

Figure 9. Histological characterization of LacZ expression [as a surrogate for Sostdc1 expression] in Sostdc1+/LacZ mice. Sostdc1 is pressed in neonatal cartilage (F, J), but not in the adult (A, E); adipocytes (B, G), vasculature (C, H) and periosteum (D, I) in both neonate and adults. m muscle; v blood vessel; p periosteum; pa patella; cb cortical bone; hc hypertrophic chondrocytes; bm bone marrow; b newly formed bone; ch chondrocytes.

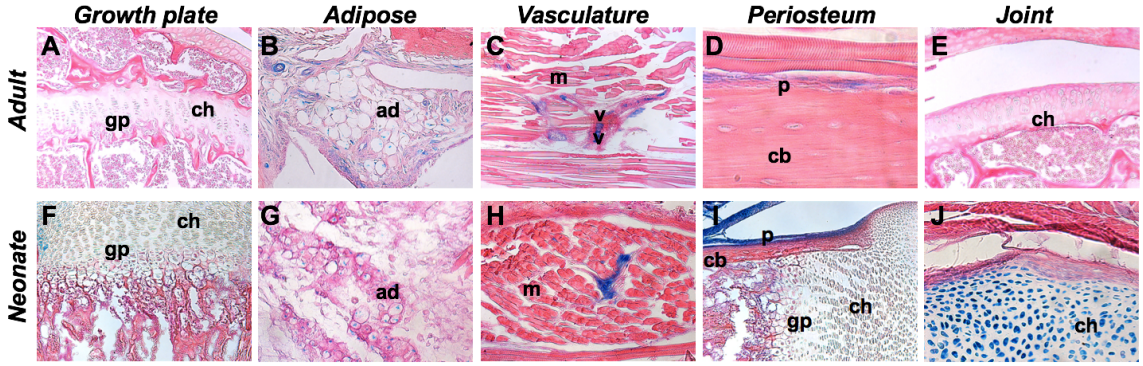

Figure 10. Histological characterization of LacZ expression [as a surrogate for Sostdc1 expression] in cartilage of Sostdc1+/LacZ mice. Sostdc1 is not expressed in adult growth plate cartilage (A), but is expressed after injury in nearby fibrocartilage associated with the patella (B). During fracture healing, weak expression is seen in chondrocytes in the callus at D7 and D10 (C, D) but disappears shortly after this time point. gp growth plate; bm bone marrow; fc fibrocartilage; ch chondrocytes.

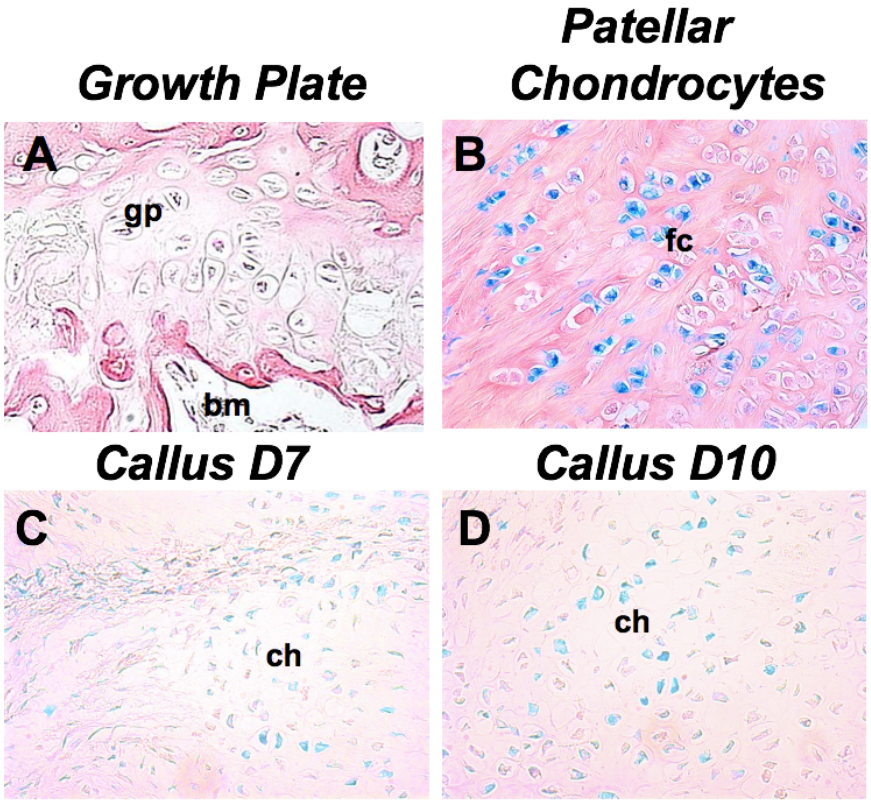

Table 1. Bone Phenotyping Based on uCT Parameters in the Cancellous Bone Compartment of the Distal Femur, L4 Vertebrae and Cortical Bone of 5.5-Month-*Old Sostdc1$^{-/-}$ Mice Compared to WT Controls.*

	Index	*WT*	*Sostdc1$^{-/-}$*
Femur	BV/TV (%)	9.50±1.20	6.50±2.00*
	Conn. Dens. (1/mm^3)	155.827±13.975	108.507±38.540*
	SMI	2.284±0.225	2.502±0.326
	Tb.N (1/mm)	4.164±0.143	3.387 ± 0.397*
	Tb.Th (mm)	0.0399 ±0.0009	0.039 ±0.006
	Tb.Sp (mm)	0.227±0.009	0.292±0.035*
	BMD (mg HA/cm^3)	913.452±14.108	935.367±15.824*
L4 Vertebrae	BV/TV (%)	19.90±0.80	12.80±2.40*
	Conn Dens. (1/mm^3)	273.007±14.759	211.350±46.188*
	SMI	0.490±0.090	1.181±0.232*
	Tb.N (1/mm)	5.270±0.154	4.155±0.428*
	Tb.Th(mm)	0.036±0.001	0.035±0.002
	Tb.Sp (mm)	0.179±0.006	0.235±0.029*
	BMD(mg HA/cm^3)	947.457±19.014	935.367±15.824*
Cortex	pMOI (mm^4)	0.47±0.063	0.592±0.145*
	TA (mm^2)	2.028±0.128	2.352±0.298*
	BA/TA (%)	42.80±1.80	40.00±2.00*
	MA (mm^2)	1.161±0.089	1.414±0.208*
	Ct.Th (mm)	0.184±0.009	0.188±0.011
	BMD (mg HA/cm^3)	1113.169±18.433	1132.091±17.407*

Data represents mean ± standard deviation for parameters measured. BV=Bone Volume; TV= Total Volume; Conn. Dens.= Connectivity Density; SMI= Structural Model Index; Tb. N= Trabecular Number; Tb.Th= Trabecular Thickness; Tb.Sp= Trabecular Separation; BMD= Bone Mineral Density; pMOI= Moment of Inertia; TA= Total Area; BA= Bone Area; MA= Marrow Area. Group size *n* = 5-10. *p-values < 0.05

Table 2. Histomorphometric analysis of Periosteal and Endocortical region of 5.5 Month-Old Sostdc1$^{-/-}$ Femurs Compared to WT Controls.

Region	Index	*WT*	*Sostdc1$^{-/-}$*	% change
Periosteal	MS/BS (%)	19.576±5.042	34.89±14.517*	+78
	MAR (μm/d)	0.025±0.005	0.019±0.005	-23
	BFR/BS (μm^3/μm^2/d)	1.794±0.667	2.333±1.115	+30
Endocortical	MS/BS (%)	47.023±9.881	51.185±13.328	+8
	MAR (μm/d)	0.027±0.004	0.016±0.003*	-42
	BFR/BS (μm^3/μm^2/d)	4.605±0.905	3.090±1.394*	-32

Data represents mean ± standard deviation for parameters measured. MS = mineralizing surface; BS = bone surface; MAR = mineral apposition rate; BFR = bone formation rate. Group size *n* = 6. *p-values < 0.05

Table 3. Biomechanical properties determined by uCT and Torsional Testing of the Mature Callus Compartment of Sostdc1$^{-/-}$ Mice Compared to WT Controls, at 28 Days Post-Fracture.

	Index	*WT*	*Sostdc1$^{-/-}$*
Callus	Callus Volume (mm^3)	17.495±5.328	28.760±9.413*
	BV (mm^3)	3.804±0.966	5.197±1.042*
	BV/TV (%)	23.30±0.88	19.10±4.40
	BMD (mg HA/cm^3)	992.936±11.032	1022.581±11.220*
Control	Stiffness (Nm/deg)	0.00171±0.0005	0.00192±0.0007
	Ult. Torque (Nm)	0.032±0.006	0.032±0.009
	Rot. Ult. Torque (degrees)	24.983±6.020	20.888±5.371
Fractured	Stiffness (Nm/deg)	0.00073±0.0005	0.00064±0.0003
	Ult. Torque (Nm)	0.021±0.009	0.018±0.005
	Rot. Ult. Torque (Degrees)	47.200±17.339	35.500±14.343

Data represents mean ± standard deviation for parameters measured. BV=Bone Volume; TV= Total Volume; BMD= Bone Mineral Density; Ult. Torque= Ultimate Torque at failure; Rot. Ult. Torque= Rotation at Ultimate Torque. Group size n= 6 *p-values < 0.05

Table 4. Cell populations in the Femur during Fracture Repair in Sostdc1-/- Mice Compared to WT Controls.

Days Post Fracture	*Mesenchymal Stem Cells*		*Osteoblasts*		*Endothelial*		*Total Cell Count*	
	WT	*Sostdc1*$^{-/-}$	*WT*	*Sostdc1*$^{-/-}$	*WT*	*Sostdc1*$^{-/-}$	*WT*	*Sostdc1*$^{-/-}$
Unfractured (N=11)	2.14±1.82	2.40±2.51	8.74±4.95	7.80±4.67	9.77±5.98	14.33±12.48	$6.80X10^5$±$2.99X10^5$	$5.37X10^5$±$2.19X10^5$
Day 5 (N=4)	1.98±0.68	5.50±1.67*	8.68±4.89	26.63±2.78*	5.77±1.99	11.32±5.7	$8.40X10^5$±$2.26X10^5$	$4.80X10^5$±$5.66X10^4$
Day 6 (N=3)	16.35±1.43	11.06±1.02*	36.31±5.89	44.49±10.83	17.03±2.92	15.98±6.59	$4.93X10^5$±$1.97X10^5$	$3.62X10^5$±$2.89X10^3$
Day 7 (N=4)	3.41±3.04	1.37±1.08	45.38±11.98	48.58±25.06	9.25±3.29	8.25±5.11	$6.00X10^5$±$2.26X10^5$	$6.20X10^5$±$2.55X10^5$
Area Under the Curve#	48.83	48.13	864.67	957.74*	129.95	168.96		

Data represents mean percentages of cells in whole digested femurs ± standard deviation for parameters measured. Total cell count data is represented as total cell count ± standard deviation. All contralateral unfractured femurs for all time-points [days 5, 6, and 7] were averaged to obtain the unfractured values for *WT* and *Sostdc1*$^{-/-}$ mice. *p-values < 0.05; #to calculate are under the curve unfractured values were used for day 0, day 14 [MSCs; ENDO] and day 35 [OBs] under the assumption that MSC and OBs would revert to unfractured levels at these time points (Figure 5C).

Chapter 5: Conclusions and Future Directions

The studies that have been discussed in this thesis have led to a better understanding of Sost and Sostdc1 role during fracture repair as well as providing evidence of the Akita mice as another diabetic model for bone and fracture studies. Based off of our experimental studies, we have come to the following overall conclusions:

1. *Study the effects of Sost antibody treatment in diabetic mice during fracture healing.* Our diabetic mice revealed a low bone mass phenotype with impaired osteogenesis due to osteoblasts ineffective activity in producing mineralized bone and decreased beta-catenin dependent Wnt signaling. Sost antibody treatment enhances osteoblast activity and beta-catenin activity, resulting in enhanced osteogenesis during repair even after termination in diabetic mice.
2. *Characterize fracture healing in Akita mice as another diabetic model for fracture healing studies.* Akita mice have decreased bone mineral density within the uninjured cortical femur region and a less mature callus with decreased bone formation during fracture healing. This suggests that the Akita mice have increased fracture risk and impaired fracture repair. Our data provides support in providing another diabetic model used for future bone metabolism and fracture studies.
3. *Determine if Sostdc1$^{-/-}$ mice have altered fracture healing. Sostdc1$^{-/-}$* mice has shown decreased trabecular bone and increased cortical bone due to a thicker periosteum in uninjured femurs. An enhanced fracture healing was observed in *Sostdc1$^{-/-}$* mice due to a rapid expansion thickening of the periosteum and increased mesenchymal stem cell and osteoblast population resulting in a more vascularized cartilage callus and thicker cortical shell during repair. Results have also suggested that Sostdc1 may promote and maintain mesenchymal stem cell quiescence within the periosteum.

Within these studies, histology analysis was heavily used in the aid of identifying what is occurring in bone homeostasis and fracture repair. Histology provides a structural visualization of bone cells and an assessment of bone phenotypes in our cohorts. A limitation in using histology is the lack of quantitative data this method provides. Instead, histology provides a qualitative assessment that requires the researcher to recognize landmarks within the bone and identify cell types upon characteristics of the cell morphology. This can lead to subjective interpretations and the lack of objectivity due to subconscious biased when comparing samples. Thus, in our experiments, multiple observers were used and blinded assessments in sample variation were conducted to minimize biased. For future work, a semi-quantitative approach may be done on histology analysis using a software algorithm in addition to microcomputed tomography to verify significant changes among studied groups.

A weakness in our studies is that male mice were only used due to the ease of reproducibility and large bone analysis literature background in males. A previous report on the comparison between human males and females revealed differences in bone parameters due to sex and age [202, 203]. Similarly, C57BL6 mice have also shown to have sex and age differences in bone parameters [143], suggesting that bone homeostasis changes are possibly due to hormone changes within sexes. These

changes in hormones among sexes and aging effects on bone metabolism can lead to variation in experimental results and data interpretations. Thus, for future studies, it is imperative to include female mice in experiments to expose sex differences and variation in results. Another comparison to include in future experiments are differences between young/adolescent and aged mice as changes due to aging can also lead to different experimental outcomes.

Our findings have revealed another therapeutic use of SOST antibody treatment as a therapy for those with difficult to heal fractures and diabetic patients with osteoporosis and impaired fracture healing. We have also revealed Sostdc1 involvement during fracture repair by maintaining mesenchymal stem cell proliferation. Our studies have contributed in examining the role of Sost and Sostdc1, two modulators of Wnt signaling, during fracture repair in normal and T1DM mice. Though SOST antibody is a promising treatment for fracture repair, there are still many unknowns in terms of SOST antibody's mechanism of action, impaired healing in T2DM patients, and whether Sost acts in an endocrine or paracrine manner. The current understanding of Sost is that osteocytes predominately secrete Sost protein, however *Sost* has also been shown to be expressed in the aorta branches of the adult heart, cerebellum, kidney, and significant protein is detected in circulation, suggesting the possibility of Sost acting in an endocrine manner instead what is understood to be a paracrine manner [83]. Sost is also expressed in some osteoblasts and osteocytes thus, understanding cell-type specific contributions of Sost to bone metabolism would be beneficial in understanding bone metabolism and fracture healing.

To study cell-type specific contributions of Sost involved in bone metabolism, a novel coin (conditionals by inversion) knockout mouse model can be used and applied in bone metabolism and fracture healing studies [204]. Sost coin mice were generated by inserting an inverted GFP cassette in the second intron of the Sost transcript [204]. Upon mating Sost coin mice with mice expressing Cre recombinase under various cell-type promoters, we can remove Sost in specific cells and examine changes in bone metabolism. For example, mating Sost coin mice with Cre under the Prx1 promoter, Col1 promoter, or DMP1 promoter will generate *Sost coinko; Prx1 cre+*, *Sost coinko; Col1 cre+* and *Sost coinko; DMP1 cre+* mice respectfully.

Prx1 is a paired-related homeobox gene expressed in undifferentiated mesenchyme targeting osteochondral progenitors (chondrocytes, adipocytes, osteoblasts, osteocytes) of the appendicular skeleton, leaving the axial skeleton unperturbed [205]. *Sost coinko; Prx1 cre+* mice will first reveal whether Sost acts in an endocrine or paracrine manner. If only the appendicular skeleton shows elevated bone mass, this will indicate Sost functioning in a paracrine manner. In contrast, if both appendicular and axial skeleton shows elevated bone mass, this will indicate Sost functioning in an endocrine manner. Additionally, since the Prx1 cre targets osteochondral progenitor cells, this will reveal if other cells besides osteocytes may express Sost.

Dentin matrix acidic phosphoprotein 1 (DMP1) is a matrix protein secreted by osteocytes. Since osteocytes are known to secrete Sost, removing Sost in osteocytes

using the DMP1 cre promoter will indicate how much Sost from osteocytes contributes in bone metabolism. If Sost is secreted only by osteocytes, we should expect to observe a high bone mass phenotype that recapitulates the bone phenotype in *Sost* knockout mice (*Sost*$^{-/-}$) mice. Fracture healing can also be examined to reveal if repair in *Sost coinko; DMP1 cre+* mice is also enhanced as observed in *Sost*$^{-/-}$ mice.

Since osteocytes mature from osteoblasts, *Sost coinko; Col1 cre+* mice will remove Sost in all osteoblasts and osteocytes. We have previously shown that conditionally knocking out a transcription factor, Mef2C, of Sost in osteoblasts results in a high bone mass phenotype similar to *Sost*$^{-/-}$ mice [83], which we would also expect to observe in *Sost coinko; Col1 cre+*.

Using these conditional knockout mice: *Sost coinko; Prrx1 cre+*, *Sost coinko; Col1 cre+*, and *Sost coinko, DMP1 cre+* mice would first provide insight in understanding cell specific Sost contributions to bone metabolism. Secondly, these conditional knockout mice can also be used in fracture repair studies to understand what target cell type might be responding the most to Sost antibody. This may also provide insight in the role of Sost during fracture healing since mesenchymal stem cells express Sostdc1 during fracture repair.

As previously discussed, Sost antibody has been shown to be a potent anabolic drug to promote bone formation as well as improving impaired fracture healing in a drug induced diabetic mouse model, STZ. However, it is still not well understood in terms of how Sost antibody functions. Sost coin mice bred with Akita (Ins2$^{+/-}$) mice or treated with STZ, can be also used to examine changes in bone metabolism in a hyperglycemic environment. Cell specific Sost knockouts in a hyperglycemic environment may provide some insights in terms of which cells may have the greatest anabolic effect upon knocking out Sost in a diabetic mouse model, as well as providing insight in terms of how SOST antibody treatment work mechanistically in a hyperglycemic environment.

In conclusion, our findings in all three studies incorporate systems levels that aid in evaluating the effects of Sost antibody treatment or in understanding more about Sost role in bone formation. For example, we aid in bridging diabetes to osteoporosis in chapter 2 and 3 and revealed systemic effects on Sost antibody treatment in bone metabolism and repair in chapter 2. We also linked periosteum and stem cells involved during fracture repair in chapter 4. Lastly in future studies, systems level approaches can be found using Sost coin knockout mice in distinguishing the differences between endocrine and paracrine effects of Sost on bone metabolism.

References

1. Wodarz, A. and R. Nusse, *Mechanisms of Wnt signaling in development.* Annu Rev Cell Dev Biol, 1998. **14**: p. 59-88.
2. Baron, R. and M. Kneissel, *WNT signaling in bone homeostasis and disease: from human mutations to treatments.* Nat Med, 2013. **19**(2): p. 179-92.
3. Ahn, Y., et al., *Inhibition of Wnt signaling by Wise (Sostdc1) and negative feedback from Shh controls tooth number and patterning.* Development, 2010. **137**(19): p. 3221-31.
4. Wang, J., et al., *A mutation in the insulin 2 gene induces diabetes with severe pancreatic beta-cell dysfunction in the Mody mouse.* J Clin Invest, 1999. **103**(1): p. 27-37.
5. Phillips, A.M., *Overview of the fracture healing cascade.* Injury, 2005. **36 Suppl 3**: p. S5-7.
6. Dana T. Graves, J.A., David N. Paglia, Jeames Patrick O'Connor, Sheldon Lin, *Impact of Diabetes on Fracture Healing.* Journal of Experimental and Clinical Medicine, 2011. **3**(1): p. 3-8.
7. Gerstenfeld, L.C., et al., *Fracture healing as a post-natal developmental process: molecular, spatial, and temporal aspects of its regulation.* J Cell Biochem, 2003. **88**(5): p. 873-84.
8. Munoz-Pinedo, A.C.-M.a.C., *Dying for Something to Eat: How Cells Respond to Starvation.* The Open Cell Signaling Journal, 2011. **3**: p. 42-51.
9. Rorsman, F.M.A.a.P., *Diabetes Mellitus and the beta Cell: The Last Ten Years.* Cell, 2012. **148**: p. 1160-1171.
10. Vincenzo Carnevale, E.R., Emilio D'Erasmo, *Skeletal involvement in patients with diabetes mellitus.* Diabetes Metab Res Rev, 2004. **20**: p. 196-204.
11. Tilman D. Rachner, S.K., and Lorenz C. Hofbauer, *New Horizons in Osteoporosis.* Lancet, 2011. **377**(9773): p. 1276-1287.
12. Lorenz C Hofbauer, C.C.B., Shiv K Singh, and Harald Dobnig, *Osteoprosis in Patients with Diabetes Mellitus.* Journal of Bone and Mineral Research, 2007. **22**(9): p. 1317-1328.
13. McCabe, K.M.a.L.R., *Streptozotocin, Type 1 Diabetes Severity and Bone.* Biological Procedures Online, 2009. **11**(1): p. 296-315.
14. McCabe, S.B.a.L.R., *Bone Loss and Increased Bone Adiposity in Spontaneous and Pharmacologically Induced Diabetic Mice.* Endocrinology, 2007. **148**(1): p. 198-205.
15. Blakytny, R., M. Spraul, and E.B. Jude, *Review: The diabetic bone: a cellular and molecular perspective.* Int J Low Extrem Wounds, 2011. **10**(1): p. 16-32.
16. Robert Blakytny, M.S., and Edward B. Jude, *The Diabetic Bone: A Celluar and Molecular Perspective.* The International Journal of Lower Extremity Wounds, 2011. **10**(1): p. 16-31.
17. Silva, M.J., et al., *Type 1 diabetes in young rats leads to progressive trabecular bone loss, cessation of cortical bone growth, and diminished whole bone strength and fatigue life.* J Bone Miner Res, 2009. **24**(9): p. 1618-27.

18. Valerio, G., et al., *The lumbar bone mineral density is affected by long-term poor metabolic control in adolescents with type 1 diabetes mellitus.* Horm Res, 2002. **58**(6): p. 266-72.
19. Graves, D.T., et al., *Impact of Diabetes on Fracture Healing.* Journal of Experimental & Clinical Medicine, 2011. **3**(1): p. 3-8.
20. Alblowi, J., et al., *High levels of tumor necrosis factor-alpha contribute to accelerated loss of cartilage in diabetic fracture healing.* Am J Pathol, 2009. **175**(4): p. 1574-85.
21. Gooch, H.L., et al., *Alterations of cartilage and collagen expression during fracture healing in experimental diabetes.* Connect Tissue Res, 2000. **41**(2): p. 81-91.
22. Toshiyuki Kasahara, S.I., Hideto Kojima, Miwako Katagi, Hiroshi Kimura, Lawrence Chan, Yoshitaka Matsusue, *Malfunction of bone marrow-derived osteoclasts and the delay of bone fracture healing in diabetic mice.* Bone, 2010. **47**: p. 617-625.
23. Fulzele, K. and T.L. Clemens, *Novel functions for insulin in bone.* Bone, 2012. **50**(2): p. 452-6.
24. Guo, S., *Insulin signaling, resistance, and the metabolic syndrome: insights from mouse models into disease mechanisms.* J Endocrinol, 2014. **220**(2): p. T1-T23.
25. Siddle, K., *Signalling by insulin and IGF receptors: supporting acts and new players.* J Mol Endocrinol, 2011. **47**(1): p. R1-10.
26. Wang, Y., Y. Zhou, and D.T. Graves, *FOXO Transcription Factors: Their Clinical Significance and Regulation.* BioMed Research International, 2014. **2014**: p. 13.
27. Zhang, X., et al., *Akt, FoxO and regulation of apoptosis.* Biochim Biophys Acta, 2011. **1813**(11): p. 1978-86.
28. Iyer, S., et al., *FOXOs attenuate bone formation by suppressing Wnt signaling.* J Clin Invest, 2013. **123**(8): p. 3409-19.
29. Jiao, H., E. Xiao, and D.T. Graves, *Diabetes and Its Effect on Bone and Fracture Healing.* Curr Osteoporos Rep, 2015. **13**(5): p. 327-35.
30. Roszer, T., *Inflammation as death or life signal in diabetic fracture healing.* Inflamm Res, 2011. **60**(1): p. 3-10.
31. Accili, D., et al., *Early neonatal death in mice homozygous for a null allele of the insulin receptor gene.* Nat Genet, 1996. **12**(1): p. 106-9.
32. Joshi, R.L., et al., *Targeted disruption of the insulin receptor gene in the mouse results in neonatal lethality.* EMBO J, 1996. **15**(7): p. 1542-7.
33. Thrailkill, K.M., et al., *Is insulin an anabolic agent in bone? Dissecting the diabetic bone for clues.* Am J Physiol Endocrinol Metab, 2005. **289**(5): p. E735-45.
34. Gandhi, A., et al., *The effects of local insulin delivery on diabetic fracture healing.* Bone, 2005. **37**(4): p. 482-90.
35. Beam, H.A., J.R. Parsons, and S.S. Lin, *The effects of blood glucose control upon fracture healing in the BB Wistar rat with diabetes mellitus.* J Orthop Res, 2002. **20**(6): p. 1210-6.

36. Erdal, N., et al., *The effect of insulin therapy on biomechanical deterioration of bone in streptozotocin (STZ)-induced type 1 diabetes mellitus in rats.* Diabetes Res Clin Pract, 2012. **97**(3): p. 461-7.
37. Ferron, M., et al., *Insulin signaling in osteoblasts integrates bone remodeling and energy metabolism.* Cell, 2010. **142**(2): p. 296-308.
38. Capulli, M., R. Paone, and N. Rucci, *Osteoblast and osteocyte: games without frontiers.* Arch Biochem Biophys, 2014. **561**: p. 3-12.
39. Katayama, Y., et al., *Role of nonenzymatic glycosylation of type I collagen in diabetic osteopenia.* J Bone Miner Res, 1996. **11**(7): p. 931-7.
40. Alikhani, M., et al., *Advanced glycation end products stimulate osteoblast apoptosis via the MAP kinase and cytosolic apoptotic pathways.* Bone, 2007. **40**(2): p. 345-53.
41. Franke, S., et al., *Advanced glycation endproducts influence the mRNA expression of RAGE, RANKL and various osteoblastic genes in human osteoblasts.* Arch Physiol Biochem, 2007. **113**(3): p. 154-61.
42. Hamada, Y., et al., *Histomorphometric analysis of diabetic osteopenia in streptozotocin-induced diabetic mice: a possible role of oxidative stress.* Bone, 2007. **40**(5): p. 1408-14.
43. Bai, X.C., et al., *Oxidative stress inhibits osteoblastic differentiation of bone cells by ERK and NF-kappaB.* Biochem Biophys Res Commun, 2004. **314**(1): p. 197-207.
44. Suda, N., et al., *Participation of oxidative stress in the process of osteoclast differentiation.* Biochim Biophys Acta, 1993. **1157**(3): p. 318-23.
45. McCabe, L.R., *Understanding the pathology and mechanisms of type I diabetic bone loss.* J Cell Biochem, 2007. **102**(6): p. 1343-57.
46. Botolin, S. and L.R. McCabe, *Bone Loss and Increased Bone Adiposity in Spontaneous and Pharmacologically Induced Diabetic Mice.* Endocrinology, 2007. **148**(1): p. 198-205.
47. Maggio, A.B., et al., *Decreased bone turnover in children and adolescents with well controlled type 1 diabetes.* J Pediatr Endocrinol Metab, 2010. **23**(7): p. 697-707.
48. Khan, T.S. and L.A. Fraser, *Type 1 diabetes and osteoporosis: from molecular pathways to bone phenotype.* J Osteoporos, 2015. **2015**: p. 174186.
49. Hie, M., et al., *Increased cathepsin K and tartrate-resistant acid phosphatase expression in bone of streptozotocin-induced diabetic rats.* Bone, 2007. **41**(6): p. 1045-50.
50. Hie, M., et al., *Insulin-dependent diabetes mellitus decreases osteoblastogenesis associated with the inhibition of Wnt signaling through increased expression of Sost and Dkk1 and inhibition of Akt activation.* Int J Mol Med, 2011. **28**(3): p. 455-62.
51. Iitsuka, N., M. Hie, and I. Tsukamoto, *Zinc supplementation inhibits the increase in osteoclastogenesis and decrease in osteoblastogenesis in streptozotocin-induced diabetic rats.* Eur J Pharmacol, 2013. **714**(1-3): p. 41-7.

52. Coe, L.M., J. Zhang, and L.R. McCabe, *Both spontaneous Ins2(+/-) and streptozotocin-induced type I diabetes cause bone loss in young mice.* J Cell Physiol, 2013. **228**(4): p. 689-95.
53. Gennari, L., et al., *Treatment needs and current options for postmenopausal osteoporosis.* Expert Opin Pharmacother, 2016. **17**(8): p. 1141-52.
54. Michael J. Rogers, S.G., H.L. Benford, F.P. Coxon, S.P. Luckman, J. Monkkonen, J.C. Frith, *Cellular and Molecular Mechanisms of Action of Bisphosphonates.* Cancer Supplement, 2000. **88**(12): p. 2961-2978.
55. Jiliang Li, S.M., Yoshio Kaji, Tasuku Mashiba, Jun Kawanishi, and Hiromichi Norimatsu, *Effect of Bisphosphonate (Incadronate) on Fracture Healing of Long Bones in Rats.* Journal of Bone and Mineral Research, 1999. **14**(6): p. 969-979.
56. Hua Zhu Ke, W.G.R., Xiaodong Li, and Michael S. Ominsky, *Sclerostin and Dickkopf-1 as Therapeutic Targets in Bone Diseases.* Endocrine Reviews, 2012. **33**(5): p. 747-783.
57. C. Ejersted, H.O., E.F. Eriksen, and T.T. Andreassen, *Withdrawal of Parathyroid Hormone Treatment Causes Rapid Resorption of Newly Formed Verteral Cancellous and Endocortical Bone in Old Rats.* Bone, 1998. **23**(1): p. 43-52.
58. Ben-awadh, A.N., et al., *Parathyroid hormone receptor signaling induces bone resorption in the adult skeleton by directly regulating the RANKL gene in osteocytes.* Endocrinology, 2014. **155**(8): p. 2797-809.
59. Nabanita S. Datta, A.B.A.-S., *PTH and PTHrP signaling in osteoblasts.* Cellular Signaling, 2009. **21**: p. 1245-1254.
60. Luigi Gennari, D.M., Robert Valenti, Elena Ceccarelli, Martina Ruvio, Maria G. Pietrini, Cosimo Capodarca, Maria Beatrice Franci, Maria Stella Campagna, Anna Calabro, Dorica Cataldo, Konstantinos Stolakis, Francesco Dotta, and Ranuccio Nuti, *Circulating Sclerostin Levels and Bone Turnover in Type 1 and Type 2 Diabetes.* The Journal of Clinical Endocrinology & Metabolism, 2012. **97**(5): p. 1737-1744.
61. Daniel Lozano, L.F.d.C., Sonia Dapia, Irene Andrade-Zapata, Felix Manzarbeitia, M. Victoria Alvarez-Arroyo, Enrique Gomez-Barrena, and Pedro Esbrit, *Role of Parathyroid Hormone-Related Protein in the Decreased Osteoblast Function in Diabetes-Related Osteopenia.* Endorinology, 2009. **150**: p. 2027-2035.
62. Black, D.M., et al., *The effects of parathyroid hormone and alendronate alone or in combination in postmenopausal osteoporosis.* N Engl J Med, 2003. **349**(13): p. 1207-15.
63. Liu, L., et al., *Rosiglitazone inhibits bone regeneration and causes significant accumulation of fat at sites of new bone formation.* Calcif Tissue Int, 2012. **91**(2): p. 139-48.
64. King, A.J., *The use of animal models in diabetes research.* Br J Pharmacol, 2012. **166**(3): p. 877-94.
65. Diab, R.A., et al., *Immunotoxicological effects of streptozotocin and alloxan: in vitro and in vivo studies.* Immunol Lett, 2015. **163**(2): p. 193-8.

66. Szkudelski, T., *The mechanism of alloxan and streptozotocin action in B cells of the rat pancreas.* Physiol Res, 2001. **50**(6): p. 537-46.
67. Muller, Y.D., et al., *Immunosuppressive effects of streptozotocin-induced diabetes result in absolute lymphopenia and a relative increase of T regulatory cells.* Diabetes, 2011. **60**(9): p. 2331-40.
68. Lenzen, S., *The mechanisms of alloxan- and streptozotocin-induced diabetes.* Diabetologia, 2008. **51**(2): p. 216-26.
69. Pozzilli, P., et al., *NOD mouse colonies around the world--recent facts and figures.* Immunol Today, 1993. **14**(5): p. 193-6.
70. Mordes, J.P., et al., *Rat models of type 1 diabetes: genetics, environment, and autoimmunity.* ILAR J, 2004. **45**(3): p. 278-91.
71. Mathews, C.E., S.H. Langley, and E.H. Leiter, *New mouse model to study islet transplantation in insulin-dependent diabetes mellitus.* Transplantation, 2002. **73**(8): p. 1333-6.
72. Venkatesh Krishnan, H.U.B., and Ormond A. MacDougald, *Regulation of bone mass by Wnt signaling.* The Journal of Clinical Investigation, 2006. **116**(5): p. 1202-1209.
73. Hartmann, C., *A Wnt canon orchestrating osteoblastogenesis.* TRENDS in Cell Biology, 2006. **16**(3): p. 151-158.
74. Canalis, E., *Wnt signalling in osteoporosis: mechanisms and novel therapeutic approaches.* Nat Rev Endocrinol, 2013. **9**(10): p. 575-83.
75. Chen, Y., et al., *Beta-catenin signaling plays a disparate role in different phases of fracture repair: implications for therapy to improve bone healing.* PLoS Med, 2007. **4**(7): p. e249.
76. Barolo, S., *Transgenic Wnt/TCF pathway reporters: all you need is Lef?* Oncogene, 2006. **25**(57): p. 7505-11.
77. Sawakami, K., et al., *The Wnt co-receptor LRP5 is essential for skeletal mechanotransduction but not for the anabolic bone response to parathyroid hormone treatment.* J Biol Chem, 2006. **281**(33): p. 23698-711.
78. Holmen, S.L., et al., *Decreased BMD and limb deformities in mice carrying mutations in both Lrp5 and Lrp6.* J Bone Miner Res, 2004. **19**(12): p. 2033-40.
79. Nakanishi, R., et al., *Osteoblast-targeted expression of Sfrp4 in mice results in low bone mass.* J Bone Miner Res, 2008. **23**(2): p. 271-7.
80. Li, J., et al., *Dkk1-mediated inhibition of Wnt signaling in bone results in osteopenia.* Bone, 2006. **39**(4): p. 754-66.
81. Kramer, I., et al., *Parathyroid hormone (PTH)-induced bone gain is blunted in SOST overexpressing and deficient mice.* J Bone Miner Res, 2010. **25**(2): p. 178-89.
82. Li, X., et al., *Targeted deletion of the sclerostin gene in mice results in increased bone formation and bone strength.* J Bone Miner Res, 2008. **23**(6): p. 860-9.
83. Collette, N.M., et al., *Targeted deletion of Sost distal enhancer increases bone formation and bone mass.* Proc Natl Acad Sci U S A, 2012. **109**(35): p. 14092-7.

84. Boschert, V., et al., *Mutational analysis of sclerostin shows importance of the flexible loop and the cystine-knot for Wnt-signaling inhibition.* PLoS One, 2013. **8**(11): p. e81710.
85. van Dinther, M., et al., *Anti-Sclerostin antibody inhibits internalization of Sclerostin and Sclerostin-mediated antagonism of Wnt/LRP6 signaling.* PLoS One, 2013. **8**(4): p. e62295.
86. Chang, M.K., et al., *Disruption of Lrp4 function by genetic deletion or pharmacological blockade increases bone mass and serum sclerostin levels.* Proc Natl Acad Sci U S A, 2014. **111**(48): p. E5187-95.
87. Wendy Balemans, m.E., Neela Patel, Els Van Hul, Pam Olson, Marianna Dioszegi, Charlemagne Lacza, Wim Wuyts, Jenneke Van Den Ende, Patrick Willems, Auristela F. Paes-Alves, Suvimol Hill, Manuel Bueno, Feliciano J. Ramos, Paolo Tacconi, Frederik G. Dikkers, Constantine Stratakis, Klaus Llindpaintner, Brian Vickery, Dorothee Foernzler and Wim Van Hul, *Increased bond density in sclerosteosis is due to the deficiency of a novel secreted protein (SOST).* Human Nolecular Genetics, 2001. **10**(5): p. 537-543.
88. Balemans, W., et al., *Identification of a 52 kb deletion downstream of the SOST gene in patients with van Buchem disease.* J Med Genet, 2002. **39**(2): p. 91-7.
89. Nicole M. Collette, D.C.G., Aris N. Economides, LiQin Xie, Mohammad Shahnazari, Wei Yao, Nancy E. Lane, Richard M. Harland, and Gabriela G. Loots, *Targeted deletion of Sost distal enhancer increases bone formation and bone mass.* PNAS, 2012. **109**(35): p. 14092-12097.
90. Nicole M. Collette, D.C.G., Deepa Murugesh, Richard M. Harland, Gabriela G. Loots, *Genetic evidence that SOST inhibits WNT signaling in the limb.* Developmental Biology, 2010. **342**: p. 169-179.
91. Chaoyang Li, M.S.O., Hong-Lin Tan, Mauricio Barrero, Qing-Tian Niu, Franklin J. Asuncion, Edward Lee, Min Liu, William S. Simonet, Chris Paszty, Hua Zhu Ke, *Increased callus mass and enhanced strength during fracture healing in mice lacking the sclerostin gene.* Bone, 2011. **49**: p. 1178-1185.
92. Michael S Ominsky, F.V., Jacquelin Jolette, Susan Y Smith, Brian Stouch, George Doellgast, Jianhua Gong, Yongming Gao, Jin Cao, Kevin Graham, Barbara Tipton, Jill Cai, Rohini Deshpande, Lei Zhou, Michael D Hale, Daniel J Lightwood, Alistair J Henry, Andrew G Popplewell, Adrian R Moore, Martyn K Robinson, David L Lacey, W Scott Simonet, and Chris Paszty, *Two Doses of Sclerostin Antibody in Cynomolgus Monkeys Increases Bone Formation, Bone Mineral Density, and Bone Strength.* Journal of Bone and Mineral Research, 2010. **25**(5): p. 948-959.
93. Li, X., et al., *Sclerostin antibody treatment increases bone formation, bone mass, and bone strength in a rat model of postmenopausal osteoporosis.* J Bone Miner Res, 2009. **24**(4): p. 578-88.
94. Hamann, C., et al., *Sclerostin antibody treatment improves bone mass, bone strength, and bone defect regeneration in rats with type 2 diabetes mellitus.* J Bone Miner Res, 2013. **28**(3): p. 627-38.

95. Alzahrani, M.M., F. Rauch, and R.C. Hamdy, *Does Sclerostin Depletion Stimulate Fracture Healing in a Mouse Model?* Clin Orthop Relat Res, 2016. **474**(5): p. 1294-302.
96. Michael S Ominsky, C.L., Xiaodong Li, Hong L Tan, Edward Lee, Mauricio Barrero, Franklin J Asuncion, Denise Dwyer, Chun-Ya Han, Fay Vlasseros, Rana Samadfam, Jacqueline Jolette, Susan Y Smith, Marina Stolina, David L Lacey, William S Silmonet, Chris Paszty, Gang Li, and Hua Z Ke, *Inhibition of Sclerostin by Monoclonal Antibody Enhances Bone Healing and Improves Bone Density and Strength of Nonfractured Bones.* Journal of Bone and Mineral Research, 2011. **26**(5): p. 1012-1021.
97. Li, X., et al., *Increased bone formation and bone mass induced by sclerostin antibody is not affected by pretreatment or cotreatment with alendronate in osteopenic, ovariectomized rats.* Endocrinology, 2011. **152**(9): p. 3312-22.
98. Agholme, F., et al., *Efficacy of a sclerostin antibody compared to a low dose of PTH on metaphyseal bone healing.* J Orthop Res, 2014. **32**(3): p. 471-6.
99. Padhi, D., et al., *Single-dose, placebo-controlled, randomized study of AMG 785, a sclerostin monoclonal antibody.* J Bone Miner Res, 2011. **26**(1): p. 19-26.
100. Ominsky, M.S., et al., *Two doses of sclerostin antibody in cynomolgus monkeys increases bone formation, bone mineral density, and bone strength.* J Bone Miner Res, 2010. **25**(5): p. 948-59.
101. Clarke, B.L., *Anti-sclerostin antibodies: utility in treatment of osteoporosis.* Maturitas, 2014. **78**(3): p. 199-204.
102. Kiso, H., et al., *Interactions between BMP-7 and USAG-1 (uterine sensitization-associated gene-1) regulate supernumerary organ formations.* PLoS One, 2014. **9**(5): p. e96938.
103. Laurikkala, J., et al., *Identification of a secreted BMP antagonist, ectodin, integrating BMP, FGF, and SHH signals from the tooth enamel knot.* Dev Biol, 2003. **264**(1): p. 91-105.
104. Collette, N.M., et al., *Sost and its paralog Sostdc1 coordinate digit number in a Gli3-dependent manner.* Dev Biol, 2013. **383**(1): p. 90-105.
105. Colnot, C., *Skeletal cell fate decisions within periosteum and bone marrow during bone regeneration.* J Bone Miner Res, 2009. **24**(2): p. 274-82.
106. Janssens, K. and W. Van Hul, *Molecular genetics of too much bone.* Hum Mol Genet, 2002. **11**(20): p. 2385-93.
107. Gardner, J.C., et al., *Bone mineral density in sclerosteosis; affected individuals and gene carriers.* J Clin Endocrinol Metab, 2005. **90**(12): p. 6392-5.
108. Brunkow, M.E., et al., *Bone dysplasia sclerosteosis results from loss of the SOST gene product, a novel cystine knot-containing protein.* Am J Hum Genet, 2001. **68**(3): p. 577-89.
109. Beighton, P., et al., *The syndromic status of sclerosteosis and van Buchem disease.* Clin Genet, 1984. **25**(2): p. 175-81.
110. Yagi, H., et al., *Sclerosteosis (craniotubular hyperostosis-syndactyly) with complex hyperphalangy of the index finger.* Pediatr Radiol, 2015. **45**(8): p. 1239-43.

111. Hamilton, E.J., et al., *Prevalence and predictors of osteopenia and osteoporosis in adults with Type 1 diabetes.* Diabet Med, 2009. **26**(1): p. 45-52.
112. Hofbauer, L.C., et al., *Osteoporosis in patients with diabetes mellitus.* J Bone Miner Res, 2007. **22**(9): p. 1317-28.
113. Nyman, J.S., et al., *Increasing duration of type 1 diabetes perturbs the strength-structure relationship and increases brittleness of bone.* Bone, 2011. **48**(4): p. 733-40.
114. Schwartz, A.V., *Diabetes Mellitus: Does it Affect Bone?* Calcif Tissue Int, 2003. **73**(6): p. 515-9.
115. Vestergaard, P., L. Rejnmark, and L. Mosekilde, *Diabetes and its complications and their relationship with risk of fractures in type 1 and 2 diabetes.* Calcif Tissue Int, 2009. **84**(1): p. 45-55.
116. Coe, L.M., et al., *The bone marrow microenvironment contributes to type I diabetes induced osteoblast death.* J Cell Physiol, 2011. **226**(2): p. 477-83.
117. de, L., II, et al., *Bone mineral density and fracture risk in type-2 diabetes mellitus: the Rotterdam Study.* Osteoporos Int, 2005. **16**(12): p. 1713-20.
118. Issa, C., M.S. Zantout, and S.T. Azar, *Osteoporosis in men with diabetes mellitus.* J Osteoporos, 2011. **2011**: p. 651867.
119. Shu, A., et al., *Bone structure and turnover in type 2 diabetes mellitus.* Osteoporos Int, 2012. **23**(2): p. 635-41.
120. Ceriello, A., *The emerging challenge in diabetes: the "metabolic memory".* Vascul Pharmacol, 2012. **57**(5-6): p. 133-8.
121. Loder, R.T., *The influence of diabetes mellitus on the healing of closed fractures.* Clin Orthop Relat Res, 1988(232): p. 210-6.
122. Erejuwa, O.O., *Management of diabetes mellitus: could simultaneous targeting of hyperglycemia and oxidative stress be a better panacea?* Int J Mol Sci, 2012. **13**(3): p. 2965-72.
123. Campos Pastor, M.M., et al., *Intensive insulin therapy and bone mineral density in type 1 diabetes mellitus: a prospective study.* Osteoporos Int, 2000. **11**(5): p. 455-9.
124. Petersen, C.P. and P.W. Reddien, *Wnt signaling and the polarity of the primary body axis.* Cell, 2009. **139**(6): p. 1056-68.
125. Halt, K. and S. Vainio, *Coordination of kidney organogenesis by Wnt signaling.* Pediatr Nephrol, 2014. **29**(4): p. 737-44.
126. Church, V.L. and P. Francis-West, *Wnt signalling during limb development.* Int J Dev Biol, 2002. **46**(7): p. 927-36.
127. Nusse, R., *Wnt signaling.* Cold Spring Harb Perspect Biol, 2012. **4**(5).
128. Kato, M., et al., *Cbfa1-independent decrease in osteoblast proliferation, osteopenia, and persistent embryonic eye vascularization in mice deficient in Lrp5, a Wnt coreceptor.* J Cell Biol, 2002. **157**(2): p. 303-14.
129. Cui, Y., et al., *Lrp5 functions in bone to regulate bone mass.* Nat Med, 2011. **17**(6): p. 684-91.

130. Little, R.D., et al., *A mutation in the LDL receptor-related protein 5 gene results in the autosomal dominant high-bone-mass trait.* Am J Hum Genet, 2002. **70**(1): p. 11-9.
131. Babij, P., et al., *High bone mass in mice expressing a mutant LRP5 gene.* J Bone Miner Res, 2003. **18**(6): p. 960-74.
132. Arioka, M., et al., *Acceleration of bone development and regeneration through the Wnt/beta-catenin signaling pathway in mice heterozygously deficient for GSK-3beta.* Biochem Biophys Res Commun, 2013. **440**(4): p. 677-82.
133. Day, T.F., et al., *Wnt/beta-catenin signaling in mesenchymal progenitors controls osteoblast and chondrocyte differentiation during vertebrate skeletogenesis.* Dev Cell, 2005. **8**(5): p. 739-50.
134. Li, X., et al., *Sclerostin binds to LRP5/6 and antagonizes canonical Wnt signaling.* J Biol Chem, 2005. **280**(20): p. 19883-7.
135. Balemans, W., et al., *Localization of the gene for sclerosteosis to the van Buchem disease-gene region on chromosome 17q12-q21.* Am J Hum Genet, 1999. **64**(6): p. 1661-9.
136. Loots, G.G., et al., *Genomic deletion of a long-range bone enhancer misregulates sclerostin in Van Buchem disease.* Genome Res, 2005. **15**(7): p. 928-35.
137. Collette, N.M., et al., *Genetic evidence that SOST inhibits WNT signaling in the limb.* Dev Biol, 2010. **342**(2): p. 169-79.
138. Gennari, L., et al., *Circulating sclerostin levels and bone turnover in type 1 and type 2 diabetes.* J Clin Endocrinol Metab, 2012. **97**(5): p. 1737-44.
139. Suen, P.K., et al., *Sclerostin monoclonal antibody enhanced bone fracture healing in an open osteotomy model in rats.* J Orthop Res, 2014. **32**(8): p. 997-1005.
140. McDonald, M.M., et al., *Inhibition of sclerostin by systemic treatment with sclerostin antibody enhances healing of proximal tibial defects in ovariectomized rats.* J Orthop Res, 2012. **30**(10): p. 1541-8.
141. Bonnarens, F. and T.A. Einhorn, *Production of a standard closed fracture in laboratory animal bone.* J Orthop Res, 1984. **2**(1): p. 97-101.
142. Bouxsein, M.L., et al., *Guidelines for assessment of bone microstructure in rodents using micro-computed tomography.* J Bone Miner Res, 2010. **25**(7): p. 1468-86.
143. Glatt, V., et al., *Age-related changes in trabecular architecture differ in female and male C57BL/6J mice.* J Bone Miner Res, 2007. **22**(8): p. 1197-207.
144. Fowlkes, J.L., et al., *Osteo-promoting effects of insulin-like growth factor I (IGF-I) in a mouse model of type 1 diabetes.* Bone, 2013. **57**(1): p. 36-40.
145. Lopez-Herradon, A., et al., *Inhibition of the canonical Wnt pathway by high glucose can be reversed by parathyroid hormone-related protein in osteoblastic cells.* J Cell Biochem, 2013. **114**(8): p. 1908-16.
146. Motyl, K. and L.R. McCabe, *Streptozotocin, type I diabetes severity and bone.* Biol Proced Online, 2009. **11**: p. 296-315.

147. Ellies, D.L., et al., *Bone density ligand, Sclerostin, directly interacts with LRP5 but not LRP5G171V to modulate Wnt activity.* J Bone Miner Res, 2006. **21**(11): p. 1738-49.
148. Musumeci, G., et al., *An in vivo experimental study on osteopenia in diabetic rats.* Acta Histochem, 2011. **113**(6): p. 619-25.
149. Lozano, D., et al., *The C-terminal fragment of parathyroid hormone-related peptide promotes bone formation in diabetic mice with low-turnover osteopaenia.* Br J Pharmacol, 2011. **162**(6): p. 1424-38.
150. Ross, R.D., et al., *Bone matrix quality after sclerostin antibody treatment.* J Bone Miner Res, 2014. **29**(7): p. 1597-607.
151. Hassler, N., et al., *Sclerostin deficiency is linked to altered bone composition.* J Bone Miner Res, 2014. **29**(10): p. 2144-51.
152. Ominsky, M.S., et al., *Inhibition of sclerostin by monoclonal antibody enhances bone healing and improves bone density and strength of nonfractured bones.* J Bone Miner Res, 2011. **26**(5): p. 1012-21.
153. Jawad, M.U., et al., *Effects of sclerostin antibody on healing of a non-critical size femoral bone defect.* J Orthop Res, 2013. **31**(1): p. 155-63.
154. Li, C., et al., *Increased callus mass and enhanced strength during fracture healing in mice lacking the sclerostin gene.* Bone, 2011. **49**(6): p. 1178-85.
155. Feng, G., et al., *Systemic administration of sclerostin monoclonal antibody accelerates fracture healing in the femoral osteotomy model of young rats.* Int Immunopharmacol, 2015. **24**(1): p. 7-13.
156. Lu, H., et al., *Diabetes interferes with the bone formation by affecting the expression of transcription factors that regulate osteoblast differentiation.* Endocrinology, 2003. **144**(1): p. 346-52.
157. Song, L., et al., *Loss of wnt/beta-catenin signaling causes cell fate shift of preosteoblasts from osteoblasts to adipocytes.* J Bone Miner Res, 2012. **27**(11): p. 2344-58.
158. Zhang, Q., R.C. Riddle, and T.L. Clemens, *Bone and the regulation of global energy balance.* J Intern Med, 2015. **277**(6): p. 681-9.
159. Liang, J. and J.M. Slingerland, *Multiple roles of the PI3K/PKB (Akt) pathway in cell cycle progression.* Cell Cycle, 2003. **2**(4): p. 339-45.
160. Kim, J.Y., et al., *Exendin-4 increases bone mineral density in type 2 diabetic OLETF rats potentially through the down-regulation of SOST/sclerostin in osteocytes.* Life Sci, 2013. **92**(10): p. 533-40.
161. Ma, P., et al., *Glimepiride promotes osteogenic differentiation in rat osteoblasts via the PI3K/Akt/eNOS pathway in a high glucose microenvironment.* PLoS One, 2014. **9**(11): p. e112243.
162. Manolagas, S.C. and M. Almeida, *Gone with the Wnts: beta-catenin, T-cell factor, forkhead box O, and oxidative stress in age-dependent diseases of bone, lipid, and glucose metabolism.* Mol Endocrinol, 2007. **21**(11): p. 2605-14.
163. Gaudio, A., et al., *Sclerostin levels associated with inhibition of the Wnt/beta-catenin signaling and reduced bone turnover in type 2 diabetes mellitus.* J Clin Endocrinol Metab, 2012. **97**(10): p. 3744-50.

164. Abiola, M., et al., *Activation of Wnt/beta-catenin signaling increases insulin sensitivity through a reciprocal regulation of Wnt10b and SREBP-1c in skeletal muscle cells.* PLoS One, 2009. **4**(12): p. e8509.
165. Stolina, M., et al., *Temporal changes in systemic and local expression of bone turnover markers during six months of sclerostin antibody administration to ovariectomized rats.* Bone, 2014. **67**: p. 305-13.
166. Grasemann, C., et al., *Parental diabetes: the Akita mouse as a model of the effects of maternal and paternal hyperglycemia in wildtype offspring.* PLoS One, 2012. **7**(11): p. e50210.
167. Parajuli, A., et al., *Bone's responses to mechanical loading are impaired in type 1 diabetes.* Bone, 2015. **81**: p. 152-60.
168. Yeh, C.K., et al., *Hyperglycemia and xerostomia are key determinants of tooth decay in type 1 diabetic mice.* Lab Invest, 2012. **92**(6): p. 868-82.
169. Yee, C.S., et al., *Sclerostin Antibody Treatment Improves Fracture Outcomes in a Type I Diabetic Mouse Model.* Bone, 2015.
170. Sjogren, K., et al., *The gut microbiota regulates bone mass in mice.* J Bone Miner Res, 2012. **27**(6): p. 1357-67.
171. Bechtold, S., et al., *Early manifestation of type 1 diabetes in children is a risk factor for changed bone geometry: data using peripheral quantitative computed tomography.* Pediatrics, 2006. **118**(3): p. e627-34.
172. Jilka, R.L., *The relevance of mouse models for investigating age-related bone loss in humans.* J Gerontol A Biol Sci Med Sci, 2013. **68**(10): p. 1209-17.
173. Colnot, C., *Cell sources for bone tissue engineering: insights from basic science.* Tissue Eng Part B Rev, 2011. **17**(6): p. 449-57.
174. Grcevic, D., et al., *In vivo fate mapping identifies mesenchymal progenitor cells.* Stem Cells, 2012. **30**(2): p. 187-96.
175. Matthews, B.G., et al., *Analysis of alphaSMA-labeled progenitor cell commitment identifies notch signaling as an important pathway in fracture healing.* J Bone Miner Res, 2014. **29**(5): p. 1283-94.
176. Maes, C., et al., *Osteoblast precursors, but not mature osteoblasts, move into developing and fractured bones along with invading blood vessels.* Dev Cell, 2010. **19**(2): p. 329-44.
177. Yanagita, M., et al., *Uterine sensitization-associated gene-1 (USAG-1), a novel BMP antagonist expressed in the kidney, accelerates tubular injury.* J Clin Invest, 2006. **116**(1): p. 70-9.
178. Tanaka, M., et al., *Expression of BMP-7 and USAG-1 (a BMP antagonist) in kidney development and injury.* Kidney Int, 2008. **73**(2): p. 181-91.
179. Clausen, K.A., et al., *SOSTDC1 differentially modulates Smad and beta-catenin activation and is down-regulated in breast cancer.* Breast Cancer Res Treat, 2011. **129**(3): p. 737-46.
180. Ahn, Y., et al., *Lrp4 and Wise interplay controls the formation and patterning of mammary and other skin appendage placodes by modulating Wnt signaling.* Development, 2013. **140**(3): p. 583-93.

181. Simmons, D.G. and T.G. Kennedy, *Uterine sensitization-associated gene-1: a novel gene induced within the rat endometrium at the time of uterine receptivity/sensitization for the decidual cell reaction.* Biol Reprod, 2002. **67**(5): p. 1638-45.
182. Itasaki, N., et al., *Wise, a context-dependent activator and inhibitor of Wnt signalling.* Development, 2003. **130**(18): p. 4295-305.
183. Ohazama, A., et al., *Lrp4 modulates extracellular integration of cell signaling pathways in development.* PLoS One, 2008. **3**(12): p. e4092.
184. Lintern, K.B., et al., *Characterization of wise protein and its molecular mechanism to interact with both Wnt and BMP signals.* J Biol Chem, 2009. **284**(34): p. 23159-68.
185. Cho, S.W., et al., *Interactions between Shh, Sostdc1 and Wnt signaling and a new feedback loop for spatial patterning of the teeth.* Development, 2011. **138**(9): p. 1807-16.
186. Collette, N.M., et al., *Sost and its paralog Sostdc1 coordinate digit number in a Gli3-dependent manner.* Dev Biol, 2013.
187. Lobe, C.G., et al., *Z/AP, a double reporter for cre-mediated recombination.* Dev Biol, 1999. **208**(2): p. 281-92.
188. Dempster, D.W., et al., *Standardized nomenclature, symbols, and units for bone histomorphometry: a 2012 update of the report of the ASBMR Histomorphometry Nomenclature Committee.* J Bone Miner Res, 2013. **28**(1): p. 2-17.
189. Kedlaya, R., et al., *Sclerostin inhibition reverses skeletal fragility in an Lrp5-deficient mouse model of OPPG syndrome.* Sci Transl Med, 2013. **5**(211): p. 211ra158.
190. Schepers, K., et al., *Activated Gs signaling in osteoblastic cells alters the hematopoietic stem cell niche in mice.* Blood, 2012. **120**(17): p. 3425-35.
191. Birbrair, A., et al., *Nestin-GFP transgene reveals neural precursor cells in adult skeletal muscle.* PLoS One, 2011. **6**(2): p. e16816.
192. Baek, W.Y., et al., *Positive regulation of adult bone formation by osteoblast-specific transcription factor osterix.* J Bone Miner Res, 2009. **24**(6): p. 1055-65.
193. Lama, G., et al., *Progenitor/Stem Cell Markers in Brain Adjacent to Glioblastoma: GD3 Ganglioside and NG2 Proteoglycan Expression.* J Neuropathol Exp Neurol, 2016.
194. Murao, H., et al., *Periosteal cells are a major source of soft callus in bone fracture.* J Bone Miner Metab, 2013. **31**(4): p. 390-8.
195. He, J.W., et al., *Contribution of the sclerostin domain-containing protein 1 (SOSTDC1) gene to normal variation of peak bone mineral density in Chinese women and men.* J Bone Miner Metab, 2011. **29**(5): p. 571-81.
196. Semenov, M., K. Tamai, and X. He, *SOST is a ligand for LRP5/LRP6 and a Wnt signaling inhibitor.* J Biol Chem, 2005. **280**(29): p. 26770-5.
197. Liu, Y., et al., *Effects of Sclerostin Antibody on the Healing of Femoral Fractures in Ovariectomised Rats.* Calcif Tissue Int, 2016. **98**(3): p. 263-74.

198. Friedman, M.S., S.M. Oyserman, and K.D. Hankenson, *Wnt11 promotes osteoblast maturation and mineralization through R-spondin 2.* J Biol Chem, 2009. **284**(21): p. 14117-25.
199. Liu, S., et al., *Overexpression of Wnt11 promotes chondrogenic differentiation of bone marrow-derived mesenchymal stem cells in synergism with TGF-beta.* Mol Cell Biochem, 2014. **390**(1-2): p. 123-31.
200. Yano, F., et al., *The canonical Wnt signaling pathway promotes chondrocyte differentiation in a Sox9-dependent manner.* Biochem Biophys Res Commun, 2005. **333**(4): p. 1300-8.
201. Boland, G.M., et al., *Wnt 3a promotes proliferation and suppresses osteogenic differentiation of adult human mesenchymal stem cells.* J Cell Biochem, 2004. **93**(6): p. 1210-30.
202. Khosla, S., et al., *Effects of sex and age on bone microstructure at the ultradistal radius: a population-based noninvasive in vivo assessment.* J Bone Miner Res, 2006. **21**(1): p. 124-31.
203. Riggs, B.L., et al., *Population-based study of age and sex differences in bone volumetric density, size, geometry, and structure at different skeletal sites.* J Bone Miner Res, 2004. **19**(12): p. 1945-54.
204. Economides, A.N., et al., *Conditionals by inversion provide a universal method for the generation of conditional alleles.* Proc Natl Acad Sci U S A, 2013. **110**(34): p. E3179-88.
205. Logan, M., et al., *Expression of Cre Recombinase in the developing mouse limb bud driven by a Prxl enhancer.* Genesis, 2002. **33**(2): p. 77-80.